INELASTIC INTERACTIONS OF 200 GeV AND 300 GeV PROTONS WITH EMULSION NUCLEI

V. H. Areti

Thesis submitted to the School of Graduate Studies
in partial fulfillment of the requirements for the
degree of Ph.D. in Physics

UNIVERSITY OF OTTAWA
OTTAWA, CANADA, 1976

ABSTRACT

Proton-nucleus interactions, in nuclear emulsion, at incident proton energies of 200 GeV and 300 GeV are studied. The emulsion stacks were exposed with the emulsion surface perpendicular to the beam direction. The results obtained are found to be compatible with those obtained, by scanning along the track of the incident proton, in the horizontally exposed stacks.

The inelastic mean-free-path is essentially the same at the two energies: 33.4 ± 2.6 cm at 200 GeV 34.6 ± 1.8 cm at 300 GeV. The average number of black tracks and the average number of grey tracks are also observed to be the same at both energies: $\langle N_b \rangle = 5.9\pm0.4$, $\langle N_g \rangle = 1.7\pm0.2$ at 200 GeV and $\langle N_b \rangle = 6.1\pm0.3$, $\langle N_g \rangle = 1.7\pm0.1$ at 300 GeV. The average number of shower particles, $\langle n_s \rangle$, increases from 13.4 ± 0.6 at 200 GeV to 15.2 ± 0.4 at 300 GeV. $\langle n_s \rangle$ may be given by $\langle n_s \rangle = 1.85\ s^{1/3}$, where s is the square of the C.M. energy of the nucleon-nucleon system.

It is shown that the ratio of dispersion D to the average multiplicity in proton-nucleus collisions is independent of the target nucleus. It is also shown that the multiplicity distribution (in emulsion) obeys the KNO

semi-inclusive scaling law in the energy range of 6.2 GeV to 300 GeV. The scaling function applied by Buras et al to the proton-proton multiplicity distributions was used.

It is argued that the proper quantity that gives the correct A dependence of the production of particles in proton-nucleus collisions is the ratio of created charges in proton-nucleus and proton-proton interactions. The predictions for the average multiplicity and the above mentioned ratio, from various models, are compared with the experimental values. The predictions of the models discussed agree reasonably well with the experimental results.

The rapidity distribution provides a crucial test for the models considered. The models' prediction that there should be no difference between proton-nucleus and proton-proton distributions, in the foreward region of the rapidity (in this case ln tan $\theta_L/2$) plots is verified. It is concluded that with extensive data using various nuclear targets, it should be possible to eliminate some of the models since the models differ in the prediction of the boundary of the region where the excess number of particles (compared with proton-proton distribution at the same energy) should appear.

ACKNOWLEDGMENTS

The author expresses his gratitude to Prof. J. Hebert for his help and guidance throughout the course of this work.

It is a pleasure to thank Dr. C. J. D. Hebert, who was extremely helpful through all the stages of this work; from processing of the emulsion stacks to the editing of the manuscript. The author benefited greatly from the many interesting discussions with her.

The author wishes to thank the members of the collaboration for making their data available.

Thanks are due to Dr. L. Voyvodic and the FNAL staff for the exposure of the emulsion stacks.

Thanks are also due to Dr. A. Van Ginneken for useful discussions and suggestions and Dr. J. J. Lord for keeping us informed of the results of their work.

The partial financial support provided by Prof. Hebert, from his I.P.P. and N.R.C. grants is gratefully acknowledged.

CONTENTS

LIST OF ILLUSTRATIONS

LIST OF TABLES

INTRODUCTION

In recent years attention has been focussed on hadron-hadron collisions at high energies as a means of understanding strong interaction dynamics. Since multiple particle production is the dominating process accounting for approximately three-quarters of the total cross-section, it has been the subject of intensive study. Until recently, cosmic ray experiments, especially nuclear emulsions exposed at high altitudes to energetic cosmic ray primaries, were the source of information regarding multiple production processes at ultra-high energies. The advent of a new generation of accelerators made possible the study of high-multiplicity events in the laboratory under more controllable conditions and with a higher degree of precision than could be achieved in cosmic ray experiments.

The main area of interest in cosmic ray studies was the extraction of information concerning hadron-hadron interactions from hadron-nucleus interactions. Since nuclear emulsion presents a composite target to the

incoming primary, the isolation of hadron-hadron events was carried out by selecting those events in which the number of evaporation tracks from the target nucleus was small.

Interest in hadron-nucleus interactions

During the past few years the situation has changed and the study of hadron-nucleus interactions is attracting the interest of many physicists.[1-8] There are several reasons for this. The idea that it may be possible to test different classes of models of multiple particle production in hadron-hadron collisions by a study of hadron-nucleus collisions is very attractive.[9-10] Moreover, experiments using nuclei as targets may yield information regarding the space-time development of the production process and could be of more fundamental importance than the asymptotic hadron-nucleon collision. Another reason for studying hadron-nucleus interactions is the coherent production of states that have the same intrinsic quantum numbers as the incident particle. If these states are long-lived, it would be possible to study their decay modes, interaction cross-sections with nucleons etc..[11]

In cosmic ray experiments, using nuclear emulsions, the incident hadron energy is estimated by using the Castagnoli relation[12]

$$\langle \log_{10} \mathrm{ctg}\, \theta_L \rangle = \log \gamma_c \ ,$$

where θ_L is the emission angle of the secondary in the laboratory frame, and γ_c is the Lorentz factor of the centre of momentum of the hadron-nucleon system. It was pointed out by Hebert et al[13] that, in 200 GeV proton-nucleus interactions, the incident proton energy estimated using this method exceeds the true energy by 40% when the number of evaporation prongs from the target nucleus is less than 2. In fact, the $\langle \log_{10} \mathrm{ctg}\, \theta_L \rangle$ value decreases as the number of slow particles, resulting from the fragmentation of the target nucleus, increases. Gibbs et al[14] made use of this fact in re-estimating the energies of some cosmic ray primaries. Thus, a study of hadron-nucleus interactions at known energies leads to a more accurate estimate of the energies of cosmic ray primaries interacting with a nuclear target in emulsions. Also, if the target nucleons in the path of the incident particle interact simultaneously with it, the centre of momentum energy available would be greater than for a hadron-nucleon collision by a factor equal to the square root of the number of nucleons involved. If this is the case, the

energy boost has important consequences for the production of heavy particles hitherto unobserved in proton-proton collisions at the available accelerator energies.[15]

Some features of high energy hadron-nucleus interactions

A proton-nucleus interaction may be represented by

$$p+A \longrightarrow a+b+c+\ldots+A'$$

where A and A' are the target nucleus in its initial and final states, and a,b,c etc. are the final state particles produced as a result of the collision. In a coherent production process, A and A' are the same. In an inelastic interaction, the target nucleus is often left in an excited state and it evaporates nucleons or nuclear fragments, whose typical energies are of the order of 10 MeV.

From cosmic ray experiments and from ISR results, it is established that 80% of the produced secondaries are pions.[16,17] The transverse momentum distribution of the primaries falls off rather sharply, and the value of $\langle p_t \rangle$ is about 0.3-0.4 Gev/c. There are indications that at large transverse momenta, heavy particle production becomes important.

The average number of fast charged particles from a proton-nucleus interaction $\langle n_s \rangle$ is only weakly dependent on the incident energy and the atomic weight of the target nucleus. A particularly useful parameter that allows a comparison between $\langle n_s \rangle$ and $\langle n_{ch} \rangle$ (the number of charged particles in the final state of proton-proton collisions at the same energy), is [9]

$$R_A = \langle n_s \rangle_{p-A} / \langle n_{ch} \rangle$$

The dependence of R_A on A is normally expressed by the relation $R_A \propto A^{\alpha}$. The value of R_A (and thus α) increases with energy and seems to have reached a constant value at the highest available accelerator energies.

Proton-nucleus interactions at high energies (>30 GeV) investigated using emulsions as detectors also show a constancy in the value of the average number of slow particles resulting from the break up of the target nucleus. The coefficient of inelasticity K, which is a measure of the energy spent by the incident particle in producing secondaries, is on the average considerably less than unity, implying that a good fraction of the incident energy is carried away by a final particle. This feature of the hadron interactions at high energies is called the leading particle effect.

An important feature of hadron-nucleus interactions seems to be the apparent transparency of the nucleus towards the newly produced particles, as evidenced by the angular distributions of the secondaries and the absence of internal cascading.

These and some other features of particle production at incident proton energies of 200 GeV and 300 GeV are presented in this work.

Chapter 1

EXPERIMENTAL TECHNIQUES

PART I: EMULSION TECHNIQUES

1.1 INTRODUCTION

Nuclear emulsions are used both as targets and detectors in studying various nuclear phenomena. As detectors, nuclear emulsions are compact and economical, requiring only a small amount of accelerator time. The small grain size of emulsions provides excellent spatial resolution. Emulsions of different grain sizes and sensitivities are manufactured by Ilford Ltd. The two most widely used electron sensitive emulsions are G-5 and K-5. K-5 emulsions have smaller grains than G-5 emulsions (≈ 0.2 um before processing) and thus provide better resolution. This is important because, at high energies, the majority of the fast particles are produced in a narrow forward cone and are very close to one another.

Emulsion presents a composite target to the incoming particles, since it consists of nearly equal volumes of silver halide crystals and a matrix material which is mainly gelatine. The chemical composition of standard G-5

emulsion of density 3.83 g/ml. at 58% R.H. is given by Barkas.[18] At first sight, it would appear that the fixed composition of emulsion limits the experimenter to the study of particle interactions in the constituent nuclei only. However, grains of various materials can be either suspended in the emulsion or deposited between two layers of emulsion. These loading and sandwich techniques were experimented with in this laboratory and the results are promising. The experiments of Florian et al,[4] who studied the interactions of high energy protons with tungsten nuclei, also indicates that emulsion can be effectively used in studying particle interactions in nuclei other than those of emulsion.

1.2 COMPOSITION OF EMULSION

The densities of the emulsions used in the 200 GeV and 300 GeV exposures were found to be 3.72 g/ml. and 3.85 g/ml. respectively. The lower value of the emulsion density in the case of the 200 GeV exposure is attributable to the fact that the pellicles were not completely dry. Taking the higher water content into consideration, the chemical composition of this emulsion can be calculated from the composition of standard emulsion. The results of the calculations are presented

in Table 1.1. The table also gives the probability of an interaction taking place with each of the constituent nuclei of the emulsion. The interaction probabilities are calculated assuming a cross-section dependence of $A^{2/3}$, where A is the atomic weight of the target.

Table 1.1

Chemical Composition of Emulsion

Element	Z	A	No. of atoms/ml. ($\times 10^{20}$)		interaction probabilities	
			200 GeV	300 GeV	200 GeV	300 GeV
Ag	47	107.88	97.10	101.01	0.37	0.38
Br	35	79.92	96.50	100.41	0.30	0.31
C	6	12.00	133.20	138.30	0.12	0.12
N	7	14.01	30.45	31.68	0.03	0.03
O	8	16.00	106.40	94.97	0.11	0.10
H	1	1.008	338.50	321.56	0.06	0.05
I	53	126.93	0.55	0.57	0.003	0.003
S	16	32.06	1.30	1.35	0.003	0.003

Based on the chemical composition, the <A> for emulsion is 27.82 and 29.10, respectively, for the stacks exposed to the 200 GeV and 300 GeV proton beams. The corresponding values of <A> calculated from the partial cross-sections are 68.54 and 69.76.

1.3 PARTICLE IDENTIFICATION AND ENERGY MEASUREMENTS

A charged particle traversing a medium dissipates its kinetic energy through ionization. In emulsion, the

energy absorbed by the silver halide crystals renders them developable. After processing, the track of a charged particle appears as a trail of small dark grains when the emulsion is viewed under a microscope. The grain density, i.e. the number of grains per unit length of track, and scattering measurements, are two of the techniques that enable one to identify the particle and measure its energy. These methods are briefly discussed below.

1.3.1 Grain density

The grain density 'g' is usually expressed in terms of 'g_o', the grain density of the track produced by an extremely relativistic particle. g_o is proportional to the specific ionization, up to the point where g is less than $4g_o$.

The energy loss, due to ionization, of a relativistic particle of kinetic energy T, is given by the Bethe-Bloch formula,[19]

$$\frac{dT}{dx} = 5.685\, NZ\frac{z^2}{\beta^2}\left(0.22 + \ln\frac{\beta^2}{I(1-\beta^2)} - \beta^2\right) \text{ MeV/cm}$$

where,

z = the charge number of the incident particle

Z = the charge number of the atoms of the medium

N = atomic density of the medium

I = the ionization potential of the medium.

For a compound medium, the above formula can be modified using the following procedure, mentioned in the UCRL reports.[20] Consider a compound of molecular weight A_M and density ρ_M. The 'i' elements constituting the material have densities ρ_i and atomic weights A_i and each element has i atoms per molecule. Then,

$$\left(\frac{dT}{dx}\right)_M = \sum_i \left(\frac{dT}{dx}\right)_i \rho_M A_i / \rho_i A_M$$

The plots of energy losses of protons and pions in Ilford G-5 emulsion, calculated by the above method, are reproduced from the UCRL reports in figure 1.1. Since the composition of G-5 and K-5 emulsions is the same, these plots also apply to K-5 emulsion.

In order to determine the energy of the particle from the grain density of its track, one should first measure g_o. This should be done for each plate, since g_o depends on the sensitivity of the emulsion, the degree of development and the time lapse between exposure and processing. In the present experiment, g_o is simply the grain density of the relativistic primary proton tracks. If the identity of the particle producing the track is known, its energy can be obtained from the normalized grain density (g/g_o) of the track. If, however, its

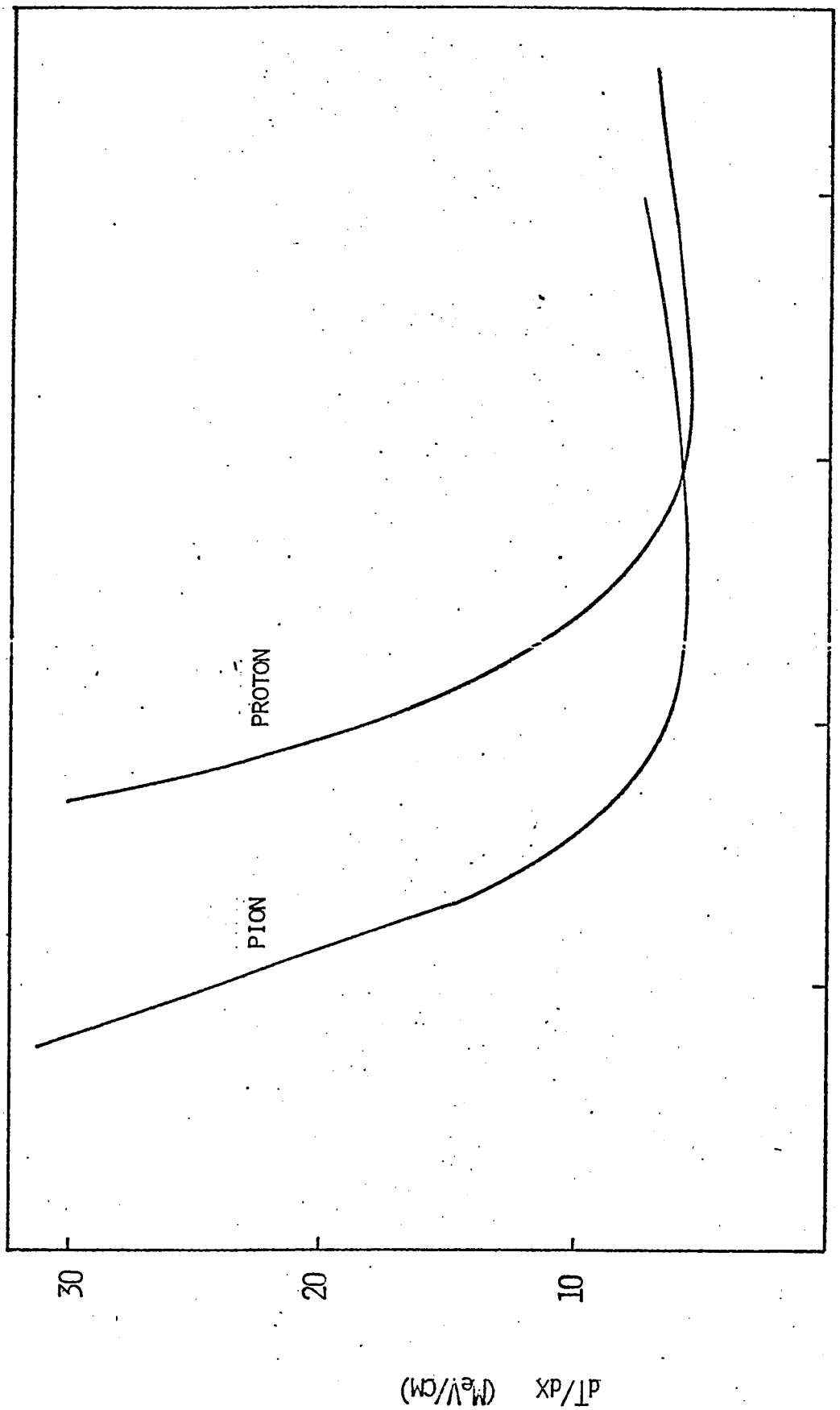

FIGURE 1.1 ENERGY LOSS AS A FUNCTION OF KINETIC ENERGY (IN EMULSION)

identity is unknown, measurements of grain density for two or more different segments of the track are needed in order to identify the particle and obtain its energy.

1.3.2 Scattering measurements

A charged particle traversing a medium continually changes its direction due to scattering by the Coulomb fields of the nuclei. For a particle of sufficiently high energy, the scattering angle α is small and its average value is given by

$$\langle\alpha\rangle = Kz\,t^{1/2}/p\beta$$

where K is a nearly constant quantity for given values of β and cell length t (measured in microns) over which the angle is measured and z and P are the charge and momentum (in MeV/c) of the particle. A knowledge of $\langle\alpha\rangle$ thus enables one to determine P and hence the energy of the particle. In measuring $\langle\alpha\rangle$, however, one has to apply corrections for various errors introduced by: a) the uncertainty in determining the centre of the track, b) the non-rectilinear motion of the microscope stage, c) the differential expansion of the parts of the microscope caused by temperature changes and d) spurious scattering which is the result of macroscopic distortions of emulsion.[21]

Following this brief introduction to the emulsion technique, the remainder of the chapter is devoted to the details of the experiment.

PART II: EXPERIMENTAL PROCEDURES

1.4 PREPARATION OF STACKS

All the emulsion stacks were prepared at the Centre de Recherches Nucleaires, Strasbourg, France. Tne stacks were composed of Ilford K-5 emulsion, 600 um thick, in addition to some emulsion plates. The composition of each of the stacks, exposed to the 200 GeV and 300 GeV proton beams, is given in Table 1.2.

Table 1.2

Composition of Stacks

No. of stacks	No. of pellicles per stack	Dimensions of pellicles	Incident energy in GeV
2	40	20cmx5cmx600um	200
1	20	5cmx5cmx600um	200
1	36	15cmx5cmx600um	300
1 (*)	6	15cmx5cmx600um	300
3 (**)	10	5cmx5cmx600um	300
2	12	5cmx5cmx600um	300

(*) glass backed emulsion.
(**) contains 8 glass backed emulsion and 2 pellicles.

1.5 EXPOSURE TO BEAM

The exposure of the emulsion stacks to the 200 GeV proton beam (NAL Expt. # 116) was carried out at the Meson Target Area of the Fermi National Accelerator Laboratory

(FNAL) by Dr. R. Kaiser and Dr. J. P. Massue, of the Strasbourg Laboratory. The 300 GeV exposure (NAL Expt. # 233) took place at the Neutrino Area of the FNAL. The persons invloved were the author, Dr. R. Kaiser and Dr. M.-A. Vincent, CRESALA, Universite du Quebec.

The stacks were placed at a distance of 50 meters from the window from which the 200 GeV proton beam emerged. The amount of air the beam passes through is equivalent to 1.5 cm of emulsion. By the time the beam reaches the target, it would be highly contaminated. To reduce this contamination of the beam, a plastic bag filled with helium gas (at atmospheric pressure) was placed in the path of the beam. In the case of the 300 GeV exposure, the beam passes through only 1.5 meters of air and thus the introduction of helium in the path of the beam was not essential.

The beam dimensions, in both the experiments, were 7.5 cm x 3.5 cm. The pulse rate was 10 pulses per minute. The beam was located by exposing polaroid films and the flux of protons was determined by irradiating test plates. This value was found to be 0.3×10^4 protons/cm^2/pulse.

Two techniques of exposure were used: i) the horizontal exposure, where the beam direction was parallel

to the emulsion surface and ii) the vertical exposure where the beam direction was perpendicular to the emulsion surface. The stacks containing emulsion pellicles (and/or plates) of dimensions 5 cm x 5 cm x 600 um were exposed vertically to a total flux of approximately 10^6 protons and the rest of the stacks were exposed horizontally to a total flux of nearly 2×10^4 protons.

1.6 PROCESSING OF THE EMULSION STACKS

The stacks that were exposed horizontally (at both energies) and three of the vertically exposed stacks (at 300 GeV) were processed at Centre de Recherches Nucleaires, Strasbourg, France. The remaining stacks were processed at the University of Ottawa. The steps involved in processing are outlined here. The detailed procedure is presented in Appendix 1.

Prior to development of the stacks, a grid was printed on the lower surface of each pellicle so as to provide a co-ordinate system for the location of events.

The aim, in processing the emulsion stacks, was to achieve uniform development throughout the thickness of the emulsion, with low distortions. Since unsupported emulsion undergoes dimensional changes in all directions, it was necessary to restrict at least the lateral

expansion of the pellicles by mounting them on pre-treated glass. The development technique used was the two-temperature method introduced by Dilworth, Occhialini and Payne.[22] The first stage of this method consists in presoaking the emulsion in distilled water. During this stage the emulsion swells but the swelling is kept to a minimum by keeping the distilled water at 4° C. In the following stage the plates were placed in developer solution at 4° C. The pre-soak in distilled water facilitates the penetration of the developer into the emulsion. The developer solution used was Brussels amidol developer. Amidol is a strong reducing agent that penetrates the emulsion faster than most other chemicals used for this purpose and it can function at low pH. The low pH is important in avoiding excess swelling of the emulsion. The action of the developer starts during the warm stage of development. In the dry warm stage, which was used in developing these stacks, the cold developer solution was poured out and the temperature of the plates was allowed to rise to 24° C. During both the cold and warm stages of development, at the University of Ottawa, filtered nitrogen gas was circulated in the developing tank. This prevents the oxidation of amidol which gives a yellow tinge to the processed emulsion.

The action of the developer was arrested by placing the plates in a weak (0.6%) solution of acetic acid. The plates were then transferred to the fixing solution. Fixing is rapid at high temperatures and with high pH solutions. This would make the emulsion swell greatly and would cause distortions. Fixing at low temperatures with low pH solutions is slower. Moreover, too low a pH for the fixer tends to etch the grains of the tracks. Fixing can be accelerated by stirring the solution and also by maintaining the concentration of the solution by periodically adding fresh fixer. In this laboratory, stirring of the solution was accomplished by a gentle flow of nitrogen gas into the fixer. The temperature of the stop bath and fixer were kept at a constant 12°C.

On the completion of fixing, the fixer solution was very slowly diluted by allowing filtered demineralized water to flow into the solution. The temperature during this stage was the same as for the fixing stage. This stage is very critical, for rapid dilution causes bubbles to form , especially in the places where the contact between emulsion and the glass support is weak. The osmotic pressure resulting from the different concentrations of the liquids inside and outside the bubble, makes the bubbles swell. When bubbles formed,

these were punctured in order to avoid distortions in other parts of the emulsion, which could be caused by the growth in size of the bubbles. Once the fixer was removed, the plates were washed in rapidly flowing filtered demineralized water (at 12°C) and then were dried in a series of solutions containing progressively stronger percentage of ethanol. This type of drying reduces distortions and also prevents the growth of micro-organisms in the emulsion. Finally, the plates were left to dry in air at a constant temperature and humidity (55% R.H.).

During the dilution stage of one of the 300 GeV stacks, the temperature of the bath was accidentally allowed to rise to 20° C for about 12 hours. This, unfortunately, introduced distortions in these plates.

After drying, the thickness of the processed emulsion is about one half of the initial thickness, owing to the removal of the undeveloped silver halide during fixing. The shrinkage factor, i.e. the ratio of the original thickness of the emulsion to its thickness after processing, should be determined for each plate.

1.7 DISTRIBUTION OF STACKS

The plates were distributed to the members of our collaboration, consisting of groups from Paris, Rome, Valence, Belgrade, Lund, University of Ottawa and McGill University. The horizontally exposed plates were distributed to the European groups mentioned above. The group from McGill was involved in the 200 GeV experiment only. At the University of Ottawa, some horizontally exposed plates were used, but the work done for this thesis was confined exclusively to the vertically exposed stacks. Data from the rest of the collaboration are used for comparison purposes and also when good statistics were necessary in analyzing the data.

1.8 SCANNING AND MEASUREMENT IN VERTICALLY EXPOSED PLATES

In the vertically exposed plates the proton beam appears as a matrix of dots, when the emulsion is viewed under a microscope. These dots appear to move into and out of the emulsion depending on the sense of the z motion of the microscope stage. The shrinkage of the emulsion, after processing, helps maintain the continuity of each track as it travels into or out of the emulsion.

1.8.1 Measurement of flux

The flux of protons in each plate was measured by means of a Leitz microscope fitted with a 100x oil immersion (Apochromat) objective and a pair of 10x oculars (Periplan). One of the oculars contained a graticule with a grid of 10 x 10 squares inscribed on its surface. The dimensions of the grid were calibrated against a stage micrometer. The total number of protons traversing the area of the grid was counted at five different areas in each 0.5 mm x0.5 mm square of the emulsion area that was scanned.

1.8.2 Scanning

A graticule placed in one of the oculars of the microscope aided in dividing the field of view into 9 squares. Originally, the plates exposed to the 200 GeV proton beam were scanned using a 40x air objective (Apochromat) and a pair of 10x oculars. However, noticing the inefficiency in the observation of events with one or no nuclear fragments, this objective was replaced by a 53x oil immersion objective (Apochromat). Groups of primaries traversing each part of the field of view were carefully followed and possible proton-nucleus interactions were recorded by noting the x,y and z coordinates of each event. The x and y coordinates were fixed by observing

the position of each event on a grid printed on the emulsion or on a grid that was attached to the glass plate supporting the emulsion. The z coordinate was measured relative to either the top or bottom surface of the emulsion, using the z micrometer of the microscope. The scanning procedure was repeated by changing the field of view by means of the x and y micrometers of the microscope stage. This method of scanning is a hybrid between area scanning and along-the-track scanning techniques. Though an area of emulsion was scanned, it was the tracks of a group of particles that were followed in each field of view.

As experience in scanning increased, it was realized that comparable detection efficiency, with increased speed of scanning, can be achieved by scanning the plates at lower magnification. Consequently, the plates exposed to the 300 GeV proton beam were scanned using a 22x oil immersion objective (Apochromat) along with a pair of 10x oculars.

1.8.3 Criteria for selection of events

Though many possible proton-nucleus interactions were detected while scanning, only those events that satisfied certain criteria were considered to be genuine events. An event was considered to be genuine only if the incident

particle was parallel to the beam particles. To enforce this criterion, events within 40 um (sometimes 60 um) from the top of the emulsion surface were excluded. Events within 60 um from the bottom surface of the emulsion were also excluded for the reason that small events are harder to notice if the lower portion of the emulsion is not as well developed as the upper portion. The limits of cut-off were different in different regions of the plates, depending on the local conditions of distortion, development etc.. For a given area, of the order of a few square millimeters, these limits were the same through out that area.

1.8.4 Classification of tracks

A charged particle track is classified as black, grey or minimum according to its grain density g. The grain density g_o of a minimum track in a well-developed plate is about 25 grains/100 um. This value shows a slight variation with depth in the emulsion due to the non-uniformity in development. Based on g_o , the classification of tracks is as follows:

1) Black tracks: Blacks tracks are produced by low energy particles,resulting from the evaporation of the struck nucleus. They have a grain density which is greater than

4 g_o . This corresponds to protons of energies up to 75 MeV and pions of energies up to 12 MeV. Stopping particles of unit charge are easy to recognize from the scattering at the end of the track, although deuterons and tritons cannnot be separated from protons without performing scattering measurements.

2) Grey tracks: In this work grey tracks are tracks with $4\ g_o \geq g > 1.4\ g_o$ and are frequently associated with protons of energy between 75 MeV and 400 MeV, or pions of energy between 12 MeV and 60 MeV.

3) Shower tracks: The grain density of a shower track is to be $g \leq 1.4\ g_o$ and corresponds to proton and pion energies in excess of 400 MeV and 60 MeV, respectively.

1.8.5 Measurement of the number of slow particles

The field of view was divided into 4 quadrants (with the aid of a graticule placed in one of the oculars) and the number of black and grey tracks in each quadrant were counted. The number of heavy tracks N_h is the sum of the black tracks N_b and the grey tracks N_g . For events with a great number of tracks, the counting was performed by making a rough drawing of the star, in order to avoid counting the same track twice. The division of tracks into black and grey was done by eye. Difficulties in the

classification of the tracks were due to the non-uniform development of the emulsion with depth and the large dip angles of the tracks under consideration. The grain density of a track going into or out of the emulsion can be corrected if the shrinkage factor and the approximate dip angle of the track are known. One also has to account for the variation of grain density with depth. Fortunately, in the vertically exposed plates, the majority of the black and grey tracks have small dip angles and are fairly easy to classify.

1.8.6 Measurement of the number of shower particles

The method used in counting the number of shower particles is the same as that used in counting the black and grey tracks. The severe limits of cut-off in depth ensured that the grain density of tracks is reasonably uniform in the area used. Grain count was performed only in doubtful cases.

1.8.7 Measurement of angles

The distortions in some regions of the plate selected for our study at 200 GeV, were very low and the primary protons were perpendicular to the emulsion surface with a slope that was not more than 6'. To measure the angles of the charged shower particles from a proton-nuclear

encounter, the following procedure was adopted. One of the oculars contained a graticule with a scale inscribed on its surface, and this scale was calibrated against a stage micrometer. The other ocular contained a protractcr-graticule that was used to measure the azimuthal angles of the shower particles. For the measurement of angles, a 53x oil objective was used at both energies.

The space angle of each shower particle was determined by noting a) the height 'h' of the event from the bottom surface of the emulsion as measured by the z micrometer and b) the projected length of the track of the shower particle from the centre of the star to the point where it left the emulsion, as measured by the calibrated scale in the ocular. The real height of the event, i.e. the height of the event in unprocessed emulsion, is given by $h.s$, where s is the shrinkage factor.

The shower particles from most of the events are in a very forward cone and leave the emulsion in the field of view. The space angle of any particle, that leaves the field of view before leaving the emulsion, was determined by measuring the height of the star from the plane where the particle disappeared from the field of view to the point of interaction, and the projected length of the

particle track on this plane. Since the objective used introduced distortions at the edge of the field of view, a shower particle was considered to be out of the field of view as it reached the distorted region.

This simple method of measuring angles could not be used with the plates exposed to the 300 GeV proton beam, due to the distortions introduced during processing these plates. To overcome this difficulty, instead of a pair of 10x oculars, a pair of Leitz Wetzlar 12x oculars equipped with screw micrometer eypieces was used. The rotation of the micrometer screw caused a straight wire to move across a scale inside the oculars. With the aid of these oculars an x-y coordinate system was superimposed on the field of view. The height of the star was measured from the top of the emulsion surface (the proton beam entered the emulsion from the lower surface of the plate) and the x,y coordinates of the event and each of the shower particles were obtained. Corrections to the angles were made by measuring the slopes of a few primary tracks near the event, in the same vertical distance as that traversed by the shower particles.

The two types of angular measurements are illustrated in figure 1.2.

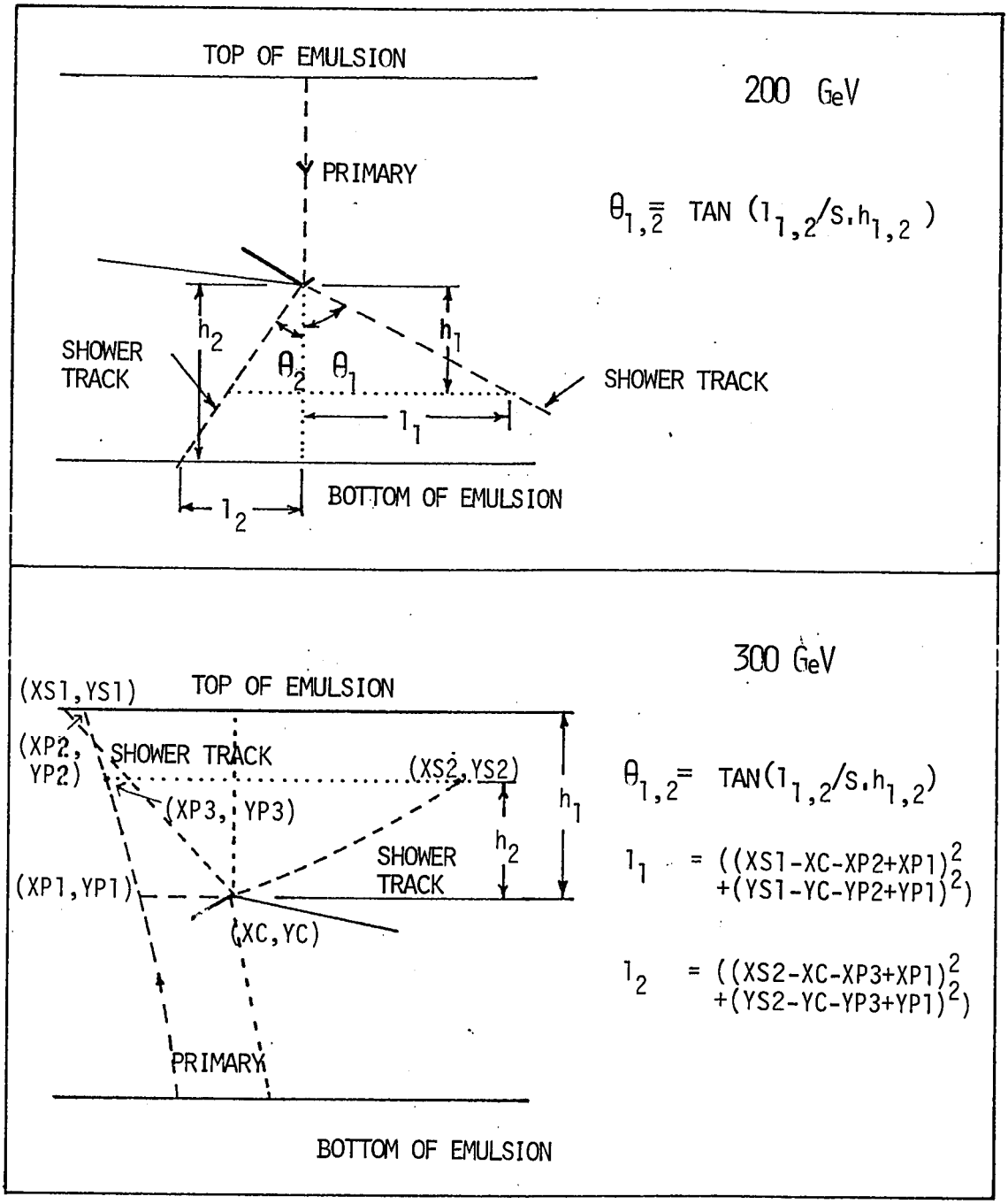

FIGURE 1.2 MEASUREMENT OF ANGLES

1.9 SCANNING AND MEASUREMENT IN HORIZONTALLY EXPOSED PLATES

1.9.1 Flux measurement

The flux of protons entering a horizontally exposed plate is obtained by counting the number of primary tracks that enter a given area of the emulsion.

1.9.2 Scanning

There are two ways of scanning for events in horizontally exposed plates; area scanning and along-the-track scanning. In the former method, one selects an area in the emulsion and scans that area systematically. This technique cannot be relied on to yield an unbiased sample of events. Since the secondaries produced in most events, especially those with a small number of slow particle, are strongly collimated in the forward direction, events with a very small number of charged shower particles escape detection. Moreover, events produced by secondary particles, whose slopes cannot be differentiated from those of the primaries by eye, would be confused with genuine events. For these reasons, the slower but more reliable along-the-track scanning technique is used by most experimenters.

In the along-the-track scanning method, one starts at

the edge of the plate where the beam enters, selects the primaries to be followed (by measuring the divergence of the beam, the dip angles of the tracks etc.) and then follows each primary until either an interaction is observed or up to a pre-determined length of track.

1.9.3 Counting of tracks

The method used for counting the number of slow particles was the same as that described for the vertical exposure. However, in horizontally exposed plates, the method of counting shower tracks is different since the geometry of the event is different. The counting was performed at a short distance from the centre of the event to ensure that the tracks are well separated. In all cases, diagrams of the stars were drawn.

1.9.4 Measurement of angles

Two plates that were exposed to 300 GeV protons were scanned in Ottawa by this method using a Leitz microscope equipped with a 32x air objective and a pair of 10x oculars. After the scanning was completed, the 32x air objective was replaced by a 53x oil objective, in order to measure the angles of the secondaries. One of the oculars was fitted with a calibrated scale, while the other contained a protractor-graticule. The dip angle of each

shower particle was measured at a distance of 100 um, and in some cases at 50 um or 200 um, from the centre of the event. The azimuthal angle of the shower track was measured using the protractor-graticule or when this angle was small, by fixing the x and y coordinates of the track with respect to the centre of the event. From the dip angle and the azimuthal angle of each secondary, its space angle was obtained.

1.10 COMPARISON OF TECHNIQUES

The efficiency of detection of events by along-the-track scanning is very high even for those events with low N_h and low n_s. However, events with $N_h = 0$ and $n_s = 1$ were only found by experienced scanners. Delta rays and lepton pairs produced directly by the incoming primaries appear similar to genuine 2-prong and 3-prong events having no nuclear fragmentation, nuclear recoil or electron track at the origin. In horizontally exposed plates, one can (in principle) follow the secondary tracks for long distances and establish the nature of the secondaries.

In vertically exposed plates, the beam flux can be higher than in horizontally exposed plates without introducing confusion of shower particles with primary protons near the event. The distance over which the

multiplicity is counted, is normally greater than 150 um and due to the shrinkage of the emulsion after processing, the forward cone appears to be wider by a factor 2, which is an advantage in counting shower multiplicities. In horizontally exposed plates, on the other hand, the same shrinkage of the emulsion makes the cone flatter in the z direction. In vertically exposed plates, the angles of the shower particles can be measured without having to change the field of view, thus minimizing the errors that could be introduced. But the measurement of angles greater than 85° is less precise, unless the field of view is changed and the track is followed over a longer distance.

1.11 EFFICIENCIES

In this section the efficiencies of scanning and measurements made in the vertically exposed plates are presented.

1.11.1 Scanning

Before going into the discussion of scanning efficiency, it is convenient to introduce the terminology commonly used in describing events in emulsion.

A proton-nucleus interaction is referred to as a star or an event. A 'clean' star does not have a nuclear

recoil or an electron track at the origin. The term 'dirty' star refers to an event with either a nuclear recoil, an electron track or both at the centre of the event. Stars with no black or grey tracks are called 'white' stars. Events with N_h=0,1 are also called 'quasi-nucleon' events. Stars with 'n' shower particles are sometimes referred to as n-prong events.

The efficiency of detecting events in vertically exposed plates depends on many factors, the most important being the experience of the scanner. The other factors are: the number of slow particles, the number of fast particles and their angles of emission. In the case of events with N_h <2, the more numerous the shower particles, the greater the chance of detecting the event. Among the N_h <2 low n_s events, the stars in which the secondaries are emitted at small angles are easier to observe than those where the secondaries are emitted at large angles.

In Table 1.3 results of scanning a particular area in a plate exposed to 300 GeV protons is presented. Scan 1 was performed by the author and scan 2 was performed by Mrs. V. Dandapani.

Table 1.3

Efficiency of Scanning

N_h group	Number of events observed	
	Scan 1	Scan 2
0	16	10
1	11	8
2	8	9
>3	65	65

The results indicate that the scanning efficiency is close to 100% except for the events with $N_h<2$.

Some of the events in the $N_h= 0$ group are not only difficult to detect, but are also difficult to interpret. These are clean white stars with $n_s =1,2$ or 3. No clean stars with $n_s =1$ were observed in the areas scanned at either energy. The contribution of these events to the proton-nucleus inelastic cross-section is expected to be small.[23] Some events with $n_s =2$ were observed, but these can easily be attributed to high energy delta ray production by the incident protons. The mean free path, in emulsion, for the production of delta rays with energies in excess of 50 MeV can be calculated to be close to 2.5 meters. (See Appendix 2). These events were considered to be genuine inelastic interactions only if the final particle trajectories showed appreciable

deviation from the incident particle direction and if the tracks did not show multiple scattering characteristic of a low energy electron.

Clean inelastic events with $n_s = 3$ may be confused with e^+ e^- materialization coincident with the beam tracks, lepton pairs directly produced by the incident protons or, as in the case of $n_s = 1$ events, coherent interactions between beam protons and target nuclei. A rough calculation using Bhabha's theory yields a mean free path for direct electron pair production, (with sufficient pair energies to be mistaken for genuine events), which is compatible with the number of events observed. (See Appendix 2). If there is an observable deviation of the primary track, the event can not be interpreted as pair production. In all such cases, the criterion $\sum_{i=1}^{n_s} \sin\theta_i \leqslant 0.3$ (see section 1.12.2) for coherent production was satisfied.

In Table 1.4, the percentages of events in different N_h groups are compared with those obtained by the collaboration using along-the-track scanning. There are no significant differences between the values obtained.

Table 1.4

Percentage of events in different N_h groups

N_h group	% of events in vertical exposure		% of events in horizontal exposure	
	200 GeV	300 GeV	200 GeV	300 GeV
0- 1	25±4	24±2	28±2	28±1
2- 5	25±4	27±3	27±2	29±1
6-10	20±3	18±2	17±1	17±1
>10	30±4	31±3	28±2	26±1

1.11.2 Counting efficiencies

Results of a check on the counting of charged particle multiplicities are presented as histograms in figure 1.3. The second set of measurements (dashed histograms) were obtained while performing the angular measurements. Since each track had to be studied individually, the classification of tracks as grey or shower tracks was carried out more rigorously. Since the grey tracks are found mainly in the larger stars, this would account for the differences between the two sets of data.

1.11.3 Measurement of angles of shower particles

The efficiencies of measuring angles at 200 GeV are presented in Table 1.5. These events were remeasured

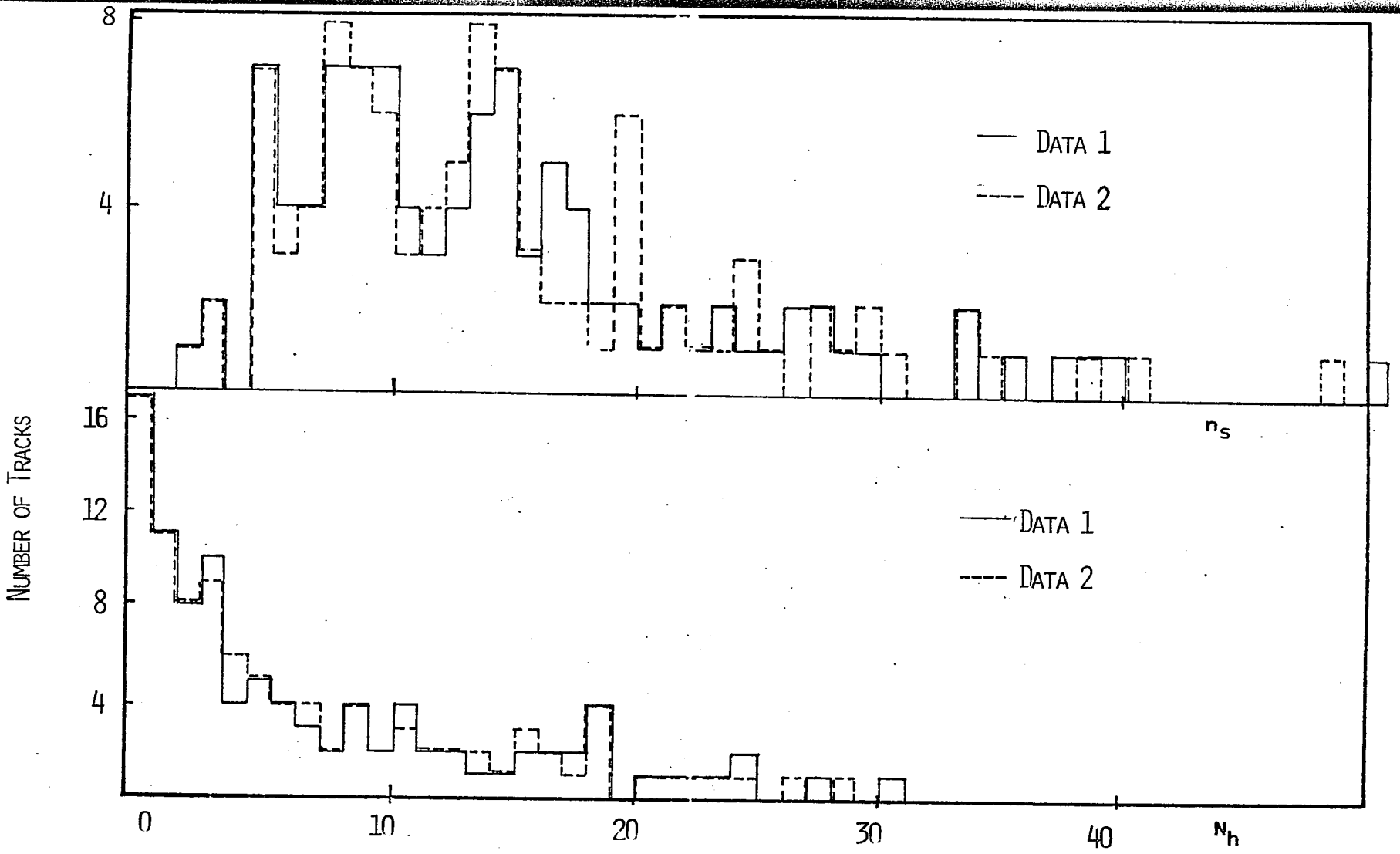

FIGURE 1.3 COUNTING EFFICIENCY

Table 1.5

Measurement of angles at 200 GeV

Trial 1	Trial 2	Error	Trial 1	Trial 2	Error
0.256	0.226	0.010	0.180	0.155	0.006
0.256	0.226	0.010	0.029	0.028	0.003
0.150	0.151	0.006	0.034	0.033	0.003
0.063	0.063	0.003	0.086	0.085	0.004
0.054	0.055	0.003	0.043	0.040	0.003
0.260	0.251	0.009	0.133	0.131	0.005
0.182	0.183	0.007	0.019	0.019	0.003
0.110	0.110	0.005	0.019	0.019	0.003
0.085	0.085	0.004	0.119	0.108	0.005
0.060	0.042	0.003	0.050	0.050	0.003
0.075	0.070	0.004	0.728	0.739	0.089
0.014	0.014	0.002	0.312	0.307	0.018
0.092	0.092	0.004	0.329	0.317	0.019
0.027	0.024	0.002	1.065	1.055	0.183
0.572	0.589	0.058	0.477	0.502	0.042
0.320	0.315	0.025	0.309	0.303	0.013
1.150	1.500	0.335	0.297	0.286	0.016
0.333	0.324	0.025	0.380	0.375	0.022
0.357	0.355	0.031	0.290	0.281	0.015
0.323	-	0.026	0.261	0.260	0.013

All angles are in radians.
- track not found.
The errors are based on errors in measurement.

Table 1.6

Measurement of angles at 300 GeV

Trial 1	Trial 2	Error	Trial 1	Trial 2	Error
0.015	0.016	0.001	0.001	0.0004	0.002
0.006	0.008	0.001	0.014	0.014	0.002
0.004	0.004	0.001	0.013	0.014	0.001
0.003	0.002	0.001	0.114	0.115	0.006
0.066	0.067	0.003	0.136	0.133	0.006
0.017	0.016	0.001	0.113	0.112	0.005
0.027	0.025	0.001	0.038	0.040	0.003
0.039	0.038	0.002	0.190	0.191	0.010
0.038	0.043	0.002	0.136	0.136	0.006
0.038	0.034	0.002	0.226	0.224	0.010
0.071	0.066	0.003	0.396	0.414	0.028
0.042	0.039	0.002	0.266	0.283	0.015
0.052	0.052	0.002	0.178	0.188	0.010
0.151	0.157	0.006	0.169	0.172	0.008
0.168	0.177	0.007			
0.096	0.100	0.004			
0.512	0.568	0.107			
0.643	0.655	0.065			
0.344	0.355	0.253			
0.364	0.369	0.029			
0.141	-	0.006			
-	0.104	0.004			

All angles are in radians.
- track not found

The errors are based on errors in measurement.

accidentally, without any intention of checking the accuracies of the measurements. The results of remeasuring angles at 300 GeV are presented in Table 1.6. This time a check on accuracy was intended. Correspondence between tracks was made by a knowledge of their approximate azimuthal angles.

The errors are based on reading errors only. The errors do seem to be overestimated, since in the majority of cases, the difference between the two measurements is much smaller than the estimated error.

1.12 CLASSIFICATION OF STARS

1.12.1 Events belonging to light and heavy groups

It is convenient to consider emulsion as consisting of hydrogen, a light group of elements (C,N,O) and a heavy group of elements (Ag,Br). It would be worthwhile to try to separate the events into groups in order to study the dependence of the average charged shower multiplicity and the angular distribution of the shower particles on the mass of the target nucleus.

The guideline for classification of events is the number of slow particles from the target nucleus. Though a complete break up of an oxygen nucleus can give eight

slow charged particles, Lohrman and Teucher[24] report that in experiments done with pure gelatine no events with $N_h > 6$ were recorded. Nearly 45% of the observed events, at both energies, have $N_h > 6$ and thus can be readily classified under 'heavy group'. Since 70% of the total number of events in emulsion are expected to be due to proton heavy-nucleus encounters, this means that 45% of the remaining events must also belong to the heavy group. Also, according to Lohrman and Teucher, 94% of the interactions in gelatine have atleast one black track of range less than 65 um. This was used as the criterion to identify the events belonging to the light group. A similar criterion was employed by the Soviet group.[31] In the present analysis, in ambiguous cases, nuclear recoils were also considered. In some small events ($N_h < 4$), the observation of a very short ($\approx$2 um) recoil was considered to be an indication that the star belonged to the 'heavy group'. The same criterion was extended to stars with $N_h = 0$. Proton-proton events were removed from 'clean' $N_h = 0, 1$ events by making use of the bubble chamber data[27,28] at both incident energies.

1.12.2 Coherent events

Consider a hadron-nucleus interaction, where the momentum transfer to the nucleus is small. In such cases,

the nucleus takes part in the interaction as a single body and its internal structure is of no importance in the description of the production process. The nucleus acts coherently and the production process is external to it.

Coherent production is characterized by a) the absence of break up or even excitation of the target nucleus, b) the narrowness of the angular distribution of the secondaries produced and c) the conservation of quantum numbers of the initial and final states.

The first two characteristics of coherent production process are easily observable in nuclear emulsions. The excellent spatial resolution of the detector makes the observation of small recoils (≈ 2 um) and measurements of small angles (≈ 1 mrad) possible.

The small momentum transfer involved in a coherent process demands that $\sum_{i=1}^{n_s} \sin\theta_i \leq 0.3$.[25] Clean $N_h = 0$ events with odd number of shower particles are possible coherent events. Some of the incoherently produced events also satisfy the restriction on angular distribution. Thus a correction for the background could be made and the true number of coherently produced events can be estimated.

Chapter 2

EXPERIMENTAL RESULTS

2.1 INTRODUCTION

In this chapter, the experimental data on proton-nucleus interactions at 200 GeV and 300 GeV are presented. Unless specified, the results refer to the work done in the vertically exposed stacks, which were studied exclusively in Ottawa. The data are compared and in some cases combined with the results of the rest of the collaboration. The latter results were obtained by scanning stacks that were irradiated with the beam direction parallel to the surface of the emulsion. Due to the difference in the degree of development of vertically and horizontally exposed stacks, the counting efficiencies for the two types of exposure are not the same. No attempt has been made to account for this factor.

2.2 INELASTIC MEAN-FREE-PATH

The effective track length followed was computed from the dimensions of the regions scanned, the flux of protons and the limits of cut-off applied for that region. No

corrections for scanning efficiency were made, nor were probable coherent events with n_s=3,5 or 7, excluded. The measured values of the inelastic mean-free-path are presented in Table 2.1 and are compared with those obtained by along-the-track scanning. The errors are based on the number of observed events. Results obtained by the two scanning techniques are in agreement within the limits of statistical errors. The value of the inelastic mean-free-path from the combined results is 35.0 $\pm$ 0.8 cm at 200 GeV and 34.9 $\pm$ 0.7 at 300 GeV. As expected, the mean-free-path remains constant in this energy region.

2.3 DISTRIBUTION OF SLOW PARTICLES

The distribution of black tracks observed at 200 GeV and 300 GeV are shown in figure 2.1. In figure 2.2, the corresponding distributions of grey tracks are plotted. The average number of black tracks ($\langle N_b \rangle$) in vertically exposed plates are 5.9 $\pm$ 0.4 at 200 GeV and 6.1 $\pm$ 0.3 at 300 GeV, with corresponding values of 1.7 $\pm$ 0.2 and 1.7 $\pm$ 0.1 for the average number of grey tracks ($\langle N_g \rangle$). Insofar as the slow particles are concerned there does not appear to be any difference between the stars produced at 200 GeV and 300 GeV.

The combined distributions of slow (black and grey

Table 2.1

Inelastic mean-free-path

Incident energy in GeV	Type of exposure	Length of track in meters	No. of events	Mean free path in centimeters
200	vertical	55.48	166	33.4 ± 2.6
200	horizontal	564.01	1605	35.1 ± 0.9
300	vertical	134.00	388	34.6 ± 1.8
300	horizontal	708.18	2025	35.0 ± 0.8

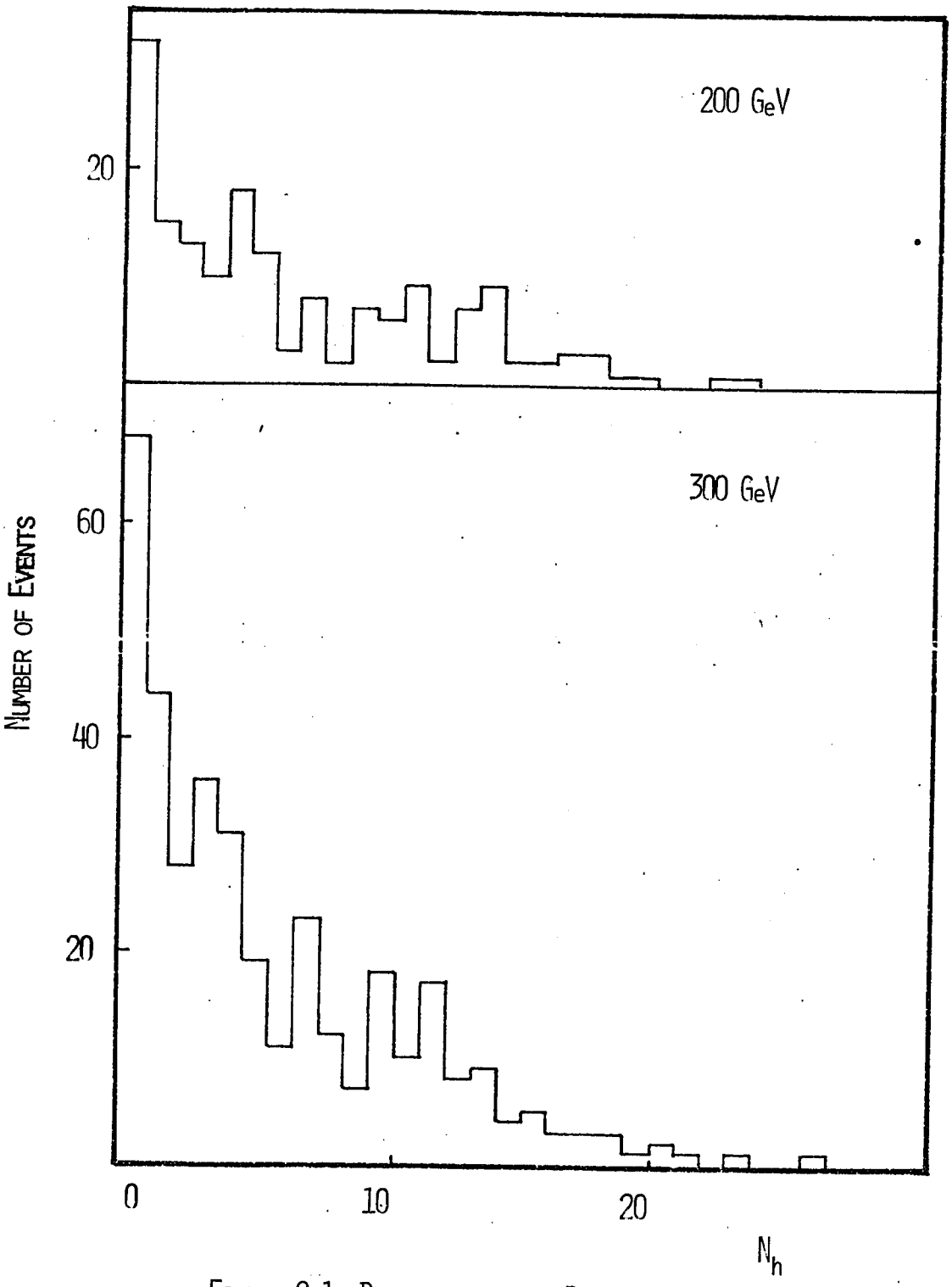

FIGURE 2.1 DISTRIBUTION OF BLACK TRACKS

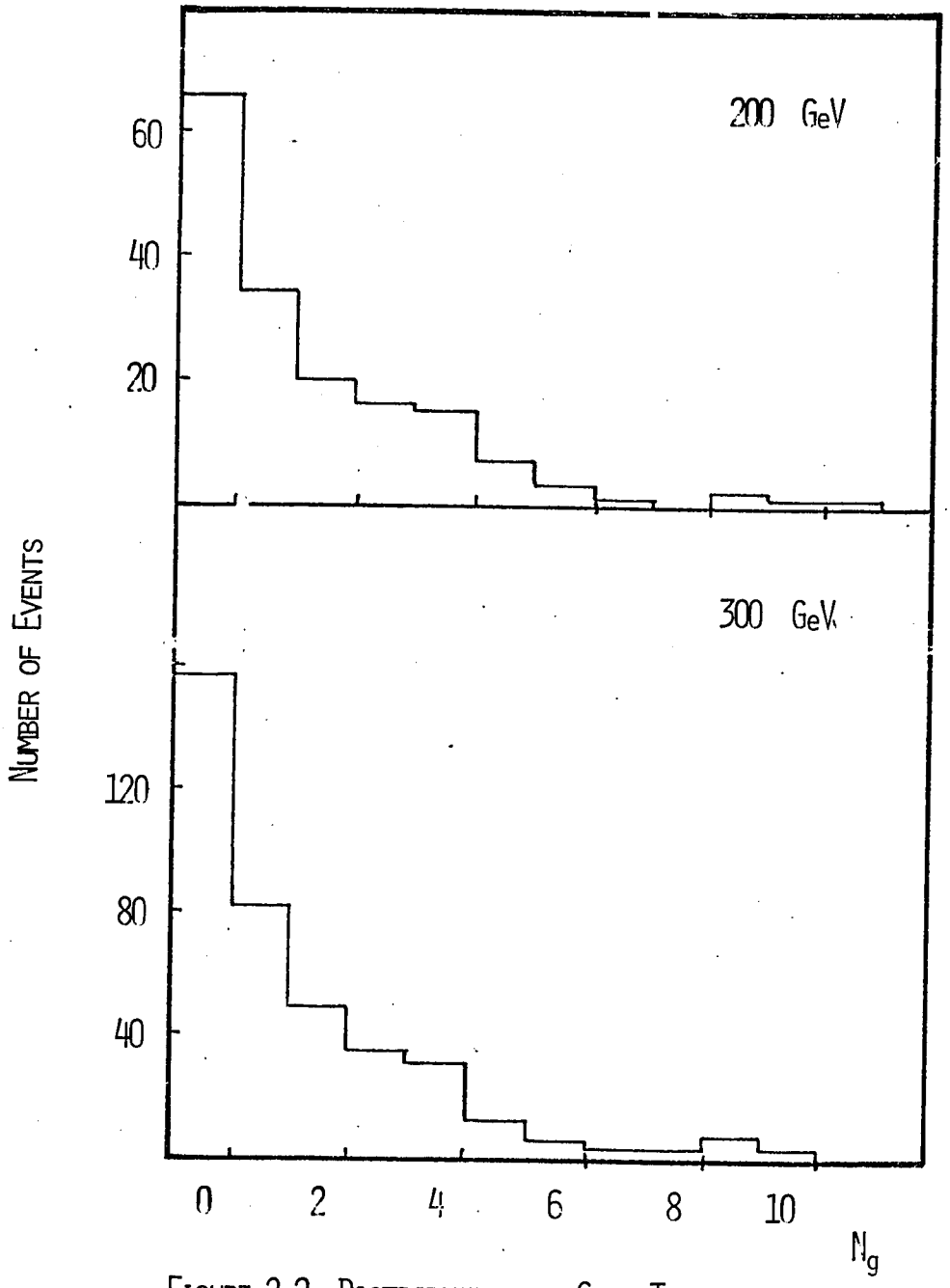

FIGURE 2.2 DISTRIBUTION OF GREY TRACKS

tracks) are shown in figure 2.3. The dotted histograms are obtained by combining our results with the results from the rest of our collaboration. The average numbers of slow particles ($\langle N_h \rangle$) are 7.6 ± 0.6 at 200 GeV and 7.8 ± 0.4 at 300 GeV. For the entire collaboration, these values are 7.6 ± 0.2 and 7.1 ± 0.1 respectively. The difference between the two results at 300 GeV could be attributed to the under-development of some of the plates used by our collaboration.

2.4 DISTRIBUTION OF SHOWER PARTICLES

The distribution of shower particles are presented in figure 2.4. The average number of shower particles ($\langle n_s \rangle$) are 13.4 ± 0.6 at 200 GeV and 15.2 ± 0.4 at 300 GeV. The dotted histograms correspond to the results of the entire collaboration. For these data, the values of $\langle n_s \rangle$ are 13.2 ± 0.2 at 200 GeV and 15.1 ± 0.2 at 300 GeV. As expected, there is an increase in the average number of shower particles from 200 GeV to 300 GeV. $\langle n_s \rangle$ may be described by the empirical relation $\langle n_s \rangle = 1.85\ s^{1/3}$, where s is the square of the centre-of-momentum energy in nucleon-nucleon collisions.

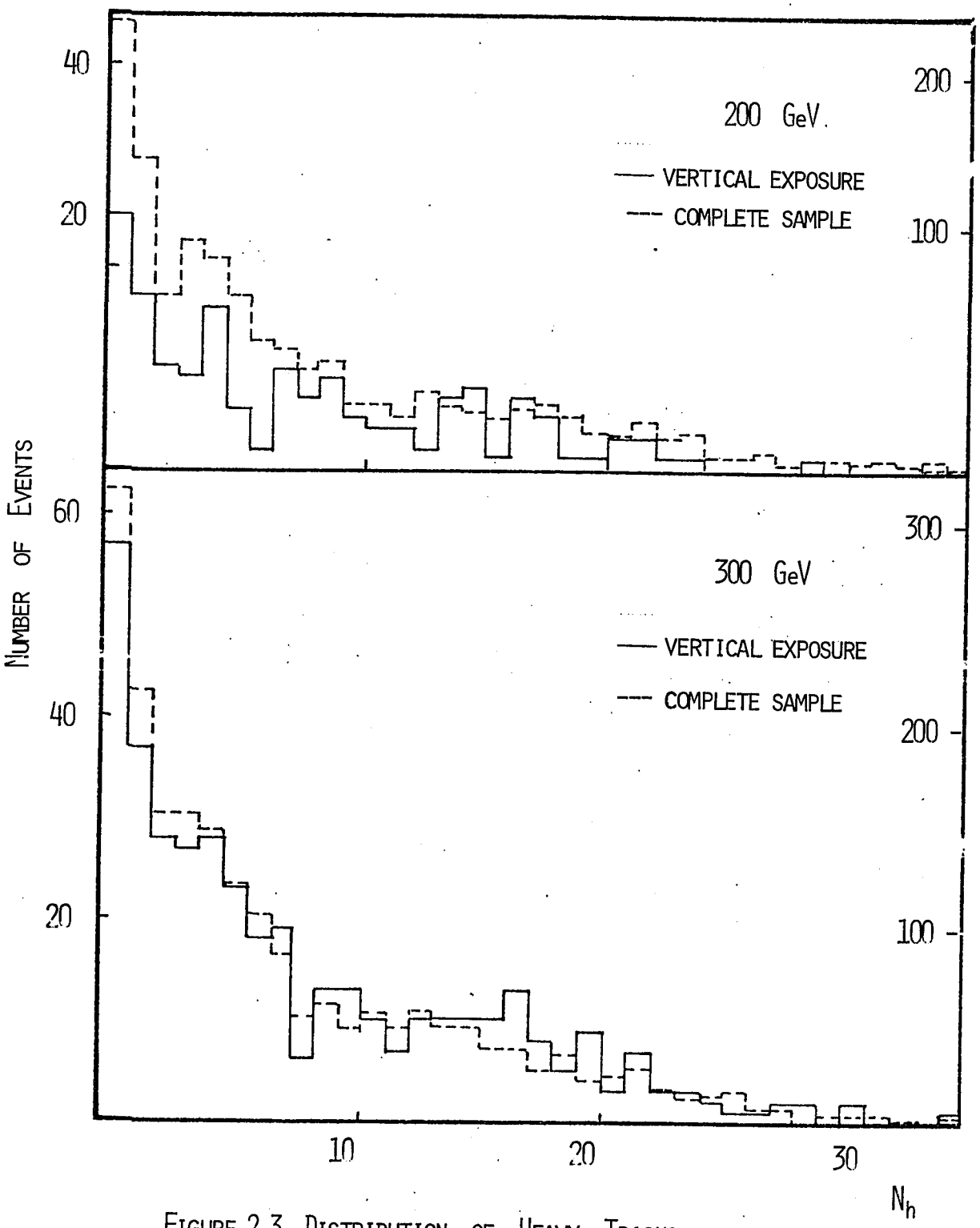

FIGURE 2.3 DISTRIBUTION OF HEAVY TRACKS

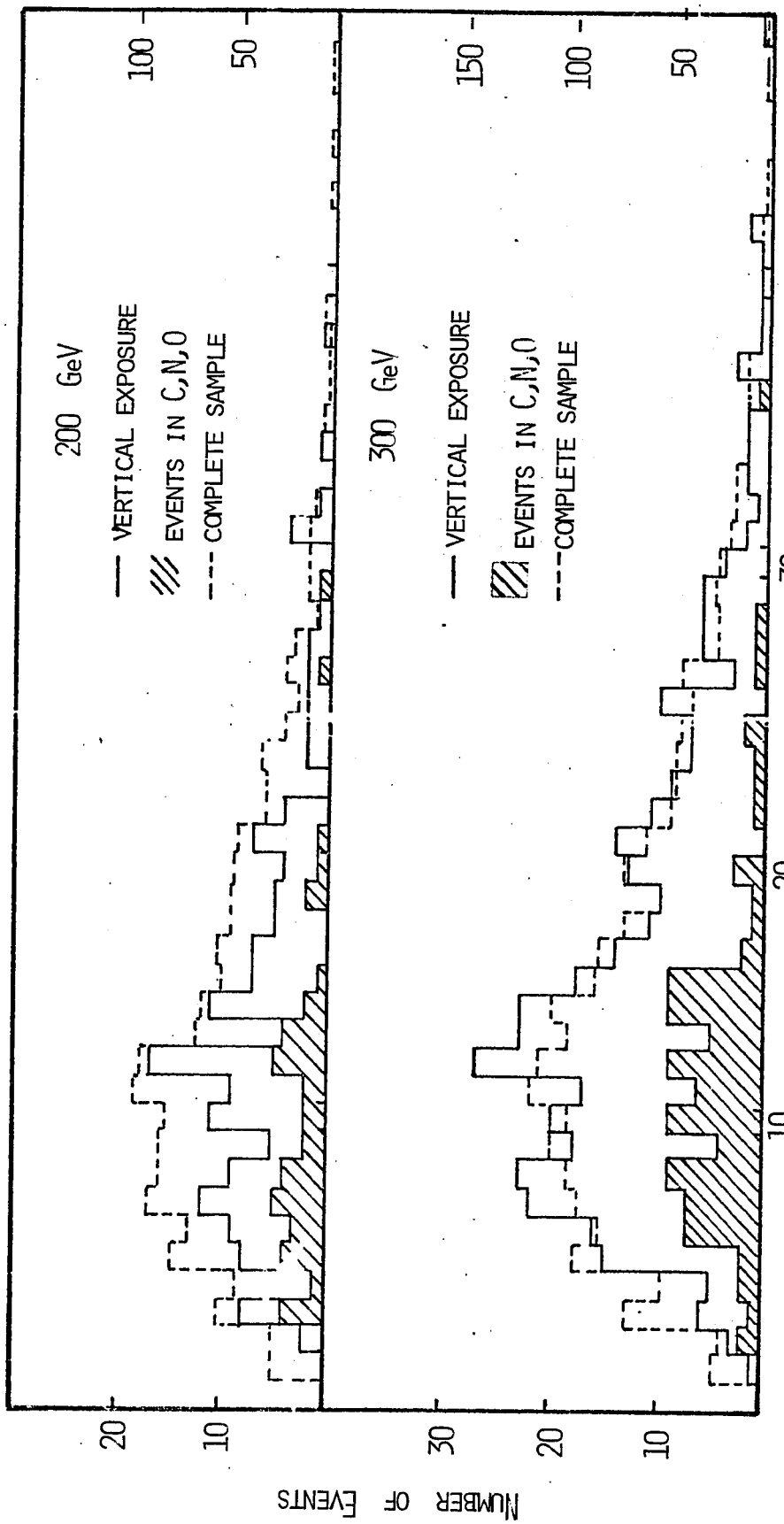

FIGURE 2.4 DISTRIBUTION OF SHOWER TRACKS

2.5 DISPERSION OF SHOWER PARTICLE DISTRIBUTION

The dispersion of the shower particle distribution is given by

$$D^2 = \langle n_s^2 \rangle - \langle n_s \rangle^2$$

The values of dispersion obtained are 7.4 ± 0.3 at 200 GeV and 8.3 ± 0.2 at 300 GeV, for the vertical exposure. For the complete sample, these values are 7.8 ± 0.2 and 9.0 ± 0.2 respectively. The larger dispersions of the complete data are to be expected, since all the scanners are not equally efficient in counting. This results in the distribution becoming broader than the distribution for a single sample.

The dispersion of the shower particle distribution is a quantity of considerable interest. The relationship that exists between D and $\langle n_s \rangle$ and its relevance to scaling of the multiplicity distribution are discussed in the next chapter.

2.6 RELATIONSHIP BETWEEN $\langle N_h \rangle$ AND $\langle n_s \rangle$

In order to bring out the relationship between $\langle N_h \rangle$ and $\langle n_s \rangle$, the complete data at 200 GeV and 300 GeV are separately divided into a number of N_h groups. The groups considered are N_h =0, 1, 2-3, 4-5, 6-7, 8-9, 10-12, 13-15, 16-18, 19-22 and >22. For each N_h group the average number of

shower particles was computed. Plots of $\langle n_s \rangle$ vs. $\langle N_h \rangle$ are displayed in figure 2.5. The resulting linear relationship can be represented by

$$\langle n_s \rangle = a + b \langle N_h \rangle$$

with $a = 9.5 \pm 1.3$ and 10.7 ± 0.8 and $b = 0.52 \pm 0.13$ and 0.63 ± 0.08 at 200 GeV and 300 GeV respectively.

The values of dispersions for the groups considered are presented in Table 2.2 along with the average number of shower particles for each group. In the same table values of $D/\langle n_s \rangle$ for the groups considered are listed. Within the limits of experimental errors, this ratio is constant for majority of the groups. However, at high values of N_h, this ratio appears to decrease.

The constancy of $D/\langle n_s \rangle$ indicates that for a homogeneous target, this ratio should be independent of the target nucleus. In order to test this argument, we shall separate the emulsion data into two groups, viz., $N_h \leqslant 6$ and $N > 6$. As pointed out in the first chapter, events in the CNO group can only have $N_h \leqslant 6$. Hence the group $N_h \leqslant 6$ corresponds to all CNO events and some AgBr events in which the number of collisions of the incident particles in the target nucleus is comparable to those in CNO. This makes the group $N_h \leqslant 6$ homogeneous and the events behave as though they occur in a pure CNO target. The

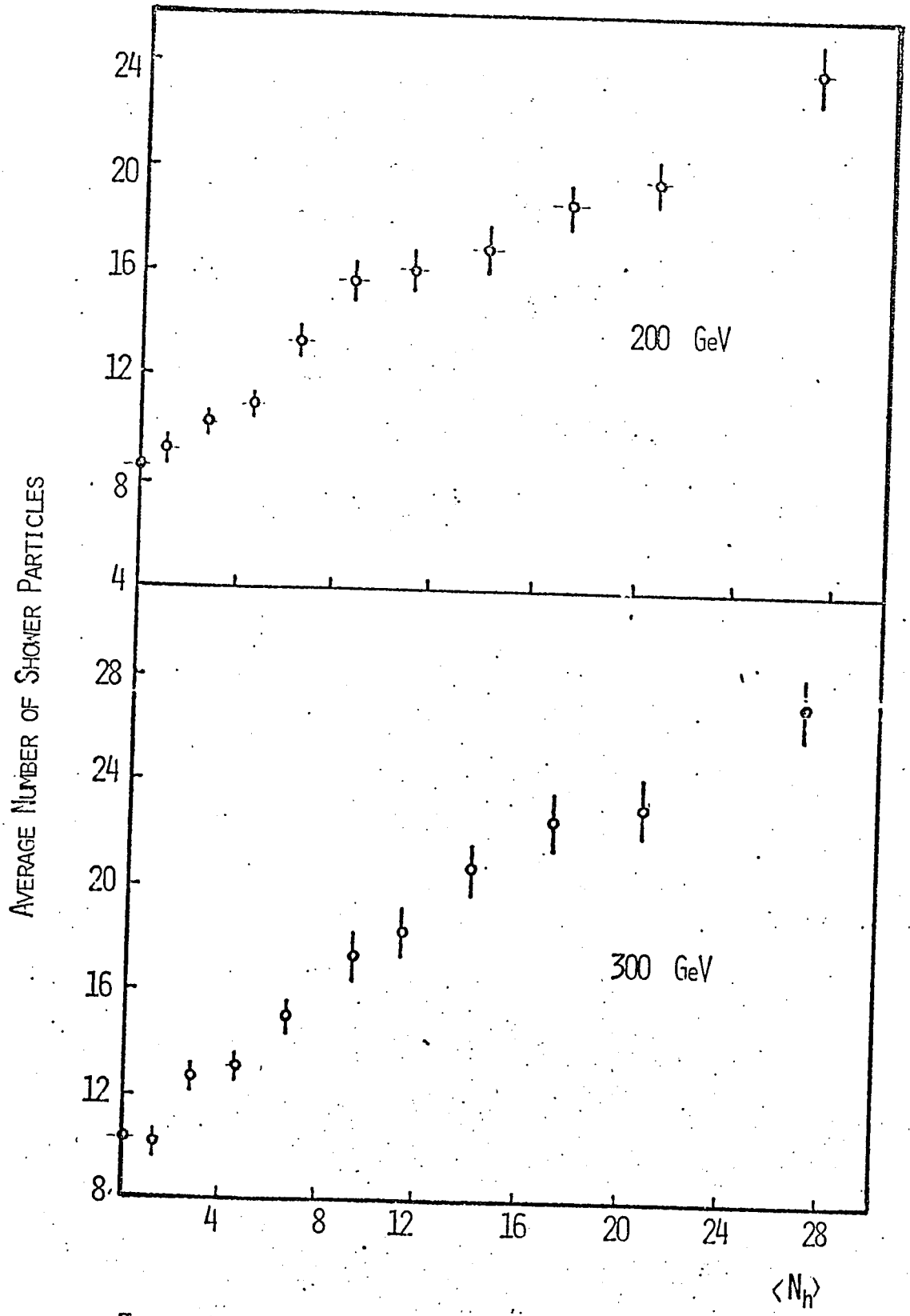

FIGURE 2.5 DEPENDENCE OF AVERAGE NUMBER OF SHOWER PARTICLES ON STAR SIZE

Table 2.2

D for various N_h groups

	200 GeV			300 GeV		
N_h	D	$\langle n_s \rangle$	$D/\langle n_s \rangle$	D	$\langle n_s \rangle$	$D/\langle n_s \rangle$
0	4.42±0.42	8.4±0.3	0.49±0.07	5.20±0.28	10.3±0.4	0.48±0.04
1	5.58±0.48	9.1±0.5	0.61±0.09	6.00±0.51	10.1±0.5	0.59±0.08
2-3	5.67±0.43	10.1±0.4	0.56±0.06	6.72±0.67	12.5±0.5	0.54±0.08
4-5	5.83±0.40	10.9±0.4	0.53±0.06	7.02±0.64	12.9±0.6	0.54±0.07
6-7	6.53±0.61	13.3±0.6	0.49±0.07	6.83±0.64	14.8±0.6	0.46±0.06
8-9	6.62±0.41	15.8±0.7	0.42±0.05	8.46±0.91	17.2±1.0	0.49±0.08
10-12	7.81±0.85	16.0±0.8	0.49±0.08	8.21±0.69	18.2±1.0	0.45±0.06
13-15	7.78±0.53	16.9±0.8	0.46±0.05	9.26±0.84	20.6±1.0	0.45±0.06
16-18	7.46±0.53	18.6±0.8	0.40±0.05	8.90±0.74	22.5±1.1	0.40±0.05
19-22	9.16±0.66	19.5±0.9	0.42±0.05	9.67±0.77	22.9±1.2	0.42±0.06
>22	9.16±0.71	23.9±1.1	0.38±0.05	9.36±0.91	26.4±1.3	0.35±0.05

angular distribution data support this argument (see section 2.10.3). The value of $D/\langle n_s \rangle$ for the $N_h \leqslant 6$ events is 0.56 ± 0.03 at 200 GeV and 0.55 ± 0.04 at 300 GeV. We can also test this conclusion by separating the emulsion data into the two constituent groups.

2.7 MULTIPLICITIES FOR THE LIGHT AND HEAVY ROUPS OF NUCLEI

The events are separated into those belonging to the light group and the heavy group, using the method discussed in the previous chapter. This separation was attempted by the group in Ottawa only.

The shower particle distributions for proton interactions with the light group, at the two incident energies, are shown as hatched distributions in figure 2.4. The values of $\langle n_s \rangle$ for the CNO group are 10.2 ± 1.0 at 200 GeV and 11.9 ±0.6 at 300 GeV. The corresponding values for the AgBr group are 14.9 ± 0.7 and 16.7 ± 0.5. The dispersions of the multiplicity distributions are

$$D_{CNO} = 5.9 \pm 0.8 \quad \text{and} \quad D_{AgBr} = 7.5 \pm 0.4$$

at 200 GeV and

$$D_{CNO} = 5.7 \pm 0.6 \quad \text{and} \quad D_{AgBr} = 8.8 \pm 0.4$$

at 300 GeV.

In table 2.3, values of $D/\langle n_s \rangle$ for CNO and AgBr

groups, along with the Chromimum (300 GeV) and Tungsten (200 GeV and 300 GeV) data of Florian et al , are presented.

Table 2.3

$D/\langle n_s \rangle$ for different nuclei

Energy in GeV	$D/\langle n_s \rangle$ CNO	AgBr	Cr	W
200	0.58 ± 0.14	0.50 ± 0.05		
300	0.48 ± 0.07	0.53 ± 0.04	0.51 ± 0.05	0.56 ± 0.04

The average numbers of heavy tracks are 2.4 ± 0.3 and 2.9 ± 0.2 for the light group and 9.9 ± 0.7 and 9.9 ± 0.5 for the heavy group at 200 GeV and 300 GeV, respectively.

2.8 EFFECT OF NUCLEAR SIZE ON MULTIPLICITY

The effect of the size of the target nucleus on particle production at high energies is usually expressed as a ratio of the average number of shower particles produced in proton-nucleus interactions to the average number of charged particles resulting from proton-proton interactions. Also, this ratio is assumed to have a simple relationship with A, the atomic weight of the target nucleus. Thus,

$$R_A = \langle n_s \rangle_{p-A} / \langle n_{ch} \rangle = A^{\alpha}$$

The value of α can be determined from the experimental data. Since emulsion is a composite target,

$$R_{em} = \sum_i p_i A^{\alpha}$$

where p_i is the probability that the incoming proton interacts with a nucleus A. The values of $\langle n_{ch} \rangle$ at 200 GeV and 300 GeV are 7.65 ± 0.16 [29] and 8.5 ± 0.12 [28] respectively. The values of R_A are given in Table 2.4.

Table 2.4

Values of R_A

Energy	R_{CNO}	R_{AgBr}	R_{em}
200 GeV	1.33 ± 0.16	1.95 ± 0.13	1.75 ± 0.12
200 GeV (*)	1.40 ± 0.09	1.92 ± 0.11	1.75 ± 0.06
300 GeV	1.40 ± 0.09	1.96 ± 0.09	1.79 ± 0.07
300 GeV (*)			1.78 ± 0.05

(*) Complete sample.

From the experimental values of R_A, the A dependence of the multiplicities can be calculated. The values of α are 0.141 ± 0.008 at 200 GeV and 0.145 ± 0.005 at 300 GeV.

2.9 COHERENT EVENTS

The number of possible coherent events observed in the vertically exposed plates is very small. This is not surprising because, the contribution from these events to the production process is only about 2%.

At 200 GeV, only one possible coherent event (n_s =7) was observed in a track length of 31.29 meters. vertically exposed plates. When corrected for background, it could be concluded that no clear coherent interaction was observed.

At 300 GeV, six possible events of this type were observed in a track length of 71.25 meters. Two of the events are 3-prong events and the rest are 5-prong events. Incoherently produced 3-prong events that satisfy the criterion for angular distribution are just as numerous as the number of possible 3-prong events, whereas only one incoherently produced 5-prong event with $\sum_{i=1}^{n_s} \sin \theta_i \leqslant 0.3$ was found. Thus, at 300 GeV three coherently produced 5-prong events were observed.

For the complete sample, the total number of coherent 3-, 5- and 7- prong events observed are 35, 2 and 1 respectively, in the case of 200 GeV exposure. The total track length was 708.18 meters. Analysis of coherent events at 300 GeV has not been completed.

2.10 ANGULAR DISTRIBUTIONS OF SHOWER PARTICLES

The angular distributions of shower particles are presented primarily in terms of the variable $U_L = -\log_{10} \tan\theta_L$ and some times in terms of the variable $\eta_L = -\ln \tan \theta_L/2$. Before presenting the results of angular measurements, the two variables U_L, and η_L are briefly discussed.

2.10.1 The U_L variable

In a nucleon-nucleon collision, if a secondary moving with a velocity β^* is emitted at an angle θ^* in the centre-of-mcmentum system, and the centre-of-momentum system is moving with a velocity β_c with respect to the laboratory system, then the emission angle of the secondary θ_L in the laboratory is related to θ^* by,

$$\tan \theta_L = \frac{1}{\gamma_c} \frac{\sin\theta^*}{\cos\theta^* + \beta_c/\beta^*}$$

From this, for $\beta_c/\beta^* = 1$,

$$\log_{10} \tan \theta_L = \log_{10} \tan \theta^*/2 - \log_{10}\gamma_c .$$

Assuming that in the centre-of-momentum system, the charged showers are emitted symmetrically with respect to 90°, we have $\langle \log_{10} \tan\theta^*/2 \rangle = 0$, giving $\langle \log_{10} \tan\theta_L \rangle = -\log_{10}\gamma_c$, which is the Castagnoli relation. Thus by measuring the angles of the charged secondaries, γ_c, the Lorentz factor

of the nucleon-nucleon centre-of-momentum system can be obtained. From this, the energy of the incident particle can be estimated.

2.10.2 The η_L variable

The relation of η_L to the longitudinal rapidity variable Y_L is discussed in a later chapter. This variable has the advantage that angles that are 90° or greater in the laboratory can be included in displaying the angular distribution of the secondaries. η_L is also called pseudo-rapidity.

An interesting discussion of the differences between η_L and y_L distributions is given by Carruthers and Minh Duong-van.[19]

2.10.3 Presentation of data

The angular distribution data are presented in two different ways. Firstly, the angular distributions for various N_h groups are examined. The groups considered are, N_h= 0-1, 2-5, 6-10 and >10. The angular distributions of shower tracks, for these groups, are plotted in figures 2.6 (200 GeV) and 2.7 (300 GeV). It can be seen from the graphs that the tendency of the distributions is to shift to higher angles as $\langle N_h \rangle$ increases. The dependence of the average value of the angular variable η_L on $\langle N_h \rangle$ is

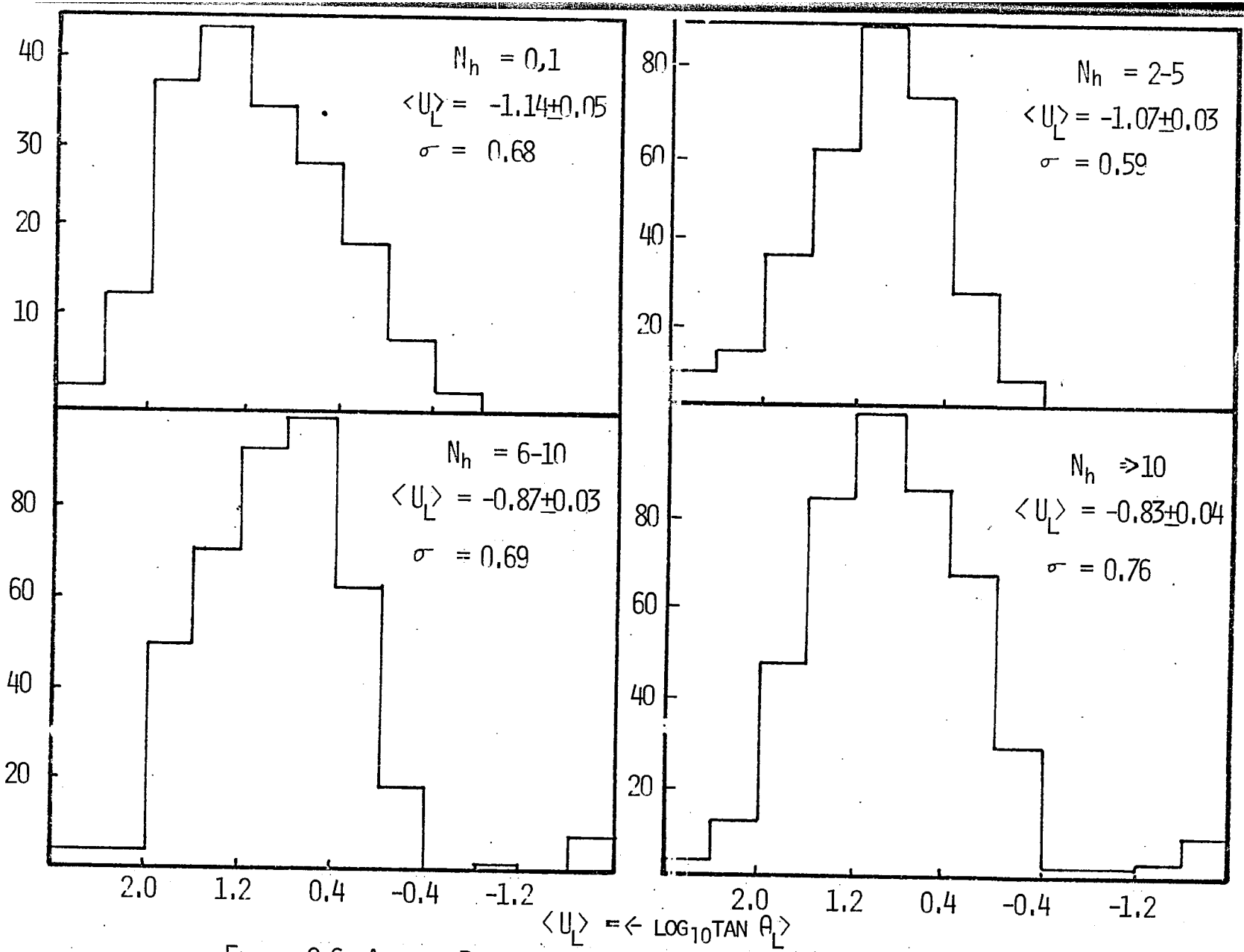

FIGURE 2.6 ANGULAR DISTRIBUTION OF SHOWER PARTICLES (200 GeV)
(FOR VARIOUS N_h GROUPS)

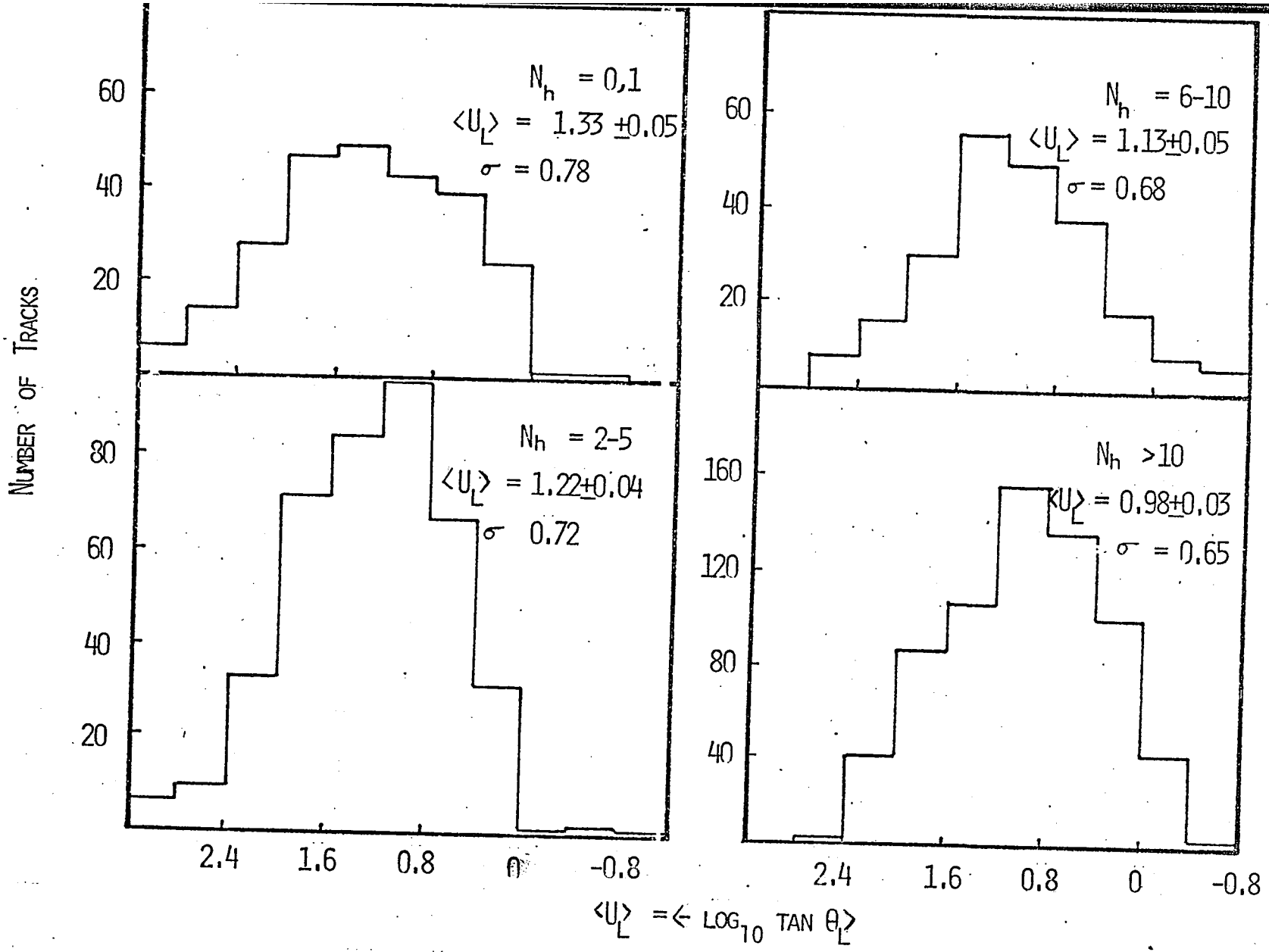

FIGURE 2.7 ANGULAR DISTRIBUTION OF SHOWER PARTICLES (300 GeV)
(FOR VARIOUS N_h GROUPS)

displayed in figure 2.8. As mentioned in the introduction, this feature of the angular distributions was used by Gibbs et al[14] in reestimating the energies of some cosmic ray primaries interacting with emulsion nuclei.

Before describing another way of presenting angular distributions, the last mentioned point will be elaborated. When applied to individual events, the energy estimation using the Castagnoli relation is not reliable. As mentioned in the beginning of this thesis, this method overestimates the incident energy by 40% when the white stars are considered. However, when the whole emulsion sample is considered, i.e., when tracks from all the events are used, the energy estimation using this relation is remarkably good. At 200 GeV, for all tracks (tracks at angles greater than or equal to 90° are excluded), $\langle \log_{10} \text{ctg}\, \theta_L \rangle = 0.97 \pm 0.02$, which gives the primary energy to be 173 (+17,-15) GeV, At 300 GeV, the value of $\langle \log_{10} \text{ctg}\, \theta_L \rangle = 1.10 \pm 0.02$, which yields a primary energy of 316 (+34, -28) GeV. Since in some cosmic ray experiments, a nearly monoenergetic beam of protons is available (from nuclear fragmentation at great energies), one can still employ the Castagnoli relation to obtain the energies of these protons, when emulsions are used as

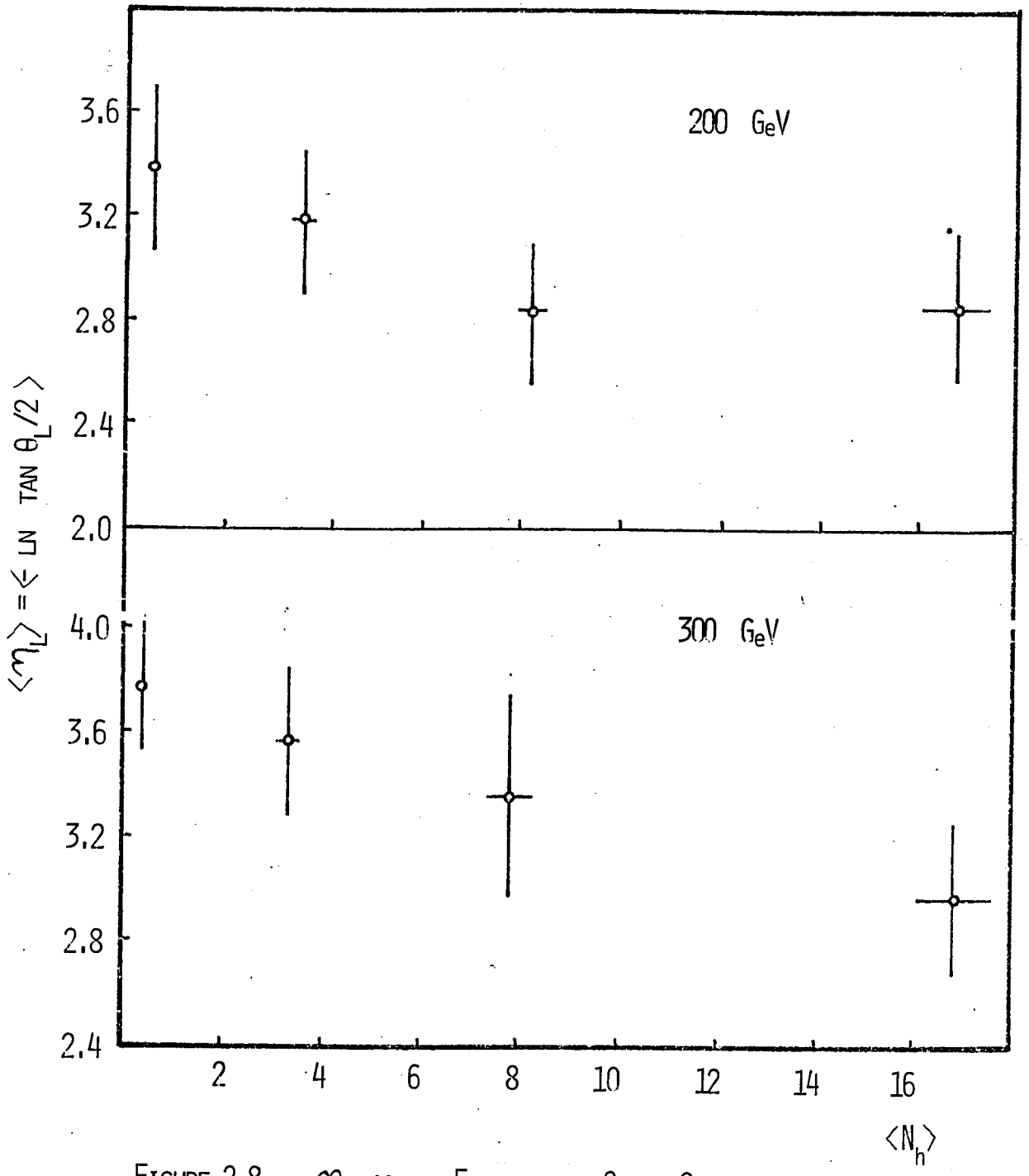

FIGURE 2.8 η_L AS A FUNCTION OF STAR SIZE

targets.

The second way of presenting the data depends on the type of target. i.e. whether the target is light (CNO) or heavy (AgBr). The heavy group is further divided into H1 group, containing events with $N_h \leq 6$ and H2 group, containing events with $N > 6$. Thus the different groups used are light, H1, H2 and heavy (H1+H2) groups. In figures 2.9 and 2.10, the angular distributions of shower particles, for these groups, are displayed. From these figures, the angular distributions for light and H1 events appear to be close to each other. This feature was also observed by the Soviet group (at 200 GeV). Since the value of $\langle N_h \rangle$ was nearly the same for the light and H1 groups, ($\langle N_h \rangle_{H1} = 1.9 \pm 0.3$ and 2.0 ± 0.2 at 200 GeV and 300 GeV respectively), this then would indicate that the angular distributions from different targets (at the same incident energy) do not particularly differ from target to target as long as $\langle N_h \rangle$ is the same.

2.11 THE COEFFICIENT OF INELASTICITY

The number of particles produced by a high energy hadron colliding with a nuclear target is much smaller than the number allowed by energy conservation. The fraction of energy spent by the incoming proton in the

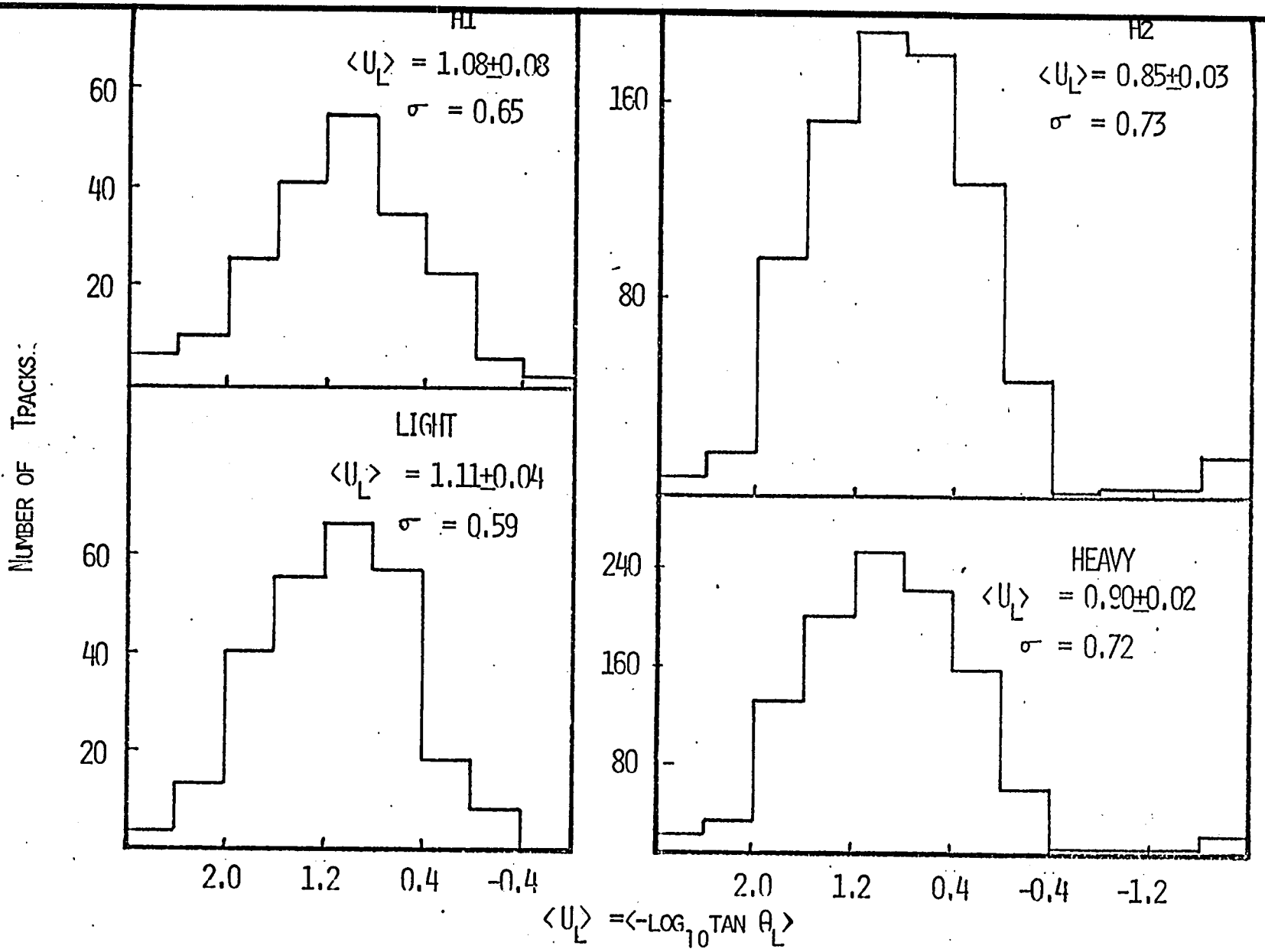

FIGURE 2.9 ANGULAR DISTRIBUTION OF SHOWER PARTICLES (200 GeV)
(FOR C,N,O AND AgBr)

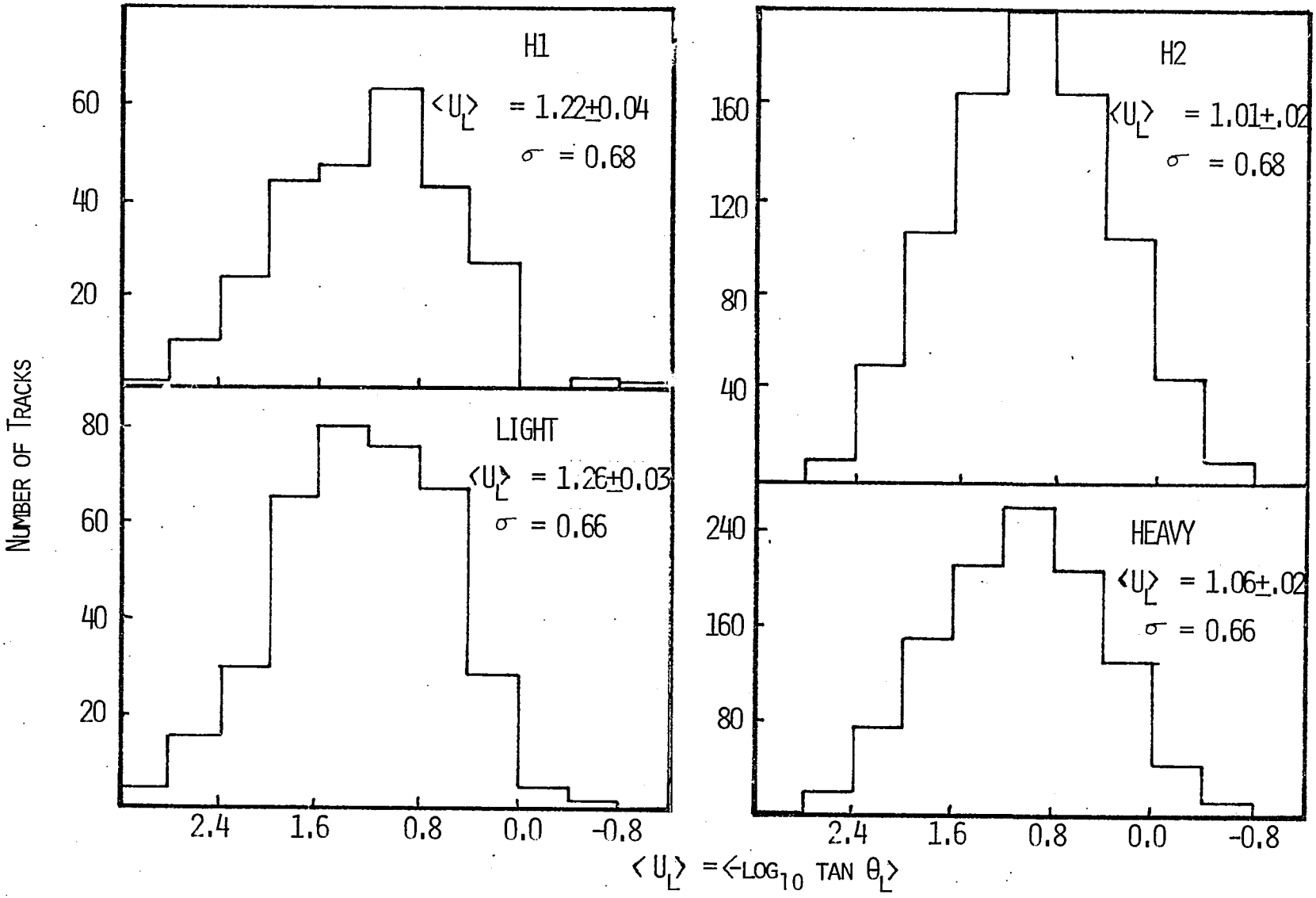

FIGURE 2.10 ANGULAR DISTRIBUTION OF SHOWER PARTICLES (300 GeV)
(FOR C,N,O AND AgBr)

production of particles is given by[30]

$$\langle K \rangle = 1.5 \langle p_t \rangle \sum_{i=2}^{n_s} \csc \theta_i / 2\gamma_c^2$$

with the inner-most track removed. The value of $\langle p_t \rangle$ was taken to be 0.35 GeV/c.

The value of $\langle K \rangle$ at 200 GeV is 0.5 ± 0.1 and its value at 300 GeV is 0.6 ± 0.1. The behaviour of $\langle K \rangle$ as a function of $\langle N_h \rangle$ is shown in figure 2.11. For the most part $\langle K \rangle$ is fairly independent of $\langle N_h \rangle$, except at small $\langle N_h \rangle$, where it has smaller values.

The values of $\langle K \rangle$ for the two different groups of nuclei, at the two energies are presented in Table 2.5. The poor statistics do not allow any definite conclusions to be drawn.

Table 2.5

Coefficient of Inelasticity

Target	200 GeV	300 GeV
CNO	0.38 ± 0.05	0.48 ± 0.06
AgBr	0.49 ± 0.03	0.48 ± 0.03

2.12 SUMMARY

In summary, the follcwing are the features of proton-nucleus interacticns at 200 GeV and 300 GeV incident

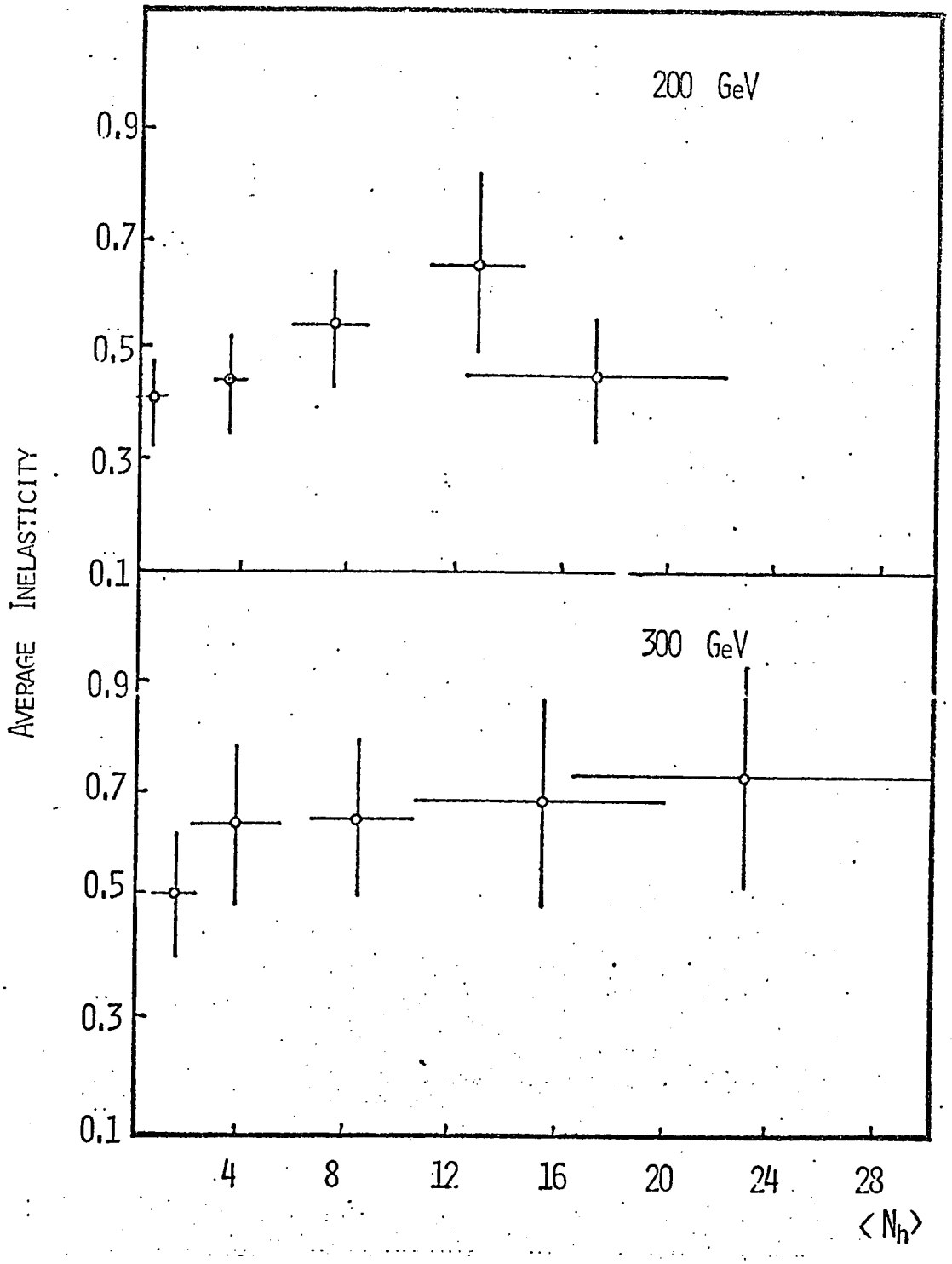

FIGURE 2.11 AVERAGE INELASTICITY AS A FUNCTION OF STAR SIZE

energies, as observed in nuclear emulsion studies.

1) The average number of fast charged particles does not show a great increase from $\langle n_s \rangle$, at the same incident energy.

2) The average number of slow tracks is practically the same at both energies. This statement is true independently for $\langle N_b \rangle$ and $\langle N_g \rangle$.

3) Comparing the normalized angular distributions (normalized to the same number of events), it can be seen that (figure 2.12) the increase in multiplicity, from 200 GeV interactions to 300 GeV interactions, is primarily in the region of small angles. In plotting these distributions, possible coherent events were excluded. In figure 2.13, the distributions of smallest angles at the two energies are compared.

4) The angular distributions, at the two incident energies, are close to being Gaussian distributions.

In Table 2.6, some of the results from the combined work of the collaboration are compared with the results obtained by other experimenters.

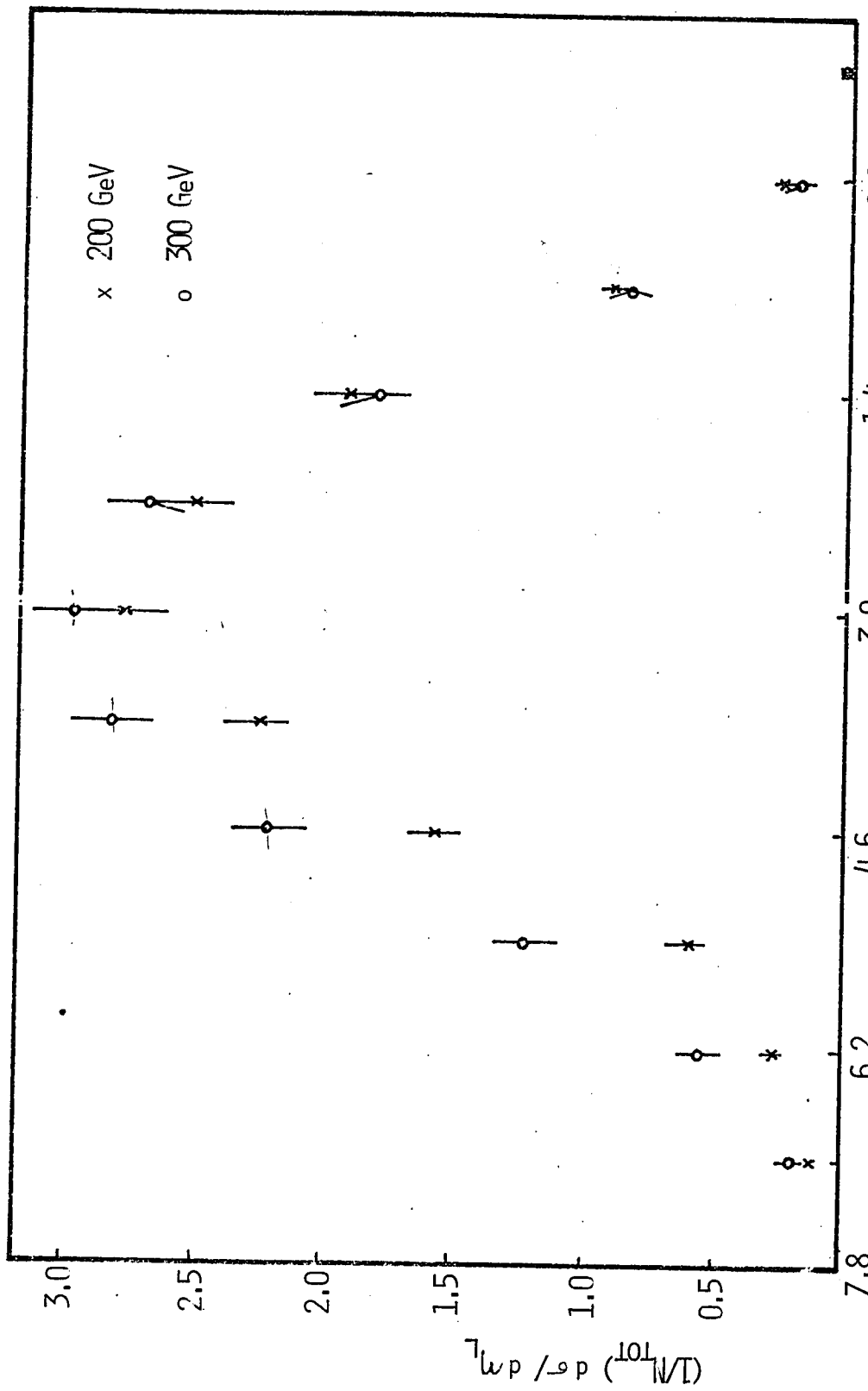

FIGURE 2.12 ANGULAR DISTRIBUTION OF SHOWER PARTICLES (200 GeV AND 300 GeV)

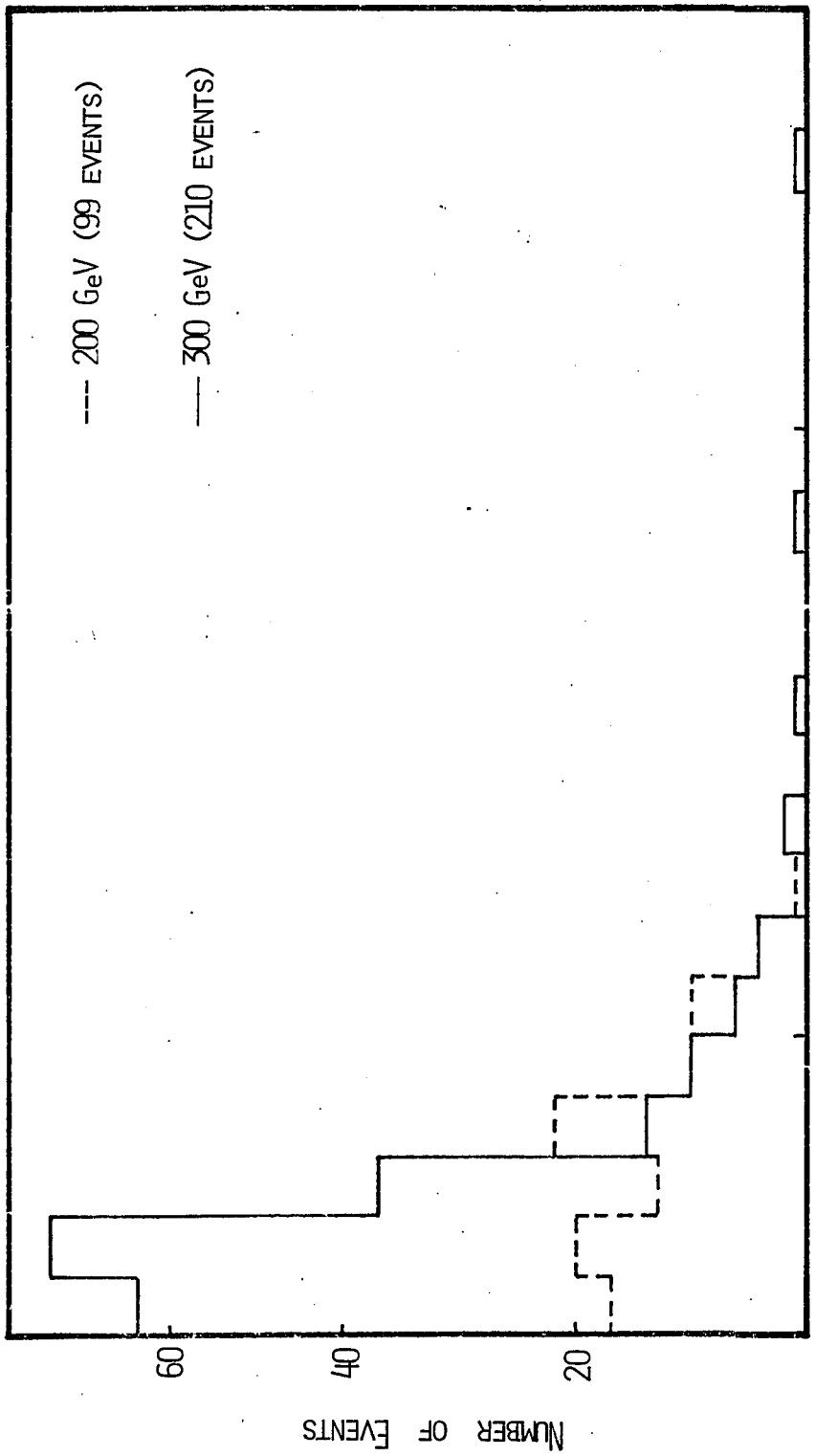

FIGURE 2.13 SMALLEST ANGLE IN LABORATORY SYSTEM (DEGREES)

Table 2.6

Comparison of results

	200 GeV			300 GeV
	This work and collaboration	Soviet group[31]	Babecki et al[2]	This work and collaboration
$\langle N_h \rangle_{em}$	7.4±0.2	7.7±0.1 7.5±0.2		7.1±0.1
$\langle N_h \rangle_{CNO}$	2.4±0.3 (*)	2.6±0.1 2.7±0.1		2.9±0.2 (*)
$\langle N_h \rangle_{AgBr}$	9.9±0.7 (*)	9.9±0.2 9.7±0.2		9.9±0.5 (*)
$\langle n_s \rangle_{em}$	13.2±0.2 (+)	14.3±0.2 14.0±0.2	13.3±0.3	15.1±0.2 (+)
$\langle n_s \rangle_{CNO}$ $\langle n_s \rangle_{AgBr}$	10.7±0.5 14.7±0.5	11.0±0.3 15.4±0.3		11.9±0.6 (*) 16.7±0.5 (*)
D_{em}	7.9±0.1	8.6±0.5 8.2±0.6	9.4±0.4	9.0±0.1
D_{CNO}	5.9±0.6 (*)	6.0±0.9		5.7±0.3 (*)
D_{AgBr}	7.5±0.4 (*)	8.7±0.8		8.8±0.3 (*)

(*)Based on vertical exposure alone.

(+) Including possible coherent events.

Chapter 3

MOMENTS OF MULTIPLICITY DISTRIBUTION AND SCALING

3.1 INTRODUCTION

The charged multiplicity distributions from proton-proton collisions and proton-nucleus collisions show some interesting regularities. These regularities are the subject matter of this chapter. A few underlying theoretical ideas are discussed before the experimental data are presented.

3.2 MULTIPLICITY DISTRIBUTION AND ITS MOMENTS

Consider the normalized single particle inclusive differential cross-section,

$$g_1(\bar{p}_c, s) = (1/\sigma_{tot})\, d\sigma(n_c, s)/dw$$

The integral,

$$F_1 = \int dw_c\; g_1(\bar{p}_c, s) = (1/\sigma_{tot}) \int dw_c\; d\sigma(n_c, s)/dw_c$$

$$= \langle n_c \rangle$$

where $\sigma(n_c, s)$ is the partial cross-section for the production of n particles of type c. F_1 can be seen to be equal to the mean number of particles of type c produced; if type c means charge, then F_1 is the mean number of charged particles produced in hadron-hadron collisions. $\sigma(n_c)/\sigma_{tot} = P(n_c, s)$ defines the charged multiplicity distribution.

Similarly, considering the two-particle inclusive cross-section,

$$g_2(\bar{p}_c, \bar{p}_d, s) = (1/\sigma_{tot})\, d\sigma(n_c n_d, s)/dw_c\, dw_d$$

$$F_2 = \int g_2(\bar{p}_c, \bar{p}_d, s) = \langle n_c n_d \rangle$$

and if n_c and n_d are the same type of particles,

$$F_2 = \langle n_c(n_c - 1) \rangle$$

If there are no correlations between c and d, then

$$g_2(\bar{p}_c, \bar{p}_d, s) = g_1(\bar{p}_c, s)\, g_1(\bar{p}_d, s)$$

But if correlations do exist, then a correlation function can be defined,

$$C(c,d) = g_2(\bar{p}_c, \bar{p}_d, s) - g_1(\bar{p}_c, s)\, g_1(\bar{p}_d, s)$$

The integral of the correlation function is given by:

$$f_2 = \int dw_c\, dw_d C(c,d) = \langle n_c n_d \rangle - \langle n_c \rangle \langle n_d \rangle$$

for c = d

$$f_2 = \langle n_c(n_c - 1) \rangle - \langle n_c \rangle^2$$

This function f_2 gives a measure of the deviation of the multiplicity distribution from a Poisson distribution.

For a Poisson distribution $f_2 = 0$; a positive value for f_2 would imply that the distribution is broader than a Poisson and a negative value would mean that the distribution is narrower than a Poisson. It is possible to define higher order of multiplicity moments F_i and the Mueller moments[34] f_i, for $i>2$.

The absolute moments of the multiplicity distribution are given by

$$C_K = \langle n^K \rangle / \langle n \rangle^K$$

and the central moments of the distribution are given by:

$$\mu_K = \sqrt[K]{\langle (n - \langle n \rangle)^K \rangle}$$

The dispersion, skewness and kurtosis of the multiplicity distribution are obtained from the central moments.

$$D^2 = \mu_2$$

$$\text{Skewness} = \mu_3 / D^3$$

$$\text{Kurtosis} = \mu_4 / D^4$$

The dispersion, the skewness and the kurtosis of the distribution measure its width, asymmetry and peakedness respectively..

3.3 EXPERIMENTAL DATA

The experimental values of the moments of the multiplicity distributions, of proton-nucleus interactions

in emulsion, are given in table 3.1 and are compared with hydrogen bubble chamber data at 200 GeV and 300 GeV incident energies.

Table 3.1

Some parameters of the multiplicity distribution

	200 GeV		300 GeV	
	Emulsion	HBC	Emulsion	HBC
$\langle n \rangle$	13.2±0.2	7.65±0.16	15.2±0.2	8.50±0.12
D	7.8±0.2	3.88±0.08	9.0±0.2	4.24±0.05
f	48.1±3.2	7.44±0.72	65.3±3.2	9.45±0.51
Skewness	1.03	0.67	0.92	0.71
Kurtosis	4.43	3.10	3.69	3.30

For emulsion data, the errors in skewness and kurtosis exceed 10%.

$\langle n \rangle = \langle n_{ch} \rangle$ for hydrogen bubble chamber data and $\langle n_s \rangle$ for emulsion data.

Of special interest is the dispersion of the distribution. It was shown by Wroblewski[35] that in proton-proton interactions, a plot of dispersion against $\langle n_{ch} \rangle$ gives a straight line that can be represented by

$$D = 0.576 \pm 0.008 \quad (\langle n_{ch} \rangle - 1)$$

A similar plot using the quantities D and $\langle n_s \rangle$, for emulsion data, also gives a straight line that can be represented by (see figure 3.1),

$$D = 0.60 \pm 0.04 \langle n_s \rangle$$

In a later chapter it will be argued that $\langle n_{ch} \rangle - 1$ and $\langle n_s \rangle$ can be interpreted as the total number of charged

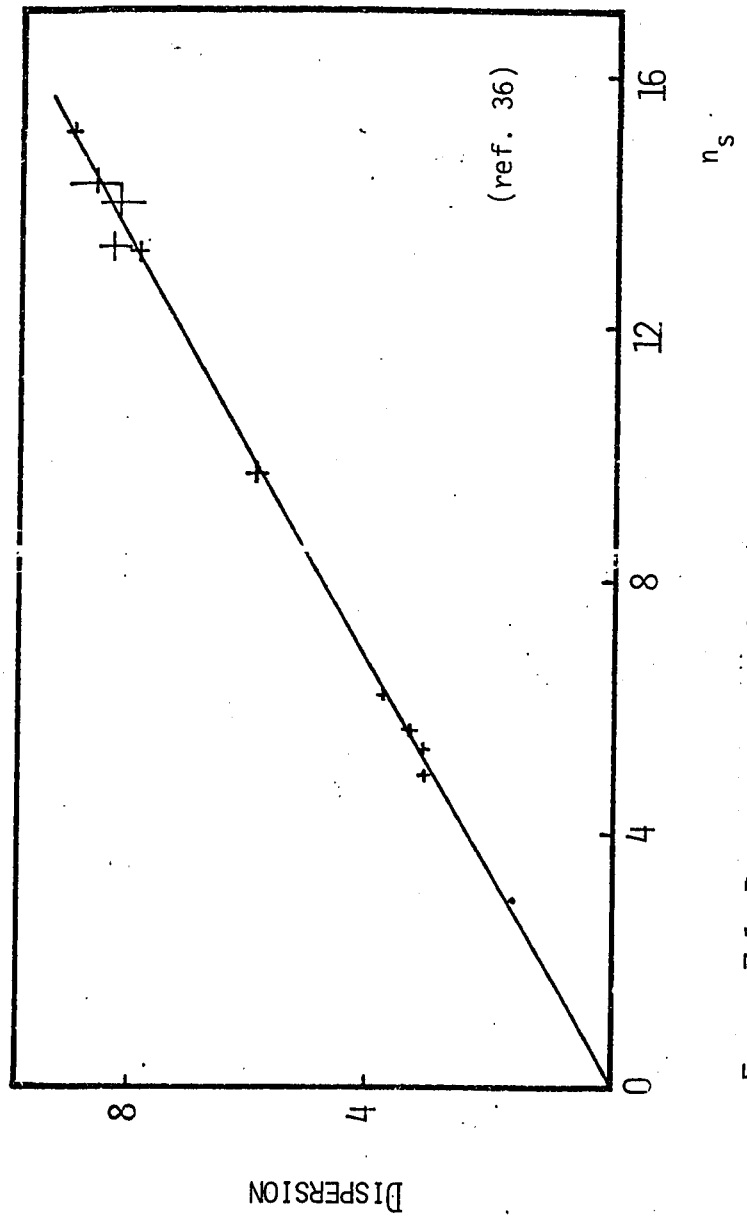

FIGURE 3.1 DISPERSION VS. AVERAGE MULTIPLICITY

particles in the final state minus the charge or charges of the target particles in the initial state of proton-proton and proton-nucleus (emulsion) interactions respectively.

The behaviour of the absolute moments C_k is relevant to the question whether the multiplicity distributions show any limiting behaviour. The values of C_k for k=2,3,4, for emulsion data,[36] are presented in table 3.2.

Table 3.2

Some absolute moments of the multiplicity distribution

Energy (GeV)	C_1	C_3	C_4
6.2	1.33±0.07	2.10±0.17	3.78±0.43
14	1.39±0.15	2.35±0.38	4.58±0.96
22.5	1.35±0.10	2.19	4.04
67	1.38±0.13	2.39	4.93
200	1.35±0.09	2.28	4.54
300	1.35±0.07	2.25	4.35

Typical errors on C_3 and C_4 are given for the data at 6.2 GeV (1768 events) and 14 GeV (526 events). Within the limits of errors C_k for k=2,3,4 has a constant value.

3.4 SCALING

The results of the previous section indicate that

$\langle n_{ch}-1\rangle/D$ and $\langle n_s\rangle/D$ do not change in the energy range $6\ \text{GeV} \leqslant E_{inc} \leqslant 300\ \text{GeV}$. Also, for the emulsion data, the values of C_K for k=2,3,4 seem to have reached their limiting values. These points suggest that the Koba, Nielsen and Olesen[37] semi-inclusive scaling law (KNO scaling) that was successfully applied to proton-proton interactions[38], would be applicable to proton-emulsion data. The KNO scaling law states that, in the asymptotic region,

$$\sigma(n)\langle n\rangle/\sigma_{tot} \quad \longrightarrow \quad \psi(z,s) \xrightarrow[s\to\infty]{} \psi(z)$$

where $z = (n)/\langle n\rangle$. It was shown by Slattery[38], that KNO scaling is applicable to proton-proton data from 50 GeV to 300 GeV. The scaling variable and function used by Slattery are

$$z = n/\langle n\rangle$$

$$\psi(z) = (Az + Bz^3 + Cz^5 + Dz^7)\ \exp(-Ez)$$

In a recent publication, Buras et al[39] have pointed out that, the Wroblewski fit

$$D = a\ (\langle n_{ch}\rangle - 1)$$

suggests that a scaling function in the variable $z = (n-1)/\langle n-1\rangle$ may extend the applicability of KNO scaling to even lower energies than 50 GeV. This is so because, while $\langle n_{ch}\rangle/D$ may be tending towards a constant value, $\langle n_{ch}-1\rangle/D$ is constant from 6 GeV upto the current

FNAL energies.

The composite nature of emulsion does not allow for a simple test of scaling. One has to first examine whether scaling holds for a pure target nucleus. That it does for π -Ne data was shown by Elliott et al.[7] It was also shown by Hebert et al[40] that if one considers the AgBr events in emulsion, (Ag and Br do not greatly differ in A), the scaling function for proton-proton data used by Slattery (all parameters except E being divided by two in order to take odd prong events into account) fits the experimental points well. Knowing the average $\langle n_s \rangle$ for each group of nuclei, it is then possible to obtain the proton-nucleus multiplicity distribution for emulsion, from the proton-proton scaling curve. There is good agreement between the experimental distributions and the expected distributions, derived from the Slattery proton-proton scaling curve, at 200 GeV and 300 GeV. This agreement is not good at lower energies.

Since $\langle n_{ch}-1\rangle/D$ and $\langle n_s\rangle/D$ exhibit similar behaviour one would expect KNO scaling to hold for proton-emulsion data even at lower energies, if the variable

$$z = (n_s)/\langle n_s \rangle$$

and the scaling function of Buras et al,

$$\psi(z) = A(z+B)\exp(Cz + Dz^2)$$

are used. The Buras et al scaling function for proton-proton data, (with the same parameters, except that A was divided by 2 in order to take care of the odd prong events), was first applied to proton-AgBr events at 300 GeV. The expected distribution and the experimental distribution are plotted in figure 3.2. The agreement between the two distributions is good with a χ^2 of 43.6 for 41 data points. The expected distributions and the observed distributions for proton-emulsion data, for various energies, are plotted in figures 3.3-3.4. The results of χ^2 tests are given in table 3.3.

Table 3.3

χ^2 tests for scaling fits

Energy (GeV)	scaling function of Buras et al		scaling function of Slattery	
	χ^2	degress of freedom	χ^2	degrees of freedom
6.2	14	8	23.3	8
14	39.1	14	47.0	11
22.5	24.2	17	59.5	15
67	38.9	31	56.3	27
200	64.6	42	66.6	38
300	74.9	52	57.4	45

At every energy considered here, events with n =0 were excluded in the computation of χ^2. The reason for this is that the efficiency of observation of these evnts is expected to be low.

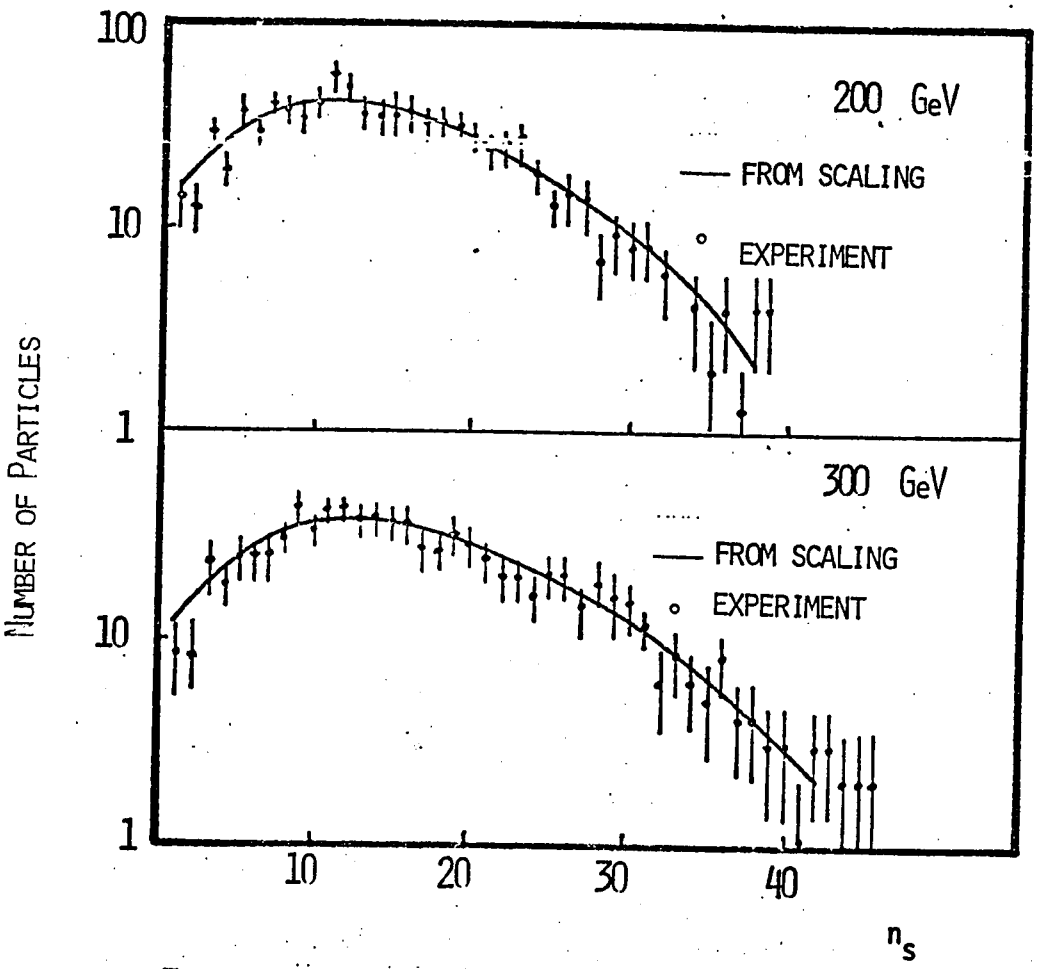

FIGURE 3.2 DISTRIBUTION OF SHOWER PARTICLES (AgBr)

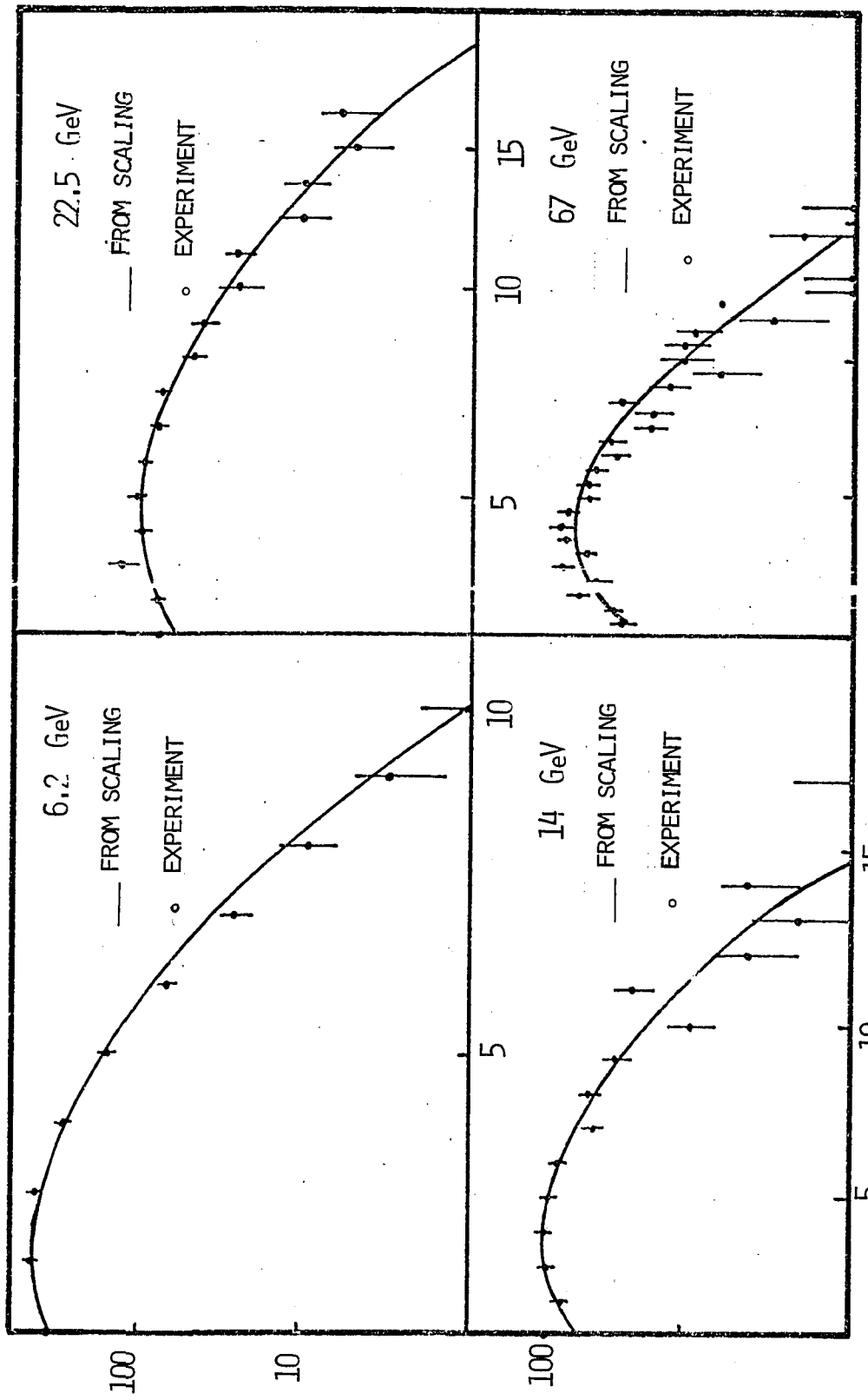

FIGURE 3.3 SHOWER PARTICLE DISTRIBUTIONS AT VARIOUS ENERGIES (EMULSION)
(BELOW 200 GeV)

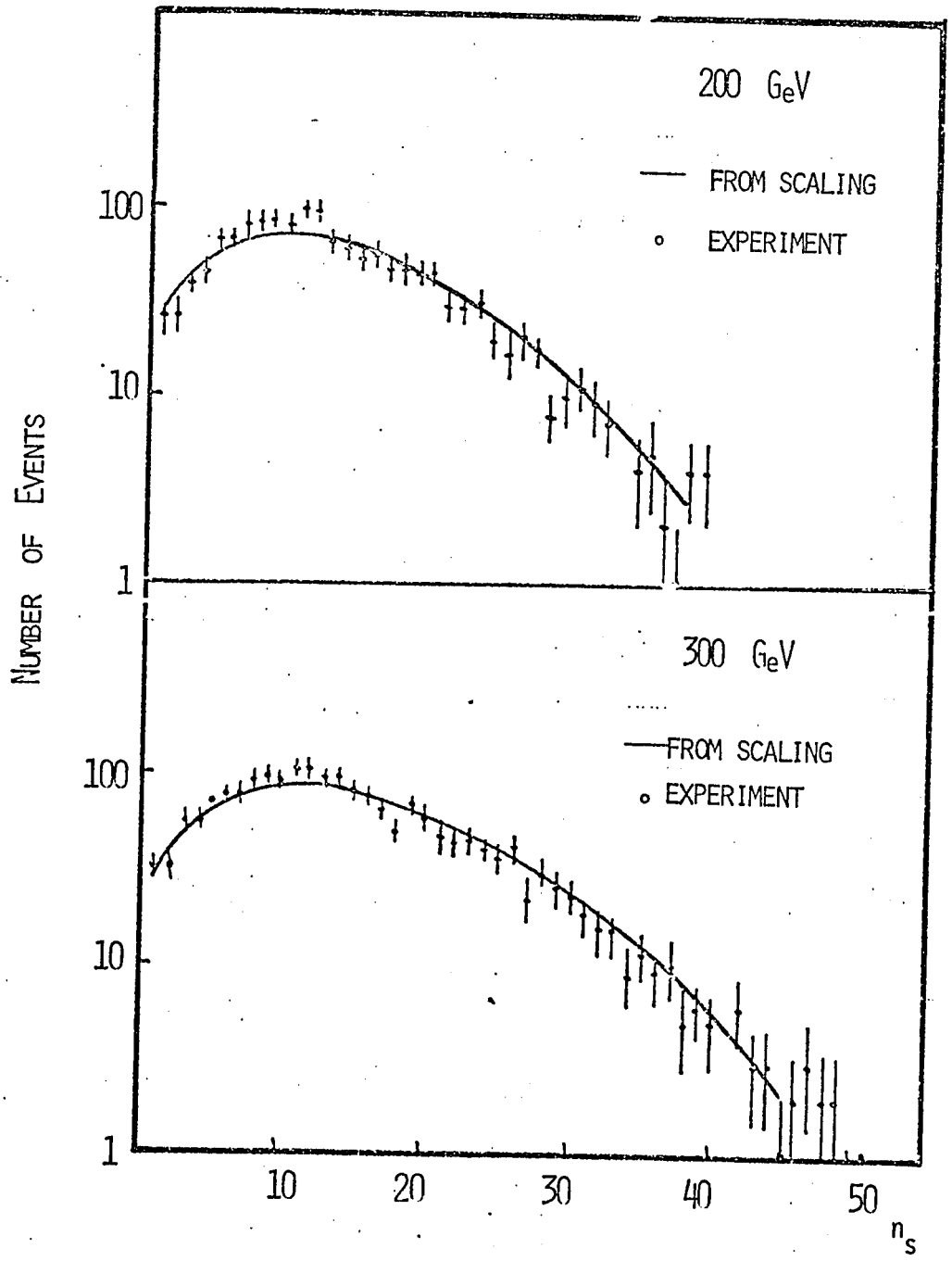

FIGURE 3.4 SHOWER PARTICLE DISTRIBUTIONS AT 200 GeV AND 300 GeV

At 14 GeV, the observed freguncy of $n_s = 1$ events is much higher than that predicted by either scaling function. Also, there is a large fluctuation in the experimental frequencies at $n_s = 10$ and 11. Combining these two frequencies and omitting the $n_s = 1$ events, we obtain a χ^2 of 10.2 for 12 degrees of fredom in the case of the scaling function of Buras et al and a χ^2 of 28.0 for 9 degrees of freedom in the case of the scaling function of Slattery. At 200 GeV and 300 GeV, the experimental distributions have higher values at $n_s = 11, 12$ than the distributions calculated from either scaling function. The Buras et al scaling function gives lower values for the frequencies than the Slattery scaling function at these points.

CHAPTER 4

MODELS OF MULTIPLE PARTICLE PRODUCTION

4.1 INTRODUCTION

The current interest in hadron-nucleus interactions stimulated a considerable theoretical activity and many new models of particle production are being proposed. To be successful, a model of hadron-nucleus interactions should be able to explain the following experimental observations:

1) The dependence of the average multiplicity on the incident energy and on the target nucleus is normally expressed as a ratio of the average multiplicity from hadron-nucleus interactions to that from hadron-nucleon (proton) interactions. This ratio is not very large even for very heavy nuclei, and would appear to be constant at the currently available accelerator energies.

2) The angular distributions of the charged shower particles, from proton-nucleus interactions show no excess of particles in the forward direction when compared with proton-proton interactions at the same energy. The ln tan $\theta/2$ plots indicate that the angular distributions in the

projectile fragmentation region are the same, independent of the size of the target nucleus.

3) The average number of heavy tracks is independent of the energy of the incident particle, in the energy range 30 GeV $\leqslant E_{inc} \leqslant$ 300 GeV.

4) The amount of energy carried away by the leading particle (50% of the incident energy), is independent of the incident energy, though it may depend weakly on the size of the target nucleus.

There are two classes of models that are readily distinguishable. These are termed one-step or incoherent production models (IPM) and two-step or coherent production models (CPM)[9,10]. In the one-step models, the final state is produced instantaneously as a result of the collision, whereas in the two-step models the final state results from the decay of a long lived intermediate state. The intra-nuclear cascade model is an example of IPM and the energy flux cascade model is an example of CPM. The CPM are also referred to as diffractive excitation or diffractive fragmentation models.

4.2 TERMINOLOGY

Before going into the description of various models some of the variables and terminology used in describing

high energy interactions will be discussed.

Consider a hadron-hadron interaction,

$$a+b\text{----}>c+d+e+\ldots\ldots$$

It is difficult to study these interactions in an exclusive manner, i.e., by measuring the momenta of all the produced particles. Instead, mainly the reactions of the type

$$a+b\text{----}>c+\text{ anything}$$

are studied, where kinematical variables of particle 'c' only are measured. This type of an experiment is called a single particle inclusive experiment. The Lorentz invariant cross-section for this reaction is defined by,

$$f\ (\bar{p}_c, s) = E_c\, d\sigma/dp_c = d\sigma/dw_c$$

p_c and E_c are the momentum and total energy of particle c, respectively, and s is the square of the centre-of-momentum energy. It is also possible to study two-particle inclusive reactions,

$$a+b\text{-----}>c+d+\text{anything},$$

with a differential cross-section,

$$f\ (\bar{p}_c, \bar{p}_d, s) = E_c\, E_d\, d\sigma/dp_c\, dp_d = d\sigma/dw\ dw$$

In a semi-inclusive reaction, the production properties of particle 'c' are studied for those reactions, where certain other properties of 'anything' are observed, but not measured. An example is,

a+b----->c+ n charged particles +neutrals.

4.2.1 The longitudinal rapidity variable

Frequently, the inclusive distributions are discussed in terms of the rapidity variable,

$$y = 1/2 \ln (E+p_{\parallel})/(E-p_{\parallel})$$

Here p is the longitudinal momentum of the particle. For the non-relativistic case $y=\beta_{\parallel}$. The advantage of using this variable is the ease of going from one reference frame to ancther. Under a Lorentz transformation, along the direction of the primary, the rapidities of the secondaries are shifted by a constant amount. Thus,

$$y_L = y^* + y_c$$

$$y_c = 1/2 \ln (1+\beta_c)/(1-\beta_c)$$

where y^* is the rapidity of the particle in the centre-of-momentum frame and y_c and β_c are the rapidity and velocity, respectively, of the centre-of-momentum frame with respect to the laboratory frame. For the non-relativistic case, this would just be the addition of velocities. Figure 4.1 is a convenient way of representing some kinematical variable of a hadron-hadron collision.[41] From the figure,

$$\tan \phi/2 = (E-p_{\parallel}/E+p_{\parallel})^{1/2}$$

or

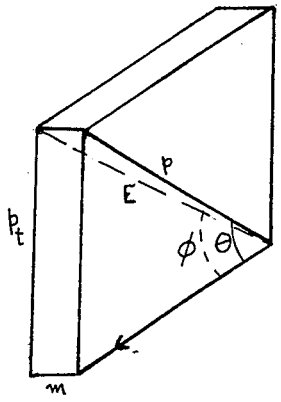

Figure 4.1

The rapidity variable

$$-\ln \tan \phi/2 = \ln(E+p_{\parallel}/E-p_{\parallel}) = y$$

For $m^2 \ll p_t^2$, can be replaced by θ. The resulting variable is used in place of y, where it is more convenient to measure the angles of emission of the secondaries, than their momenta. The invariant length of the rapidity plot, in the centre-of-momentum frame, is given by

$$Y = y_a^* - y_b^* = \ln((E_a + p_{\parallel})(E_b + p_{\parallel})/m_a m_b)$$

$$\simeq \ln(s/m_a m_b) \quad \text{for large } s$$

In the laboratory system, if b is the target ,

$$y_b = 0, \quad y_a \simeq \ln(s/m_a m_b)$$

Thus, the length of the rapidity plot grows as ln s. (See figures 4.2 and 4.3).

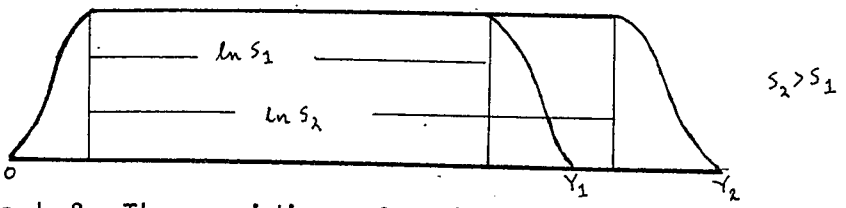

Figure 4.2 The rapidity plot in the laboratory system

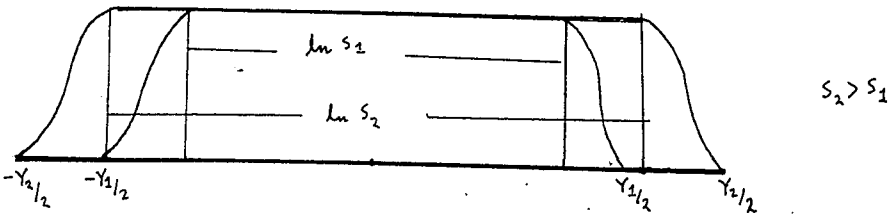

Figure 4.3 The rapidity plot in the centre-of-momentum system

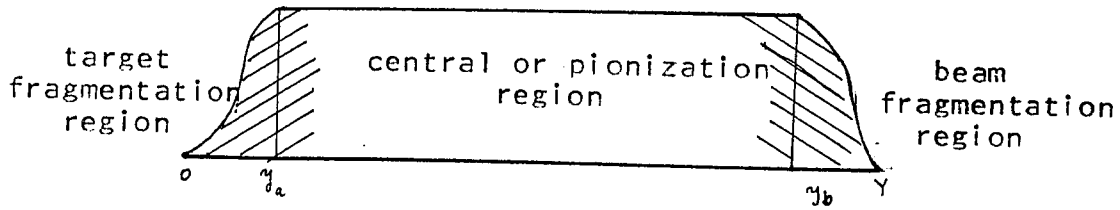

Figure 4.4 Various regions on the rapidity plot

The rapidity plot can be divided into three regions; the beam (target) fragmentation region of length L, about y_a (y_b) and the central or pionization region of length proportional to ln s. This is illustrated in figure 4.4.

4.3 INCOHERENT PRODUCTION MODELS

4.3.1 Intra-nuclear cascade model

The simplest IPM is the intra-nuclear cascade model. This model can be described as follows. The incident proton collides with a nucleon in the target nucleus, producing a number of secondary particles. These first

generation secondaries in turn give rise to a second generation of particles when they encounter other nucleons in the target. Thus an intra-nuclear cascade is set up. It is well known that this simple model grossly over estimates the number of particles produced.

Different versions of intra-nuclear cascade models, which modify the above picture were also proposed. One such version is given by Artykov et al.[42] In their calculations the authors take into account the fact that the secondaries produced in a high-energy interaction are highly collimated in the forward direction in the laboratory system. These particles, they assume, interact with one and the same nucleon inside the nucleus. In the Monte Carlo calculations, however, it turned out that only one secondary is singled out in energy and this particle determined the kinematics of the interaction with a single nucleon of many particles from the collimated beam of secondaries. In other words, the leading particle effect is taken into consideration since any cascade model that treats all the secondaries on the same footing, gives too high a multiplicity. In these calculations, it is assumed that the leading particle carries away approximately half of the incident energy. There are predictions for the average number of heavy tracks, the transeverse momenta of

the seccndaries and the half-angle of the shower particles. The half-angle is the angle in the laboratory within which half of the shower particles appear.

4.3.2 Model of Lehman and Winbow

Using Gribov's approach, Lehman and Winbow[43] have recently proposed a multi-peripheral model of particle production in hadron-nucleus interactions. The model does not lead to cascading in the central region. The particle production takes place over an extended region of space-time. In the laboratory system, many of the particles are created long before the projectile reaches the target and they miss the target altogether. Particle production throughout the central region is the same for any target and projectile and particle production outside the target fragmentation region is independent of the target. The target fragmentation region is defined by the boundary $y<y_o$, where

$$y_o = \ln (2E_o / m_{\pi t}) = \ln (4R\bar{m})$$

$R = R_o A^{1/3}$, A is the atomic weight of the target nucleus, $\bar{m}$ is a model dependent mass and $m_{\pi t}$ is the transverse mass of the pion, given by $m_{\pi t} = (m_\pi^2 + p_t^2)^{1/2}$. For emulsion, Lehman and Winbow give E_o to be 50 GeV. For $y>y_o$, the interaction takes place over the entire region of the nucleus, due to the the Lorentz contraction of the

nucleons. For $y<y_o$, the partons in the projectile and the nucleus interact only locally and the projectile partons are scattered sequentially by the target nucleons. The average total multiplicity is given by

$$m_b(A, E_{inc}) = m_b(1, E_{inc}) + 1/2(\bar{\nu} - 1) m_p(1, E_o')$$

where $y_o = 1/2 \ln(2E_o'/m)$

and $\bar{\nu} = \sigma_{\pi N} A^{1/3} / \pi R_o^2 = 0.51 A^{1/3}$

Thus, in this model, the multiplicity is a sum of a hadronic part and a nuclear part and can be written as

$$\langle n \rangle = bY + f(A)$$

As the incident energy increases, the ratio $\langle n \rangle_{p\text{-}A} / \langle n \rangle_{p\text{-}p}$ decreases. The rapidity distribution expected from this model is shown in fig 4.5. The boundary of the target fragmentation region changes with the size of the target nucleus.

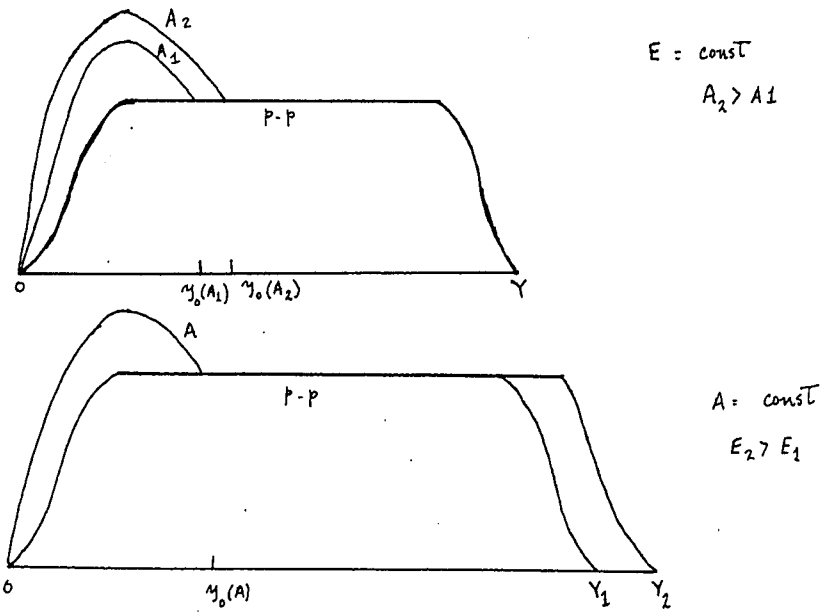

Figure 4.5 Rapidity distribution in proton-nucleus collisions in the model of Lehman and Winbow

4.3.3 Model of Cutler and Snider

A modification of the Lehman and Winbow model was carried out by Cutler and Snider[44]. In this model the average total multiplicity from hadron-nucleus interactions (for A >10) goes as

$$\langle n(p,A)\rangle = b\,\sigma_{in}(p,p)\,A^{1/3}\,Y/\pi R_o^2 + f(A)$$

Thus even at high energies there is an A dependence of average charged multiplicities. In order to compare theoretical predictions for multiplicity with the experimentally observed values, Cutler and Snider propose the use of $d\langle n\rangle/dY$ which eliminates the nuclear part. The rapidity distribution in the Cutler and Snider model is slightly different from the Lehman and Winbow model and this is illustrated in figure 4.6.

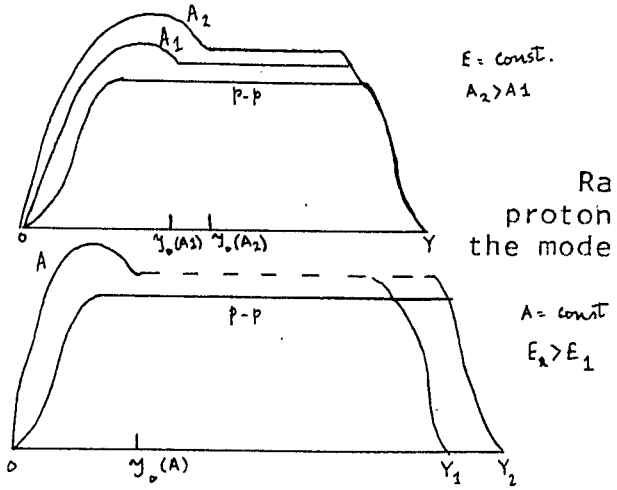

Figure 4.6
Rapidity distribution in proton-nucleus collisions in the model of Cutler and Snider

The models of Lehman and Winbow and Cutler and Snider are applicable when $Y>y_0$.

4.4 COHERENT PRODUCTION MODELS

There are two assumptions common to most CPM. One is that the life time of the excited state of the incident hadron is longer than the time needed to traverse the nucleus and the other assumption is that the cross-section for further collisions of this excited state with other nucleons is the same as for hadrons.

4.4.1 Model of Fishbane and Trefil

In a CPM proposed by Fishbane and Trefil,[45] particle production takes place as follows. The incident particle goes into an excited state after the first inelastic collision with a target nucleon. The target nucleon also goes into an excited state and its excitation is independent of the projectile excitation. The projectile excitation passing through the nucleus undergoes $\nu - 1$ more inelastic collisions, leaving $\nu - 1$ more target excitations behind. The target excitations, at the presently available FNAL energies, are not capable of particle production in inelastic encounters with other nucleons and they decay giving rise to a single particle inclusive distribution which is ν times that for a single target nucleon distribution. Thus, the projectile excitation decays resulting in $\langle n \rangle/2$ particles and the decay of the target excitations results in $\nu \langle n \rangle/2$ particles. Here

<n> is the average number of particles in the final state of hadron-nucleon interactions. The same result for <n> was obtained by Goldhaber[46] and Dar and Vary[9].

In this model, the rapidity distribution in the projectile fragmentation region is the same as for hadron-nucleon collision. But at y=Y/2, the rapidity distribution starts showing an excess of particles. Figure 4.7 is a qualitiative description of the rapidity distribution expected from this model.

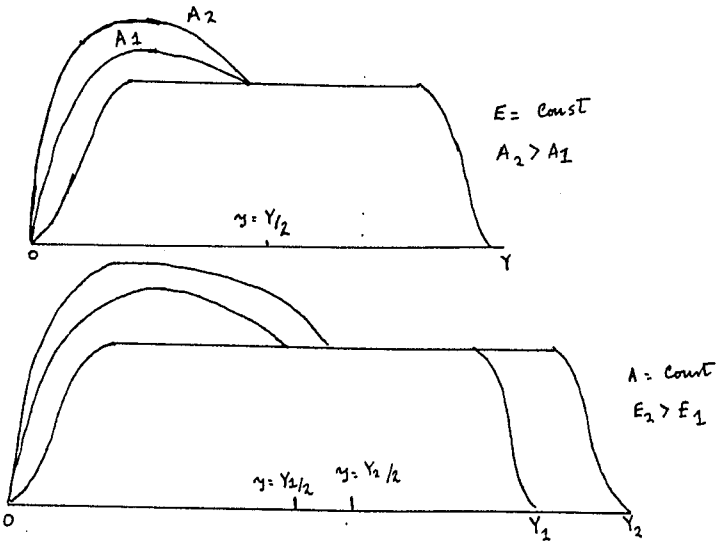

Figure 4.7
Rapidity distribution in proton-nucleus collisions in the model of Fishbane and Trefil

4.4.2 The hydrodynamical model

The hydrodynamical model, proposed by Landau in order to explain the features of nucleon-nucleon collisions is enjoying a revival[47,48]. The model was extended to the nucleon-nucleus case by Belinkii and Milekhin[49] and also by Landau and Belinkii.[50] According to Feinberg[16], the hydrodynamical model is well suited to

desribe nucleon-nucleus and nucleus- nucleus collision due to the number of particles involved in the process. The hydrodynamical model is applicable when the average number of particles in the final state is 10-15 and thus should be applicable for nucleon-nucleus collisions above 30 GeV.

Considering a nucleon-nucleon system, the mechanism of particle production in the hydrodynamical model is as follows. In the equal velocity frame (for the nucleon-nucleon case, this also is the centre-of-momentum frame), two hadronic discs collide. At that moment a compound system is formed and the energy is released into a small volume V. The mean-free-path of the 'particles' in the system is small compared to the dimensions of the system. Due to the smallness of the volume, the 'particles' interact strongly with each other and it is not proper to consider them as free particles. Thus the system is described using relativistic hydrodynamics. The number of particles is determined only at the moment of break-up of the system. The expansion of the system is considered to be adiabatic and during this stage the entropy of the system remains constant. At the moment of break-up of the system, the entropy of each small region is proportional to the number of particles in that region. Summing over all such regions, the total number of particles in the

final state (including the initial nucleons), is given by

$$N \propto S$$

$$N \propto E_L^{1/4}$$

where S is the total entropy of the system.

For the nucleon-nucleus case, Belinkii and Milekhin pointed cut that the mechanism of compression of the system at the time of collision has to be taken into consideration. The equal velocity frame of the nucleon-nucleus system is considered. In this frame, the hadronic matter resulting from the collision is at rest. The collision appears as a collision between the incident nucleon and a tube cut out of the nucleus. The final result of the calculations is that the ratio of change of entropy in proton-nucleus collisions to that in proton-proton collisions is equal to $A^{0.19}$. Thus, the ratio of the average number of particles created in a proton-nucleus interaction to the average number of particles created in a proton-proton interaction (at the same energy) is $A^{0.19}$. Due to thermodynamic description of the hydrodynamic model, the results of the calculations are expected to be insensitive to whether the collision process is sequential or simultaneous.

In the hydrodynamical model, the angular distributions of shower particles were calculated for the

case of nucleon-nucleon collisions. The agreement between the predictions of the model and the experimental distribution, in the case of proton-proton collisions was shown to be very good[29]. The angular distribution of shower particles from proton-nucleus collisions is not expected to be greatly different from the nucleon-nucleon case. Due to the number (N) of target nucleons involved in the interaction, one can expect a shift in the centre of the angular distribution. In terms of the rapidity variable, this shift would be ln <N>, towards the target fragmentation region.

4.4.3 The energy flux cascade model

The energy flux cascade model (EFC), proposed by Gottfried[11] is similar to the hydrodynamical model in that the energy flux of the hadronic matter is the essential variable. It is a cascade of this flux, and not of conventional hadrons, that occurs in proton-nucleus collisions.

After the collision between the incident proton and a target nucleon, the hadronic matter is contained within an expanding cylinder. The energy and momentum within the cylinder are obtained by assuming that the observed distributions (asymptotic) can be projected backwards in

time using the classical equations of motion of free particles.

While in the early stages of collision, the system cannot be considered as an n particle state and it is too large to be considered a single hadron. The energy flux is divided into slices, such that each slice has the appropriate thickness of a hadron moving with the mean rapidity of the matter in that slice. It is also shown that most of the incident energy (except for a small fraction) is carried by the first (or leading slice) and the rest of the slices together have an energy of the order of $s^{1/3}$, where s is the square of the centre of momentum energy in a nucleon-nucleon collision.

A hadron of incident energy would undergo inelastic interactions in the nucleus. The first collision results in the formation of the energy flux. When this flux travels a distance of one mean-free-path, it is equivalent to two hadrons H1 and H2 having energies E and $E^{1/3}$. If there are no further encounters with target nucleons, H1 will decay producing 2/3 <n> and H2 will decay producing 1/3 <n> particles. If however, another nucleon is encountered, the leading slice will interact giving rise to two more slices H1' and H2', with H1' again carrying most of the incident energy. The final multiplicity

after collisions is given by

$$\langle n(A,s)\rangle = 2/3\ \langle n(1,s)\rangle + \bar{\nu}/3\ \langle n(1,s)\rangle$$

The rapidity distribution expected from this model is shown in figure 4.8. The distribution in the forward region is the same as that from nucleon-nucleon collisions, but there is an excess of particles starting at y=Y/3, independent of the target nucleus.

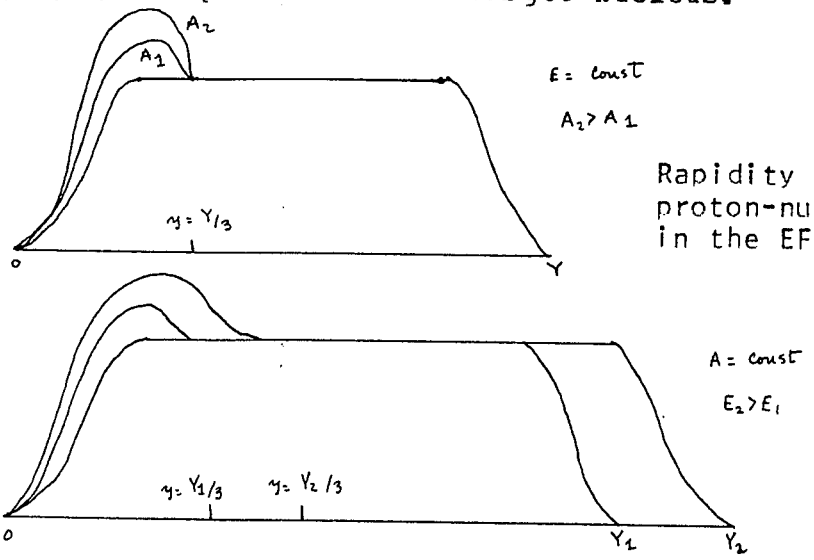

Figure 4.8
Rapidity distribtuion in proton-nucleus collisions in the EFC model

4.4.4 Model of Berlad, Dar and Eilam

Another model of particle production from nuclear targets has been proposed recently by Berlad, Dar and Eilam.[15] In this model, the 'tube' containing the target nucleons is considered to be equivalent to a single particle of mass νm, where is the number of nucleons in the 'tube' and m is the nucleon mass. The square of the centre of momentum energy is boosted by ν times compared with that available in nucleon-nucleon collisions. This

would imply that the average multiplicity goes as $\langle \nu^{1/4} \rangle$ times the average multiplicity from nucleon-nucleon collisions. If the relation $\langle n \rangle = C\ E^{1/4}$ is valid for nucelon-nucleon interactions, then $\langle n \rangle = C \langle \nu^{1/4} \rangle E^{1/4}$ and so is proportional to $A^{1/12}$, since is proportional to $A^{1/3}$, approximately.

The rapidity distribution can be expected to be similar to that from nucleon-nucleon collisions, except for a shift in the distribution towards the target fragmentation region. This is illustrated in figure 4.9.

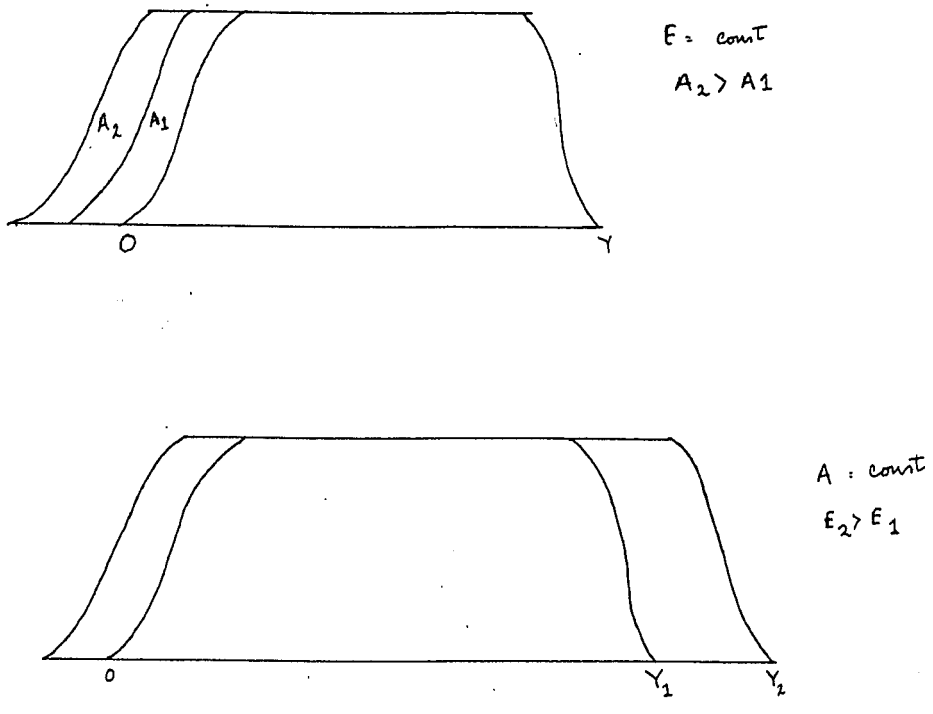

Figure 4.9 Rapidity distribution in proton-nucleus collisions in the model of Berlad, Dar and Eilam

Chapter 5

COMPARISON BETWEEN THEORY AND EXPERIMENT

5.1 INTRODUCTION

Before comparing the experimental results with the predictions of the various models, the following points must be noted.

In the models discussed in the previous chapter, the predictions for different quantities such as average multiplicities and rapidity distributions from proton-nucleus interactions are compared with the results from proton-proton interactions. A meaningful comparison can only be made when the quantities compared from the two types of interactions closely correspond to one another. Let us first consider the predictions for the average shower particle multiplicities in proton-nucleus interactions. The measured quantity in the case of proton-proton collisions is $\langle n_{ch} \rangle$, the average number of charged particles in the final state of the interaction. All charged particle tracks, whether they are black, grey or shower tracks, contribute to the value of $\langle n_{ch} \rangle$. In

the case of proton-nucleus collisions, however, the measured quantity $\langle n_s \rangle$ is the number of fast ($\beta > 0.7$) charged particles only. Thus $\langle n \rangle$ and $\langle n \rangle$ represent different quantities and should not be compared with each other.

The widespread usage of $R_A = \langle n_s \rangle_{p-A} / \langle n_{ch} \rangle$ has led to considerable difficulty in the comparison of experimental results with the predictions of theoretical models. This ratio depends on the incident energy, at least for proton-nucleus interactions below 200 GeV. The value of α in the relation $R_A = A^{\alpha}$ increases from a value which is less than zero to 0.14 at current FNAL energies. The experimental data are shown in Table 5.1. The values of α from 6.2 GeV to 67 GeV were taken from the calculations of Gurtu et al.[51]

Table 5.1

Values of R_A and α

Energy in GeV	$\langle n_s \rangle_{p-A} / \langle n_{ch} \rangle$	α
6.2	0.95 ± 0.02	-0.013 ± 0.006
9.0	0.99 ± 0.06	-0.003 ± 0.016
20.5	1.29 ± 0.03	0.064 ± 0.006
27.0	1.41 ± 0.05	0.084 ± 0.008
67	1.62 ± 0.04	0.125 ± 0.006
200	1.73 ± 0.06	0.141 ± 0.005
300	1.78 ± 0.05	0.145 ± 0.005

We feel that the proper quantities to be compared are the number of particles created in the interaction.

Consider a nucleon-nucleon interaction, where the average number of created particles is $\langle n \rangle$. At a given energy, we expect $\langle n \rangle$ to be independent of the intial nucleon charges. If we make the reasonable assumption that the number of neutrals created is half the number of charges created, then $\langle n \rangle = 3/2 \langle n_{\pm} \rangle$, where $n_{\pm}$ is the number of positive and negative charges created.

The use of $n_{\pm}$ has the advantage that the contribution of the charges in the initial state of nucleon-nucleon collisions to the average multiplicity is eliminated. Thus, at a given energy, $\langle n_{\pm} \rangle$ will be the same for proton-proton or neutron-neutron collisions. That $\langle n_{\pm} \rangle$ is the quantity that describes hadron-hadron interactions on a more universal basis is also pointed out by Frazer et al.[52] The experimental support for the use of this multiplicity is provided by neutron-proton collisions studied by Dao et al.[53] At an average neutron energy of 30 GeV, $\langle n_{-} \rangle = 1.4 \pm 0.2$, which is in excellent agreement with $\langle n_{-} \rangle = 1.3 \pm 0.04$ obtained for proton-proton interactions at 28.5 GeV. The experimental investigation of proton-deuteron interactions at 300 GeV, carried out by Sheng et al,[54] also justify the use of $\langle n_{\pm} \rangle$. In these studies, the average charged particle multiplicity from

proton-neutron interactions is 7.84 ± 0.17, which is about a unit less than the average multiplicty from proton-proton interactions at the same energy.

Since in proton-nucleus collisions we have neutron targets as well as proton targets, the elimination of the target charges is important. Thus the quantity that allows a correct comparison of proton-nucleus and proton-proton interactions is the ratio of the average number of created particles, or the ratio of the number of created charged particles.

5.2 THE AVERAGE NUMBER OF CREATED CHARGES

In proton-proton collisions, $\langle n_{\pm} \rangle$ is simply $\langle n \rangle - 2$. The incident and target protons are subtracted from the experimental values for the average charged multiplicity in hydrogen bubble chamber experiments. However, in proton-nucleus collisions, the situation is more complex. The target proton may appear among either the shower particles or the slow particles. The evaluation of $\langle n_{\pm} \rangle$ demands a knowledge of the average number of target protons.

5.2.1 The average number of target protons

The average number of target protons involved in a proton-nucleus collision may be determined from the average number of collisions, $\langle \nu \rangle$, which the incoming proton suffers inside the nucleus. $\langle \nu \rangle$ is given by

$$\langle \nu \rangle = \sigma_{in}(p,p) / \sigma_{in}(p,A)$$

Here $\sigma_{in}(p,p)$ and $\sigma_{in}(p,A)$ are the inelastic proton-proton and proton-nucleus cross-sections. Unfortunately, information regarding $\sigma_{in}(p,A)$ at all energies for all nuclei is not available. This necessitates a model dependent calculation of $\sigma_{in}(p,A)$. In the framework of the Glauber theory, $\sigma_{in}(p,A)$ has been calculated by Camillo et al[55] assuming $\sigma_{in}(p,p)$ to be 30 mb and by Gurtu et al[51] assuming $\sigma_{in}(p,p)$ to be 32 mb. Gurtu et al find that, for an incoming proton, $\langle \nu \rangle$ is well described by the empirical formula,

$$\langle \nu \rangle = 0.716\ A^{0.326}$$

for a Woods-Saxon nuclear charge density distribution.

Experimentally, $\sigma_{in}(p,A)$ has been measured, in the energy range 20 GeV - 60 GeV, for various elements by Denisov et al.[56] From their data, we obtain the empirical relation

$$\langle \nu \rangle = 0.699\ A^{0.306}$$

From the value of $\langle \nu \rangle$, the average number of target

protons $\langle \nu_p \rangle$ for the different groups of nuclei in emulsion have been calculated. These are presented in Table 5.2.

Table 5.2

Number of collisions inside a nucleus

	Gurtu et al		Denisov et al	
	$\langle \nu \rangle$	$\langle \nu_p \rangle$	$\langle \nu \rangle$	$\langle \nu_p \rangle$
CNO	1.68	0.84	1.56	0.78
AgBr	3.14	1.37	2.80	1.23
Emulsion	2.75	1.22	2.48	1.11

In order to estimate the average number of target protons that appear amongst the shower particles, we make use of the estimates of Calucci et al. From the hydrogen bubble chamber and ISR data, Calucci et al[54] estimate that in a proton-proton collision, the average number of slow particles is 0.62, out of which 0.48 are due to slow protons and 0.14 are due to slow charged pions. From this, we estimate that the number of fast target protons for proton-CNO and proton-AgBr collisions are 0.44 or 0.41 and 0.71 or 0.64, respectively. The lower values are from the empirical relation obtained from the experiments of Denisov et al and the higher values are from the relation of Gurtu et al.

In order to estimate $\langle n_\pm \rangle$ in proton-nucleus

collisions, we subtract from $\langle n_s \rangle$, the average number of fast target protons and add the average number of slow charged pions. We then obtain

$\langle n_\pm \rangle_{CNO} = \langle n_\pm \rangle + (0.24 \text{ or } 0.22) - (0.44 \text{ or } 0.41) - 1 = \langle n_s \rangle - 1.2$

$\langle n_\pm \rangle_{AgBr} = \langle n_\pm \rangle + (0.44 \text{ or } 0.39) - (0.71 \text{ or } 0.64) - 1 = \langle n_s \rangle - 1.26$

$\langle n_\pm \rangle_{em} = \langle n_\pm \rangle + (0.39 \text{ or } 0.35) - (0.63 \text{ or } 0.58) - 1 = \langle n_s \rangle - 1.24$

The quantities in parenthesis represent the values obtained from the empirical formulae of Gurtu et al and Denisov et al, respectively. The quantity 1 represents the incident proton charge.

The above considerations show that the number of fast target protons included in the shower particles is just about egual to the slow pions which are not counted.

5.2.2 Evidence for the use of $\langle n_\pm \rangle = \langle n_s \rangle - 1$

Evidence that the number of created charges is given by $\langle n_s \rangle - 1$ can be obtained from the angular distributions. Consider a neutron-neutron collision. The expected value of $\langle n_{ch} \rangle_{nn} = \langle n_{ch} \rangle - 2$. The Lorentz factor of the neutron-neutron system should be the same as for the proton-proton system at the same energy. The angular distributions from neutron-neutron collisions should be similar to those from proton-proton collisions, with the exception that the target and the incident particles are not observed. Thus, it should be expected that the quantities

$< 1/<n_{ch}>_{nn} \ln \tan \theta/2 >$ and $<1/<n_{ch}>_{p-p} \ln \tan \theta/2 >$

should have the same value.

In the case of proton-nucleus interactions, we modify the variable used by Friedlander[58] and define

$$\xi = 1/<n_{ch}> \sum_{i=2} \ln \tan \theta_i/2$$

$$\zeta = <n_s - 1> / <n_{ch} - 2>$$

The summation over $\ln \tan \theta_i/2$ for i=2 to i=n implies that the innermost track (incident track) has been removed. The experimental data were divided into different N groups and and were computed for each group. The N groups considered were N_h=0,1,2-3,4-5,6-8,9-18,>18, at 200 GeV and N_h = 0,1,2-3,4-5,6-8,9-11,12-14,15-18,19-22,>22, at 300 GeV. The data at 200 GeV is the combined data from this work and the Italian group. The data at 300 GeV is the combined data of the collaboration. When is plotted against a straight line graph is obtained for each of the two energies (see figure 5.1). The equation for these straight lines can be written as

$$<\xi> = a\ (\zeta - 1) + b$$

In fitting the data to the straight line, at both energies, the last data point was omitted due to the poor statistics in this region. Inclusion of this point has the effect of increasing the value of the intercept by about 3%. The value of the intercept, at 200 GeV, is

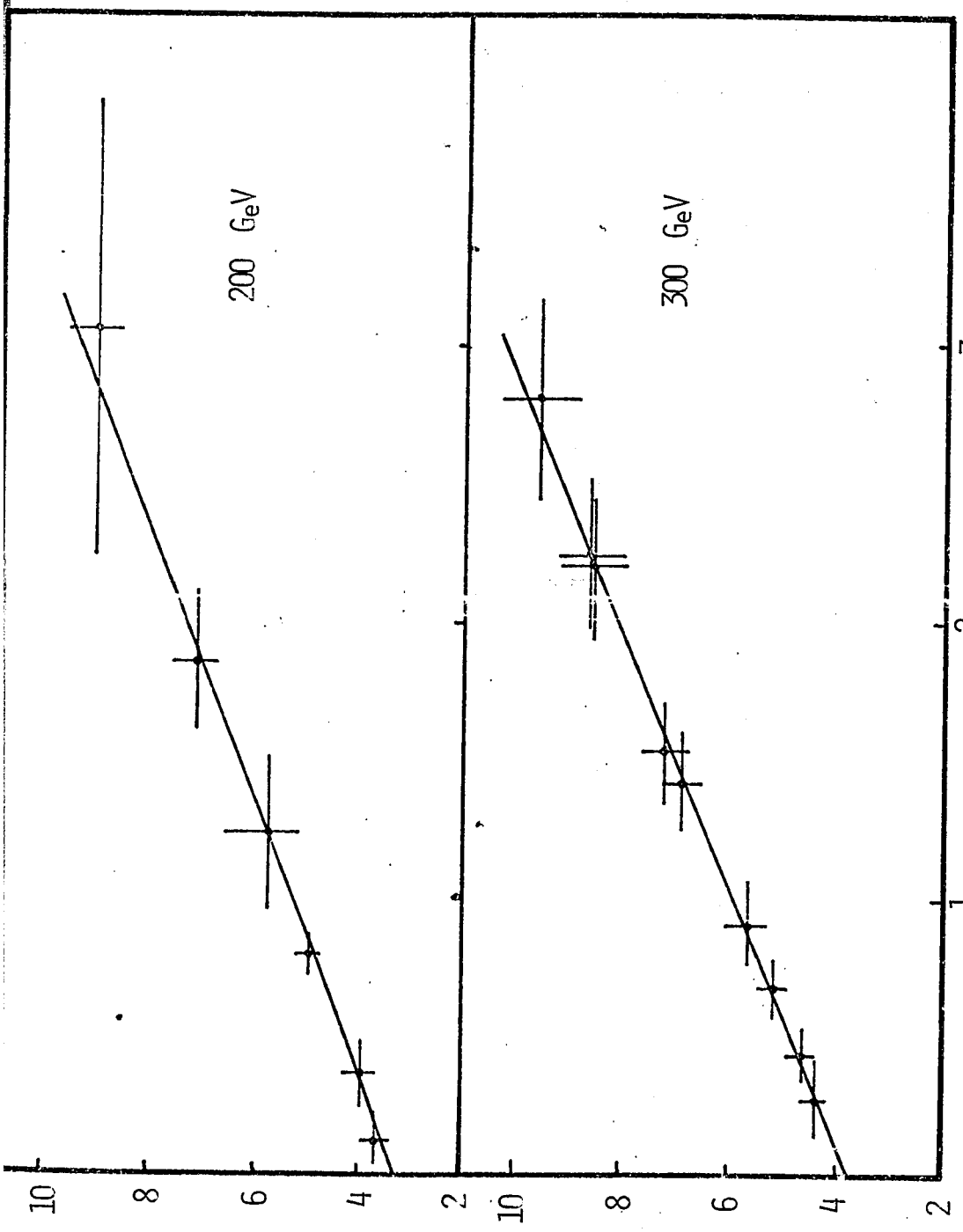

$-(1/\ n_{ch}-2\ )\ \sum_{i=2}\ \text{LN TAN}\ \theta_L/2$

vs.

$(\ n_s-1\ /\ n_{ch}-2\ )-1$

FIGURE 5.1

-3.3, which is in good agreement with the experimental value of -3.27 from proton-proton collisions.[59] Unfortunately, the value of $\langle \delta \rangle$ is not available for proton-proton interactions at 300 GeV. However, one can estimate what this value would be. At 200 GeV, the experimental value of $\langle \delta \rangle$ is approximately 10% higher than the expected value from the Lorentz factor. Thus, it can be expected that at 300 GeV, the value of $\langle \delta \rangle$ would be -3.6, which is in good agreement with the value of -3.8 obtained for the intercept. The foregoing analysis confirms that only the incident proton has to be subtracted from the shower particles.

5.3 COMPARISON OF PREDICTED AND OBSERVED MULTIPLICITIES

In order to compare the predicted and observed multiplicities, we shall examine the predictions of the models and extract the expressions for $\langle n_{\pm} \rangle$ for each model.

5.3.1 Model of Fishbane and Trefi and EFC Model

In the model of Fishbane and Trefil, the projectile excitation decays giving rise to $1/2 \langle n(1, E_{inc}) \rangle$ particles, whereas the slow target excitations decay into $\nu/2 \langle n(1, E_{inc}) \rangle$ particles. The average number of particles produced from the decay of the target excitations is

$\frac{\nu}{2}\langle n(1,E_{inc})\rangle-\nu$. Removing the incident particle from the decay of projectile excitation, the average created particle multiplicity from this part is $1/2\ \langle n(1,E_{inc})\rangle-1$. Thus, $\langle n_{\pm}\rangle$ from proton-nucleus interactions is given by

$$\langle n_{\pm}\rangle = \langle n_{ch}-2\rangle(1/2 + \bar{\nu}/2\ )$$

and the ratio R becomes

$$R_A = \langle n_{\pm}\rangle_{p\text{-}A}\ /\langle n_{\pm}\rangle_{p\text{-}p} = 1/2 + \bar{\nu}/2$$

This is exactly the relation obtained by Fishbane and Trefil. Though R_A in this model is the ratio of the created charged particles, it has been erroneously equated to $\langle n_s\rangle/\langle n_{ch}\rangle$ by some authors.

The arguments used in the case of the previous model apply to the EFC model also. From the decay of the 'soft' hadrons, i.e. the target excitations, the average number of particles produced is $\nu/3\ \langle n<1,E_{inc}\rangle-\nu$. The decay of the 'hard' hadron, i.e. the projectile excitation results in the creation of $2/3\ \langle n(1,E_{inc}\ )\rangle-1$ particles. This gives

$$\langle n_{\pm}\rangle = (2/3 + \langle\nu\rangle/3)\langle n_{\pm}\rangle_{p\text{-}p} + 2/9(1-\langle\nu\rangle)$$

5.3.2 Models of Lehman and Winbow and Cutler and Snider

The model of Lehman and Winbow predicts that the total mean multiplicities, i.e. the average number of

created particles plus the initial particles, can be given by

$$m(A,E_{inc}) = m(1,E_{inc}) + 1/2\ m'(1,E'_o)(\nu-1)$$

Here $m(A,E_{inc})$ and $m(1,E_{inc})$ are the total mean multiplicities in proton-nucleus and proton-proton collisions, respectively, and $m(1,E')$ is the total mean multiplicity in proton-proton collisions at energy E'. E' is defined by the relation,

$$2\ y_o = \ln(2E'_o/m)$$

where m is the parton mass and $E_o = 50$ GeV, for a nucleus of atomic weight $A = 67$. $\langle n_\pm \rangle$ may be estimated, if we assume that the average multiplicities in hadron-hadron collisions vary as the logarithm of the incident energy, from the relation

$$\langle n_\pm \rangle = \langle n_\pm \rangle_{p-p} + 1/2\ (\langle\nu\rangle-1)\ \langle n_\pm \rangle'(1,E_o')$$

where $\langle\nu\rangle = 0.51\ A^{1/3}$.

In the model of Cutler and Snider, the average total multiplicity is given by

$$\langle m(A,E_{inc}) = C\ A^{1/3} + f(A).$$

In order to eliminate the unknown A dependent function $f(A)$, Cutler and Snider suggest that $d\langle m(A,E_{inc})\rangle/dY$ be used. $\langle n_\pm \rangle$ may be estimated from $d\langle m(A,E_{inc})\rangle/dY = C\ A^{1/3}$. C is a constant whose value lies between 0.95 and 1.3.

5.3.3 The hydrodynamical model

In this model the quantities compared are the produced particles in both the proton-nucleus and proton-proton interactions. The ratio R then, is the ratio of the average number of charged particles produced in proton-nucleus collisions to those produced in proton-proton collisions. Since $R_A = A^{0.19}$,

$$\langle n_\pm \rangle = (2\ E^{1/4} - 2)\ A^{0.19}\ .$$

5.3.4 Model of Berlad, Dar and Eilam

In this model, the collision process involves the incident proton and a tube containing the target nucleons. This tube is considered to be equivalent to a particle of mass m, where is the number of nucleons in the tunnel. The charge of this 'particle' is equal to $\langle \nu_p \rangle$, the number of protons in the tunnel. The relation $\langle n_{ch} \rangle = C\ E^{1/4}$ that is successfully applied to proton-proton collisions is expected to hold for proton-tube collisions, except that the energy is boosted by a factor $\langle \nu \rangle^{1/4}$. The average charged particle multiplicity expected from this model is given by

$$\langle n_\pm \rangle = 2\ E^{1/4} \langle \nu \rangle^{1/4} - \text{initial charges}$$

The mechanism of particle production in this model is different from the CPM. The incoming particle or its subsequent 'excited' state does not undergo successive

collisions as in the case of CPM. Consequently, in this model is not the same as that in the other models. We can evaluate $\langle\nu\rangle$, the average number of nucleons in the tube by considering the nucleus to be a sphere of uniform density. The average length of a tube of nucleons is 1.33R where $R = R_o A^{1/3}$, is the radius of the nucleus. If the size of the incoming proton is taken to be one pion wavelength, then the average number of nucleons in the tube is 6.6 for a silver nucleus. This value is considerably higher than the average number of inelastic collisions a proton undergoes inside a silver nucleus. For emulsion as a whole, the average mass of the tube is 5.4 times the nucleon mass. Our values for ν are slightly lower than the values obtained by Berlad, Dar and Eilam. This may be due to the fact that ν is sensitive to the value of R_o used. In our calculations we took R_o to be 1.2 fm.

In Table 5.3, the theoretical and experimental values for the average number of shower particles from proton-nucleus collisions in emulsion at incident proton energies of 200 GeV and 300 GeV are presented, along with the results in tungsten and chromium obtained by Florian et al[4,26] and the Echo Lake data[6], where the targets used were

Aluminum, iron, tin and lead. In figure 5.2, the experimental values of $R_A = \langle n_\pm \rangle_{P-A} / \langle n_\pm \rangle_{P-P}$ and the theoretical predictions are shown graphically.

From the table, we see that the intra-nuclear cascade model calculations are compatible with the observed values of $\langle n_\pm \rangle$ and R_A. This would indicate that, in a successive collision picture, atleast as far as $\langle n_\pm \rangle$ is concerned, the main contribution comes from the leading 'particle'.

The predictions for R_A, for heavier nuclei, in the models of Lehman and Winbow and Cutler and Snider are in good agreement with experimental observations. The models tend to predict lower values of R_A for light nuclei. The R_A value for a given nuclear target decrease with increasing energy and this is more pronounced in the model of Lehman and Winbow than in the model of Cutler and Snider.

The predictions of the model of Berlad, Dar and Eilam are generally lower than the observed values of R_A. R_A in this model is quite sensitive to the number of nucleons in the tube, which in turn depends on the R_o value used in its computation. A lower value of R_o will result in better agreement between the models predictions and the resluts of the experiments.

Table 5.3

Comparison of predicted and observed values of multiplicities and R_A

Energy in GeV	Target	Experiment $\langle n_s \rangle$	Experiment R_A	ICM $\langle n_s \rangle$	ICM R_A	LW $\langle n_s \rangle$	LW R_A	CS $\langle n_s \rangle$	CS R_A	FT $\langle n_s \rangle$	FT R_A	EFC $\langle n_s \rangle$	EFC R_A	HM $\langle n_s \rangle$	HM R_A	BDE $\langle n_s \rangle$	BDE R_A
200	AgBr	13.6±0.7	2.41±0.19	15.0	2.65	13.4	2.37	14.5	2.57	11.7	2.07	9.2	1.63	13.1	2.37	8.2	1.49
	CNO	9.0±1.0	1.59±0.22	9.0	1.59	6.7	1.19	7.3	1.29	7.6	1.35	6.8	1.20	9.1	1.64	7.5	1.36
	Em	12.0±0.2	2.12±0.10	13.0	2.32	11.4	2.02	12.3	2.18	10.4	1.85	8.5	1.50	11.8	2.13	7.9	1.44
	W	16.8±3.8	2.97±0.76			17.4	3.08	15.8	2.80	13.9	2.46	10.5	1.86	14.9	2.69	8.4	1.53
300	AgBr	15.4±0.5	2.37±0.12	17.0	2.62	14.3	2.20	15.7	2.42	13.5	2.07	10.7	1.65	15.0	2.37	9.4	1.49
	CNO	10.7±0.6	1.65±0.12	10.0	1.54	7.6	1.17	7.9	1.22	8.7	1.35	7.8	1.20	10.4	1.64	8.6	1.36
	Em	13.9±0.2	2.14±0.07	14.8	2.28	12.3	1.89	13.4	2.06	12.0	1.85	9.8	1.51	13.5	2.13	9.1	1.44
	W	17.5±1.5	2.66±0.28			18.3	2.82	17.3	2.66	16.0	2.46	12.2	1.88	17.0	2.69	9.7	1.53
	Cr	12.5±1.2	1.92±0.22			11.5	1.77	11.1	1.71	11.7	1.80	9.6	1.48	13.4	2.12	9.2	1.45
160	Al	10.0±0.8	1.89±0.15	10.0	1.89	8.0	1.51	7.6	1.43	8.2	1.55	7.0	1.32	9.6	1.87	7.1	1.39
	Fe	11.0±0.9	2.08±0.17	11.5	2.17	10.6	2.00	9.8	1.85	9.8	1.85	7.9	1.48	11.0	2.15	7.3	1.44
	Sn	12.0±1.1	2.26±0.21			14.3	2.70	12.9	2.43	11.7	2.20	9.0	1.70	12.7	2.48	7.6	1.50
	Pb	13.5±1.4	2.55±0.26			17.9	3.38	15.7	2.96	13.4	2.54	10.0	1.89	14.1	2.75	7.7	1.51
260	Al	11.6±1.2	1.87±0.19	11.0	1.77	8.9	1.44	8.5	1.37	9.6	1.55	8.2	1.33	11.3	1.87	8.4	1.39
	Fe	11.9±1.2	1.92±0.19	13.5	2.18	11.5	1.85	11.0	1.77	11.4	1.83	9.3	1.49	13.0	2.15	8.7	1.44
	Sn	13.9±1.4	2.24±0.23			15.2	2.45	14.4	2.32	13.6	2.20	10.6	1.71	15.0	2.49	9.1	1.50
	Pb	14.3±1.5	2.31±0.24			18.8	3.03	17.5	2.82	15.7	2.54	11.9	1.91	16.6	2.75	9.3	1.54
520	Al	12.8±2.5	1.73±0.35	12.5	1.69	10.1	1.36	9.8	1.32	11.5	1.55	9.9	1.33	14.1	1.87	10.6	1.40
	Fe	14.8±2.9	2.00±0.39	16.5	2.23	12.7	1.72	12.7	1.72	13.5	1.83	11.1	1.50	16.2	2.15	11.0	1.46
	Sn	15.8±3.6	2.14±0.49			16.4	2.22	16.5	2.22	16.3	2.20	12.8	1.73	18.7	2.48	11.5	1.52

ICM - Intra-nuclear cascade model
LW - Model of Lehman and Winbow
CS - Model of Cutler and Snider
FT - Model of Fishbane and Trefil
EFC - Energy flux cascade model
HM - Hydrodynamical model
BDE - Model of Berlad, Dar and Eilam

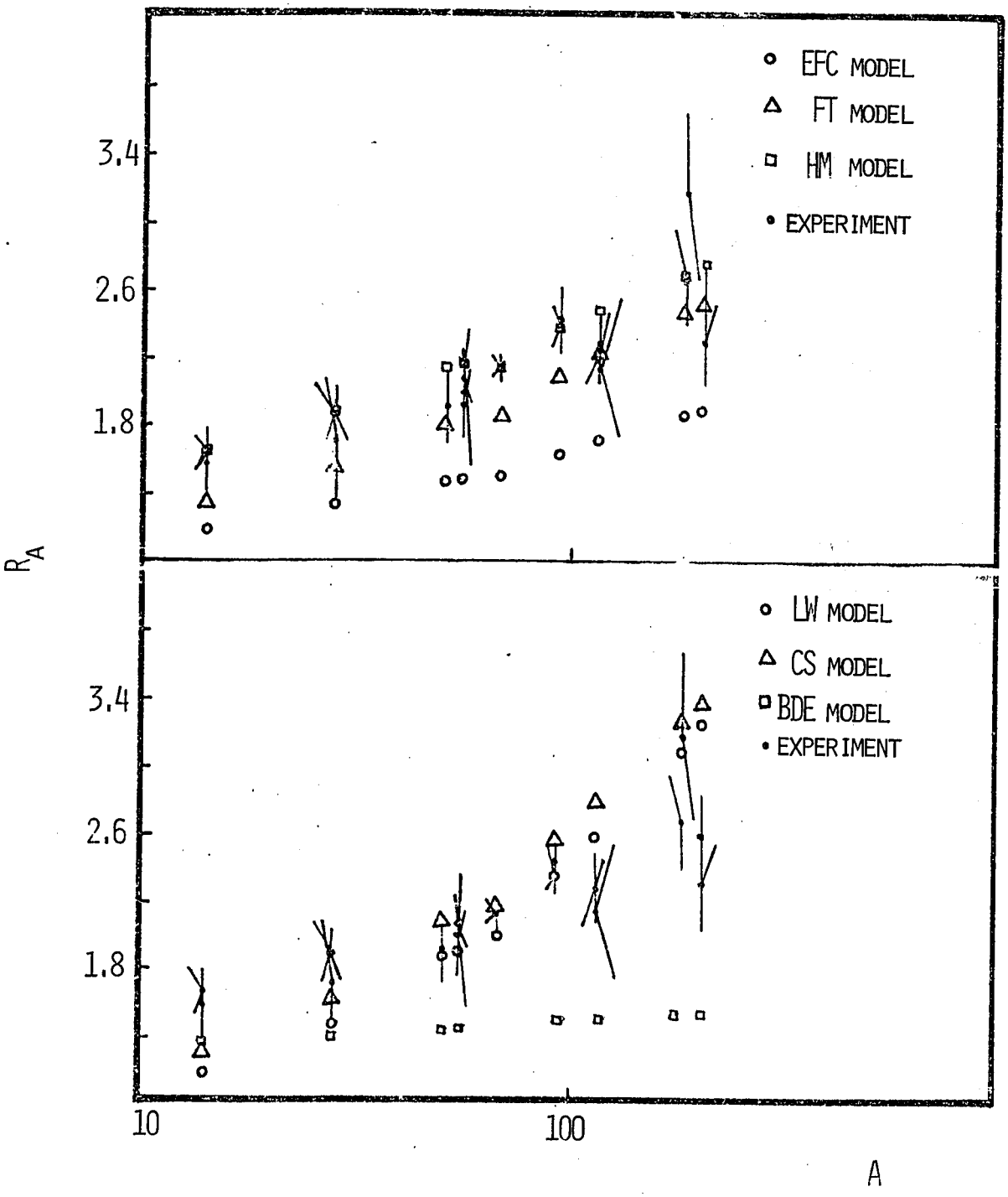

FIGURE 5.2 R_A AS A FUNCTION OF ATOMIC WEIGHT

The model of Fishbane and Trefil gives slightly higher R values than the EFC model. In these models, while calculating R_A we have used the empirical relation of Gurtu et al, which gives larger $\langle\nu\rangle$ compared with the relation obtained from the experiments of Denisov et al.

The predictions of the hydrodynamical model are in very good agreement with the experimental results. The validity of this model is not limited to FNAL energies, but may be extended to lower energies. This is shown in Table 5.4.

Table 5.4

R_A at lower energies and the predictions of the hydrodynamical model

Energy in GeV	$R_A = \langle n_\pm \rangle_{p-A} / \langle n_\pm \rangle_{p-p}$	Hydrodynamical model	Reference
6.2	1.66 ± 0.10	2.13	
9.0	1.58 ± 0.20		
20.5	1.93 ± 0.10		
22.5	1.97 ± 0.09		
27.0	2.26 ± 0.13		
27.0	2.18 ± 0.08		
30.0 (*)	2.13 ± 0.04		
67.0	2.14 ± 0.10		

(*) $\langle n_\pm \rangle$ estimated from the relation $\langle n_{ch} \rangle = 2\ E^{1/4}$.

Experimentally, for the proton-nucleus interactions studied in emulsions, the nuclear response as measured by

$\langle N_h \rangle$ appears to be the same from 30 GeV to currently available accelerator energies. A first guess would be that the particle production mechanism in proton-nucleus interactions is the same in this energy range. Hence, any model, in order to be successful, should be able to explain the experimental results from 30 GeV onwards.

5.4 NUMBER OF HEAVY TRACKS

Considering the average number of heavy tracks N_h, the cascade calculations of Artykov et al overestimate $\langle N_h \rangle$. The expected value of 13.0 from these calculations is much greater than the observed value. The Monte Carlo calculations also predict that $\langle N_h \rangle$ increases with the incident energy, which is not the experimental result. The increase in the value of $\langle N_h \rangle$, in this model, is much more dramatic at energies lower than 100 GeV. At higher energies, $\langle N_h \rangle$ increases much more slowly and seems to have reached a plateau value. The CPM, though lacking exact values for $\langle N_h \rangle$, expect it to be constant. In the models of Lehman and Winbow and Cutler and Snider, $\langle N_h \rangle$ is also expected to be constant, for $E_{inc} > 50$ GeV. This constancy is a part of the description of the mechanism of particle production. In the model of Berlad, Dar and Eilam, presumably contribution to $\langle N_h \rangle$ come from the

number of protons in the tube that collide with the incident particle. The protons do not have to be knocked out of the nucleus as individual protons; for example, they can come out as deuterons or alphas. This type of description of the collision process also leads to a constant value of $\langle N_h \rangle$. Thus, all the models except the intra-nuclear cascade model expect the nuclear response to settle down.

5.5 ANGULAR DISTRIBUTION OF SHOWER PARTICLES

The angular distributions of shower particles from proton-proton collisions and proton-nucleus collisions in emulsion are presented in figure 5.3. There is an excess of particles at larger angles as predicted by the models discussed. However, all the models have specific predictions as to where the excess of particles should begin to appear. In the case of the model of Fishbane and Trefil and EFC model, this boundary, for a given energy, is fixed independently of the target nucleus. The incident energies are not large enough to determine whether the excess appears at Y/2 (Fishbane and Trefil) or at Y/3 (EFC). In the case of the model of Berlad, Dar and Eilam, we expect the length of the rapidity plot (in our case, ln tan $\theta_L/2$ plot) to be greater than that for proton-

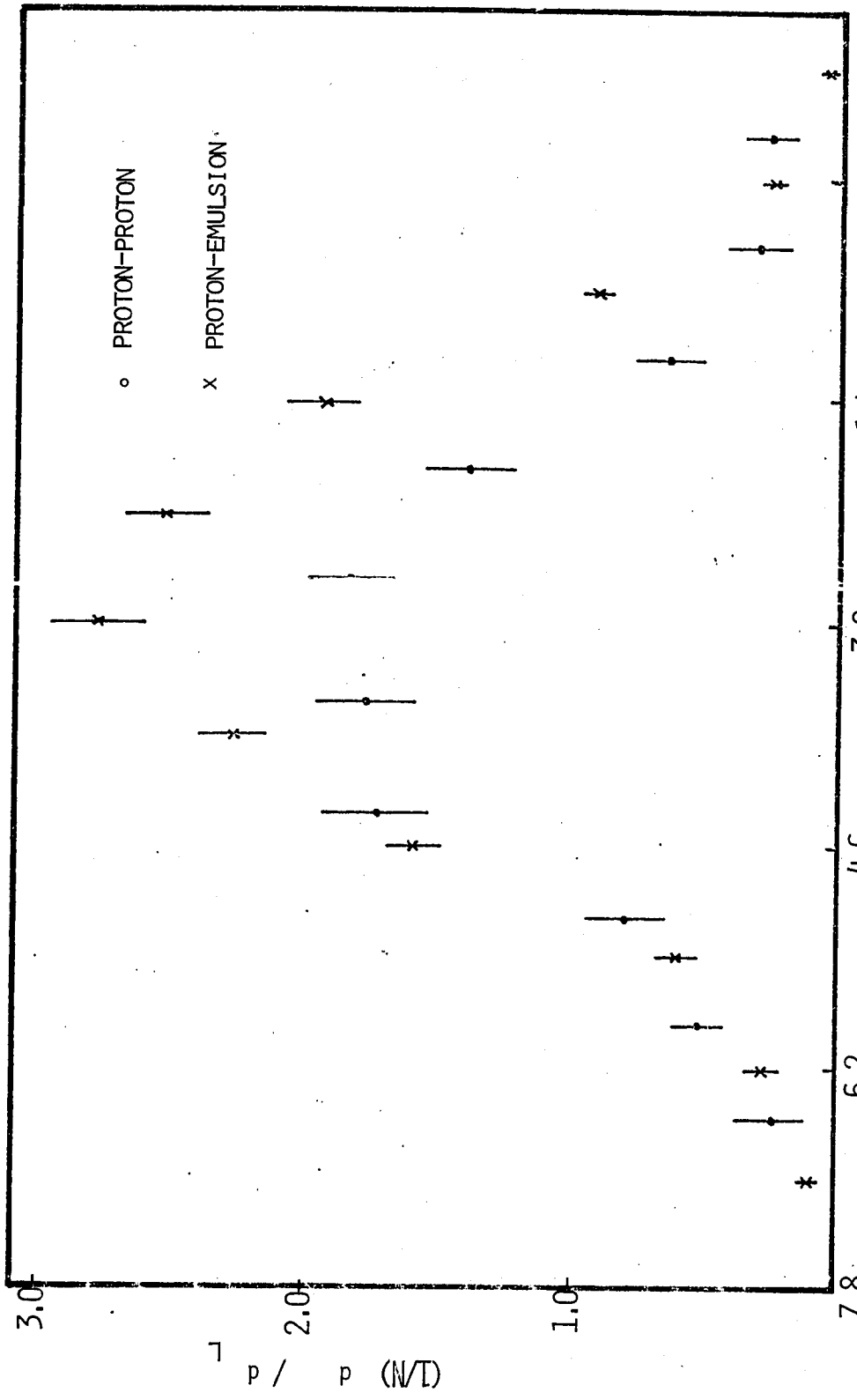

FIGURE 5.3 ANGULAR DISTRIBUTIONS OF CHARGED AND SHOWER PARTICLES

proton collisions. This does not appear to be the case. However, it must be borne in mind that in the pseudo-rapidity plot, some target protons and slow pions are not included. The angular distributions are compatible with some predictions of the hydrodynamical model. There is the expected shift of the centre of the distribution towards larger angles and the distributions are very nearly Gaussian. The predictions of the models of Lehman and Winbow and Cutler and Snider regarding the boundary point where excess particles are produced (in comparison with proton-proton data) cannot be verified with the aid of the existing data. These models, like other models do qualitatively account for the shape of the angular distributions.

CONCLUSION

Three of the important features of proton-nucleus collisions that emerge from these studies are, i) the average multiplicity depends only weakly on the atomic weight of the target nucleus, ii) in the forward region, the angular distributions of shower particles are independent of the target nucleus and iii) the ratio $D/\langle n_s \rangle$ is independent of the target nucleus.

Considering the first observation, in the literature R_A, which is the measure of the A dependence of the multiplicity, has been defined in two different ways. One is that, it is the ratio of $\langle n_s \rangle$ to $\langle n_{ch} \rangle$ and the other is that, it is the ratio of fast ($\beta > 0.7$) charged particles from proton-nucleus and proton-proton collisions, i.e. $R_A = \langle n_s \rangle / \langle n_{ch} \rangle - 0.5$.[61] Both definitions do not appear to have any arguments supporting their usage. To bring out the correct A dependence of the production process, it is logical to use the number of created particles, whether they be fast or slow.

Alsc, while comparing the angular distributions of charged particles from proton-nucleus and proton-proton interactions, it is desirable to be consistent. Thus, we feel that, only the angular distributions of the created particles should be compared.

The ratio $D/\langle n_s \rangle$ is seen to be constant for the light and heavy groups of nuclei in emulsion and also for tungsten and Chromium. For proton-neutron interactions, $D/\langle n_s \rangle$ is 0.55 ± 0.05. For proton-proton interactions, the equivalent quantity, that gives the same value for the ratio as for proton-nucleus and proton-neutron interactions, is $D/\langle n_{ch} \rangle - 1$. The interpretation of $\langle n_s \rangle$, then, is that this quantity is the total number of created charges in proton-nucleus interactions plus the incident particle.

Which of the many models of multiparticle production from nuclear targets is a valid description cannot yet be decided. Considering the average multiplicities, many models give reasonable good estimates of these quantities. However, at high energies, the model of Lehman and Winbow, predicts that the ratio $\langle n \rangle_{p\text{-}A} / \langle n \rangle_{p\text{-}p}$ decreases as the energy increases. In the hydrodynamical, Cutler and Snider and Berlad, Dar and Eilam models, there continues to be a finite A dependence of this ratio, independent of the

incident energy, whereas in the EFC model and the model of Fishbane and Trefil, this ratio depends on the behaviour of the proton-proton inelastic cross-section. Also, in these two models, as the energy increases, the energy of each of the backward clusters or slices increases. This would cause an increase in multiplicity, and the formulas need revision at high energies. If the proton-proton inelastic cross-section is constant, one would expect that the ratio, $\langle n \rangle_{p\text{-}A} / \langle n \rangle_{p\text{-}p}$, increases as the energy of the incident hadron increases. Already at 200 GeV and 300 GeV, the energy of each backward slice in the EFC model is nearly 6 GeV and if the slices behave as hadrons, this energy is sufficient to produce additional particles, though the contribution from these to the average multiplicity may be small. As a digression it is interesting to calculate the mass of each backward slice in the EFC model. Referring to figures 5.1 of chapter 5, the slopes of the straight lines may be interpreted as mean rapidities (assuming that $\ln \tan \theta/2 \approx y$), of the backward particles. From this the mass of each slice can be calculated to be 2 GeV at 200 GeV and 2.4 GeV at 300 GeV.

The rapidity distribution may prove to be more valuable than the multiplicities in testing various

models. In the models of Lehman and Winbow, and Cutler and Snider, the boundary of the target fragmentation region is different for different nuclei. The model of Cutler and Snider differs from that of Lehman and Winbow in that, the former expects a slight enhancement in rapidity distribution for proton-nucleus collisions over proton-proton collisions even in most of the forward region. To check this would require more data than is available at present. In the model of Berlad, Dar and Eilam, due to the expected energy boost, the length of the rapidity plot increases (by about 1.8 for emulsion). As far as the data allows, this does not seem to be the case. This may be because only angular distribution data is available and it is not strictly correct to equate this with the rapidity distribution. Also, the angular distribution data do not contain information regarding the slow target protons and pions. In EFC model and the model of Fishbane and Trefil, the enhancement in the rapidity distribution distribution occurs at Y/3 and Y/2 respectively, independent of the size of the target nucleus. In the hydrodynamical model, though the details are not worked out, the boundary of the target fragmentation region depends on the size of the nucleus.

Thus, the predictions for rapidity distributions are fairly distinct in each model and these could be verified at higher energies.

With extensive experimental data on the rapidity distributions, using different nuceli as targets, it may be possible to verify some of the above predictions of these models even at the present FNAL energies.

APPENDIX 1

This appendix is divided into two parts: in the first part, we shall describe the equipment used in printing the grid and processing the emulsion. In the second part we shall present the processing procedure.

PART 1: THE EQUIPMENT

a) The set up for printing grid

A sketch of this set up is shown in figure A1.1. The grid of coordinates was supplied by the Strasbourg

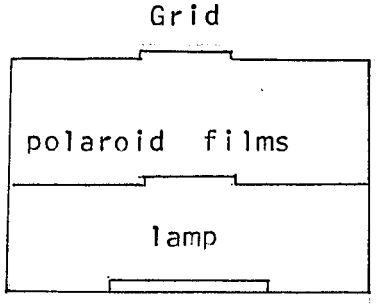

Figure A1.1 The setup for printing grid

laboratory. Each square on the grid was equal to 0.25 sq.mm. Two polaroid films were used in reducing the light intensity and a timer controlled the duration of exposure.

The pellicle was placed in contact with the grid and a small weight on the pellicle ensured good contact between the two surfaces. The timer was set and the emulsion was exposed to light for 20 seconds. The arrangement was such that a light and clearly visible grid was printed. The long exposure time left a good margin for errors.

b) The developing tank

A cross-sectional view of the developing tank is presented in figure A1.2. The developing tank and trays were made of stainless steel. The tank essentially is a rectangular container which supported a 'cave' into which

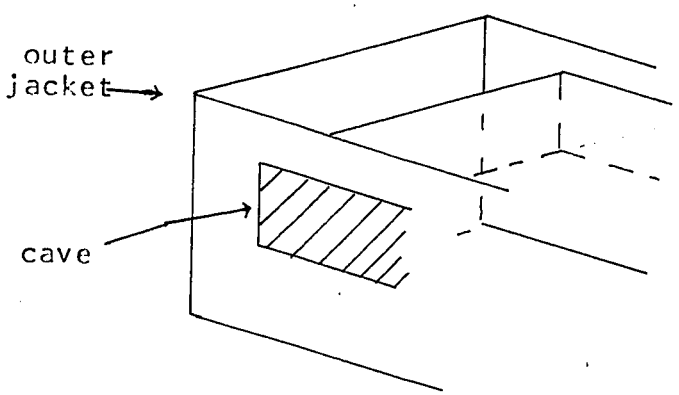

Figure A1.2 Cross-sectional view of the developing tank

trays containing the plates and solutions can be inserted. When covered with the lids and placed in the cave, the trays are light-proof. The water circulating in the tank

covered the cave on all sides and maintained its temperature at any desired value.

A larger version of the developing tank that could handle more stacks was also constructed. Instead of one cave, there are eight caves in this tank and these can accommodate wider trays than the smaller developing tank.

c) The fixing tank

This tank is also made of stainless steel and consists of an outer rectangular tank, where water at desired temperature could be circulated and an inner rectangular tank that holds the fixer solution. Stirring of the fixer can be accomplished by bubbling filtered nitrogen gas through the solution.

In a more recent design, stirring was accomplished by mechanical means. A cage made of perforated stainless steel was divided into four separate compartments, where the plates could be placed. The whole cage could be very slowly moved up and down in the fixer solution by means of a motor.

d) The set up for dilution and washing

A cartridge containing chemicals that demineralize the tap water was set up close to the fixing tank. A

constant pressure head regulates the flow of the tap water into this cartridge. The outlet of the cartridge is connected to the inlet of the fixing tank.

PART 2: PROCESSING

Prior to the commencement of processing, each pellicle or plate was labelled and its thickness was measured at five different places. A small corner was cut from a pellicle and the density of emulsion was measured using the Archimedes' principle. The liquid used was pure chlcroform.

While the plates needed no preparation, it was thought best to mount the pellicles on prepared glass plates, in order to minimize distortions that can occur during processing. The procedure described by Barkas was follcwed.

15 gms of gelatine was soaked overnight at room temperature in one litre of filtered distilled water. On the morning of processing, the solution was heated to about 50 C until all the gelatine dissolved. The solution was filtered and to this 5 c.c of glycerol and 2.5 c.c of Kodak photo-flo were added. The solution was then allowed to ccol to 27 C. This temperature was maintained during the mounting operation. An Ilford prepared glass plate

and a pellicle were immersed in the solution and the pellicle was placed on top of the glass plate. The time of immersion was not more than 10 seconds. The plate and pellicle were taken out and placed between two layers of 5 mil mylar sheets. A moderate pressure using a roller was then applied in order to drive out any air bubbles trapped between the pellicle and the glass plate and to ensure good contact between the two surfaces.

The plates were then allowed to dry in air at 4 C, for about 30 minutes.

The details of the solutions used and the temperature and duration of each stage in the processing procedure are presented in the following table.

Stage	Solution	Temperature and duration	Comments
Pre-soak	Filtered distilled water	4°C for 2 hrs.	
Cold soak	Brussels amidol developer(*) pH 6.4	4°C for 3 hrs	Filtered nitrogen gas is circulated in the tank
Warm stage	Developer solution poured out	Temperature raised to 13°C from 4°C in 10 minutes, then to 18°C in another 10 minutes, and to 20°C in 5 minutes. This temperature maintained for 1 hr.	Filtered nitrogen gas is circulated in the tank
Stop bath	6 c.c glacial acetic acid, 6 gm sodium sulfite in 1 litre of distilled water. Sodium sulfite added just before the commencement of this stage.	12°C for 1.5 hrs.	
Fixer	300 gm of sodium thiosulfate, 12 gm of sodium sulfite in 1 litre of distilled water. Sodim sulfite added just before commencement of the stage. pH 5.4;adjusted by adding acetic acid.	12°C until the plates are clear and then an additional 1/2 times the total time taken for the plates to clear.	Fixer solution changed approximately every 10 hrs. The total fixing was approximately 90 hrs.
Dilution	Filtered demineralized water, at a rate of 3 c.c/hour for 3 litres of fixer was let into the tank. After 24 hrs, the rate was increased by 50%.	12°C, until all the fixer was replaced by demineralized water.	
Washing	Filtered demineralized water at a rate of 3 litres/hr.	12°C for 3 days.	
Drying	20% ethanol, 4% glycerine and 76 % distilled water	12°C and let warm to room temperature. 1 hr.	
	40% ethanol, 4% glycerine and 56% distilled water	room temperature, 1 hr.	
	60% ethanol, 4% glycerine and 36% distilled water	room temperature. 1 hr.	
	80% ethanol, 4% glycerine and 16% distilled water	room temperature. 1 hr.	
	In air	room temperature, for two days	at 55% relative humidity

(*) Brussels amidol developer:
To 1 litre of distilled water add 35 gm of boric acid, 0.8 gms of potassium bromide. A few minutes before the commencement of cold soak, add 4.5 gm amidol and 18 gm of sodium sulfite.

APPENDIX 2

A2.1 DIRECT PAIR PRODUCTION

The probability that a proton of mass m and kinetic energy E, traversing a thickness dx (g/cm^2) of matter produces an electron pair of energy between E' and E'+dE' is given by [62]

$$P = (8N/\pi A)(\alpha z\, r_e)^2\, L(U,V)\, dE'\, dx$$

where

α = the fine structure constant

r_e = classical electron radius

N = the Avogadro number

z = the charge of the target nucleus

A = the mass number of the target nucleus

U = the total energy of the proton

V = U'/U, the ratio of the total pair energy to the total proton energy

The function L(U,V) is defined for the following extreme regions.

Region IN: pair of low energy, no shielding

$L(U,V) = 7/9\ (1/UV)\ \ln\ (k_1/(m/m_e)V)\ \ln\ (k'\ U/6m_e)$

$2\ m_e/U < V < 2\ m_e/m\ ,\quad V < 2m_e/U\alpha z^{1/3}$

Region IS: pair of low energy, complete shielding

$L(U,V) = 7/9\ (1/UV)\ \ln\ (k_2/(m/m_e)V)\ \ln\ (k_2'/\alpha Z^{1/3})$

$2\ m_e/U < V < 2\ m_e/m\ ,\quad V > 2m_e/U\alpha Z^{1/3}$

Region IIN: pair of high energy, no shileding

$L(U,V) = (1/UV^3)(m_e/m)^2\ \ln\ (k_3\ mV/\alpha Z^{1/3}\ m_e)$

$2m_e/m < V < 1,\quad V < (2m_e/m)\ \alpha Z^{1/3}\ U/m$

Region IIS: pair of high energy, complete shielding

$L(U,V) = (1/UV^3)(m_e/m)\ \ln\ (2k_4 U/m)$

$2m_e/m < V < 1,\quad V > (2m_e/m)\ \alpha Z^{1/3} U/m$

m is the mass of the electron and k and k' are constants of the order of unity. $k_1 = k_2$, $k_2' = 3k_2'$ ensures continuity at the boundary between IN and IS and $k_3 = k_4$ ensures continuity at the boundary between IIN and IIS.

Since we are interested in the events where the electron tracks are straight and thus may be confused with shower tracks, the lower limit for the pair energy is taken to be 120 MeV. At this energy, only the last three regions are relevant. For our calculations, we chose $k_2' = k_3 = k_4 = 1$. This sets $k_2 = 3$. Since these terms occur in the logarithmic function, we expect our results to be

fairly insensitive to this choice. The mean free path for direct pair production was calculated for both 200 GeV and 300 GeV protons. The results are tabulated below.

Mean free path in meters

Target	200 GeV protons	300 GeV protons
Ag	20.4	11.0
Br	35.7	19.2
C	833.	413.
N	2500.	1111.
O	625.	270.
H	10000.	4545.
Em	12.5	5.3

A2.2 KNOCK-ON ELECTRON PROBABILITIES

The collision probability for a particle of mass m and spin 1/2 with the electrons of an atom is given by [62]

$$P = 0.3\, m_e/\beta^2\, (1-\beta^2 E'/E'_m + 1/2\,(E'/E+m)^2)\, dE'/E'^2 \quad cm/gm$$

$$E' = 2\, m_e p^2/(m_e^2 + m^2 + 2m(p^2+m^2)^{1/2})$$

Here E and p are the kinetic energy and momentum of the incident particle, E' is the kinetic energy transferred to the electron and E'_m is the maximum transferable kinetic energy. Since electrons of energy lower than 60 MeV are recognizable by the scattering of their tracks, we chose this energy as the lower limit for the kinetic energy transferred by the incident proton to the electron. The mean free paths are calculated for each nucleus of the emulsion and the results are listed below.

Target	Mean free path in meters
Ag	5.1
Br	6.8
C	27.2
N	106.0
O	32.1
H	75.2
Em	2.3

The mean free paths are approximately the same for both energies.

REFERENCES

1. Barcelona-Batavia-Belgrade-Bucharest-Lund-Lyon-Montreal-Nancy-Ottawa-Paris-Rome-Strasbourg-Valencia collaboration, J. Hebert et al, Phys. Lett. 48B, 467 (1974).

2. Alma-Ata-Leningrad-Moscow-Tashkent collaboration, M. G. Antonova et al, Sov. J. Nucl. Phys. 19, 536 (1974).

3. J. Babecki, Z. Czachowska, B. Furmanska, J. Gierula, R. Holinski, A. Jurak, S. Krywdzinski, G. Nowak, B. Slezak, W. Wolter, Phys. Lett. 47B, 268 (1973).

4. J. R. Florian, Ph. D. Thesis, University of Washington (1974).

5. P. L. Jain, K. Kazuno, G. Thomas, and B. Girard, Lett. Nuovo Cimento 8, 921 (1973).

6. P. R. Viswanath, Ph. D. Thesis, University of Michigan (1974).

7. J. R. Elliott, L. R. Fortney, A. T. Goshaw, J. W. Lamsa, T. S. Loos, W. J. Robertson, W. D. Walker, and M. Yeager and M. E. Binkley, Phys. Rev. Lett. 34, 607 (1975).

8. W. Busza, J. E. Elias, D. F. Jacobs, P. A. Swartz, C. C. Young and M. R. Sogard, Phys. Rev. Lett. 34, 839 (1975).

9. A. Dar and J. Vary, Phys. Rev. D6, 2412 (1972).

10. P. M. Fishbane and J. S. Trefil, Phys. Rev. Lett. 31, 734 (1973).

11. K. Gottfried, Phys. Rev. Lett. 32, 957 (1974).

12. C. Castagnoli, G. Cortini, D. Moreno, C. Franzinetti, and A. Manfredini, Nuovo Cimento 10, 1539 (1953).

13. Barcelona-Batavia-Belgrade-Bucharest-Lund-Lyon-Montreal-Nancy-Ottawa-Paris-Rome-Strasbourg-Valencia collaboration, J. Hebert et al, Proc. AIP conf. on High-energy particle collisions, Nashville, Tenn. (1973).

14. R. E. Gibbs and J. R. Florian, L. D. Kirkpatrick, J. J. Lord and J. W. Martin, Phys. Rev. D10, 783 (1974).

15. G. Berlad, A. Dar, G. Eilam, University of Haifa Preprint (1975).

16. E. L. Feinberg, Phys. Rep. 5C, 237 (1972).

17. R. Slansky, Phys. Rep. 11C, 99 (1974).

18. W. H. Barkas, Nuclear Research Emulsions, Academic Press, vol 1, (1963).

19. R. D. Evans, The Atomic Nucleus, McGraw-Hill Book Company (1955).

20. University of California, Lawrence Radiation Laboratory, UCRL-2426, vol 2, (1966).

21. S. Biswas, B. Peters, and B. Rama, Proc. Indian Acad. Sci. A41, 154 (1955).

22. C. C. Dilworth, G. Occhialini, and R. M. Payne, Nature, 162, 102 (1948).

23. Alma-Ata-Cracow-Dubna-Leningrad-Moscow-Tashkent-Ulan Bator collaboration, M. G. Antonova et al, Phys. Lett. 39B, 285 (1972).

24. E. Lohrman and M. W. Teucher, Nuovo Cimento 25, 957 (1962).

25. C. Fisher, Ecole Internationale de la Physique des Particules Elementaires (1965).

26. J. R. Florian, M. Y. Lee, J. J. Lord, J. W. Martin, and R. J. Wilkes and R. E. Gibbs and L. D. Kirkpatrick, University of Washington Preprint (1975).

27. G. Charlton, Y. Cho, M. Derrick, R. Engelman, T. Fields, L. Hyman, K. Jaegar, U. Mehtani, B. Musgrave, Y. Oren, D. Rhines, P. Schreiner, and H. Yuta, and L. Voyvodic, R. Walker, and J. Whitmore and Z. Ming Ma, and R. G. Glasser, Phys. Rev. Lett. 29, 515 (1972).

28. A. Firestone, V. Davidson, D. Lam, F. Nagy, C. Peck, and A. Sheng, F. T. Dao, R. Hanft, J. Lach, E. Malamud, and F. Nezrick, and A. Dzierba, and R. Poster, P. Schlein, and W. Slater, Phys. Rev. D10, 2080 (1974).

29. P. Carruthers and Minh Duong-van, Phys. Rev. D8, 859 (1973).

30. D. H. Perkins, Progress in Elementary Particle and Cosmic Ray Physics, North-Holland, Amsterdam, (1960).

31. Alma-Ata-Leningrad-Moscow-Tashkent collaboration, E. V. Anzon et al, P. N. Lebedev Institute Preprint (1975).

32. K. Gottfried, Cern TH-1615 (1972).

33. N. Schmitz, Acta Physica Polonica B4, 689 (1973).

34. A. H. Mueller, Phys. Rev. D4, 150 (1971).

35. A. Wroblewski, Acta Physica Polonica B4, 857 (1973).

36. Data below 200 GeV are from: H. Winzler, Nucl. Phys. 69, 661 (1965), at 6.2 GeV and 22.5 GeV; C. Bricman, M. Csejthy-Barth, J. P. Lagnaux, and J. Sacton, Nuovo Cimento 20, 1017 (1961), at 14 GeV; H. Meyer, M. W. Teucher, E. Lohrman, Nuovo Cimento 28, 1399 (1963), and A. Barbaro-Galtieri, A. Manfredini, B. Quassiati, C. Castagnoli, A. Gainotti, and I. Ortalli, Nuovo Cimento 21, 469 (1961), at 27 GeV. The data at 200 GeV are from this work, and references 2 and 31. The data at 300 GeV are from this work.

37. Z. Koba, H. B. Nielsen, and P. Olessen, Nucl. Phys. B40, 317 (1972).

38. P. Slattery, Phys. Rev. Lett. 29, 1624 (1972).

39. A. J. Buras, J. Dias De Deus, R. Moller, Phys. Lett. 47B, 251 (1973).

40. Batavia-Belgrade-Lund-Lyon-Montreal-Nancy-Ottawa-Paris-Rome-Strasbourg-Valencia collaboration, J. Hebert et al, 14th Int. Cosmic Ray Conf. Munich, (1975).

41. P. Slattery, Proc. AIP Conf. on High-energy particle collisions, Nashville, Tenn. (1973).

42. I. Z. Artykov, V. S. Barashenkov, and S. M. Eliseev, Nucl. Phys. B6, 11 (1968).

43. E. S. Lehman and G. A. Winbow, Phys. Rev. D10, 2962 (1974).

44. R. T. Cutler and D. R. Snider, University of Illinois, Urbana, Preprint (1975).

45. P. M. Fishbane and J. S. Trefil, Phys. Rev. D9, 168 (1974).

46. A. S. Goldhaber, Phys. Rev. D7, 765 (1973).

47. P. Carruthers and Minh Duong-van, Phys. Lett. 41B, 597 (1972).

48. F. Cooper and E. Schcneberg, Phys. Rev. Lett. 30, 880 (1973).

49. S. Z. Belinkii and G. A. Milekhin, JETP 2, 14 (1956).

50. L. D. Landau and S. Z. Belinkii, Collected Papers of L. D. Landau, Ed. D. Ter Haar, Gordon and Breach, New York (1965).

51. A. Gurtu, P. K. Malhotra, and I. S. Mittra, P. M. Sood and S. C. Gupta, V. K. Gupta, G. L. Kaul, L. K. Mangotra, Y. Prakash, N. K. Rao, M. L. Sharma, Tata Institute Preprint, TIFR-Bc-74-6, (1974).

52. W. R. Frazer, R. D. Peccei, S. S. Pinsky, and Chung-I Tan, Phys. Rev D7, 2647 (1973).

53. F. T. Dao, R. Hanft, J. Lach. E. Malamud, and F. Nezrick, V. Davidson, A. Firestone, D. Lam, F. Nagy, C. Peck, and A. Sheng, R. Poster, P. Schlein, and W. Slater and A. Dzierba, Phys. Rev D10, 3588 (1974).

54. A. Sheng, A. Firestone, and C. Peck, and A. Dzierba and E. W. Anderson, H. B. Crawley, and W. J. Kernan and

J. Canter, F. T. Dao, A. Mann, and J. Schneps, and J. Poucher and S. Stone, Phys. Rev. D12, 1219 (1975).

55. P. J. Camillo, P. M. Fishbane and J. S. Trefil, Phys. Rev. Lett. 34, 622 (1975).

56. S. P. Denisov, S. V. Donskov, Yu. P. Gorin, R. N. Krasnkutsky, A. I. Petrukhin, and D. Stoyanova, Nucl. Phys. B61, 62 (1973).

57. G. Calucci, R. Jengo, and A. Pignotti, Phys. Rev. D10, 1468 (1974).

58. E. M. Friedlander, Private communication.

59. A. Van Ginneken, Private communication.

60. V. Barashenkov, V. M. Maltsev, E. K. Mikhul, Nucl. Phys. 24, 642 (1961).

61. W. Busza, Proc. AIP conf. on High-energy Physics and Nuclear Structure, Santa Fe and Los Alamos (1975).

62. B. Rossi, High-energy Particles, Prentice-Hall Inc. Englewood Cliffs, New Jersey (1956).